Published for SISSA by Springer

Received: *July 2, 2020*
Accepted: *August 17, 2020*
Published: *September 23, 2020*

q-nonabelianization for line defects

Andrew Neitzke[a] **and Fei Yan**[b,c]

[a] *Department of Mathematics, Yale University, New Haven, CT 06520, U.S.A.*
[b] *Department of Physics, The University of Texas at Austin, Austin, TX 78705, U.S.A.*
[c] *New High Energy Theory Center (NHETC) and Department of Physics and Astronomy, Rutgers University, Piscataway, NJ 08854-8019, U.S.A.*

E-mail: andrew.neitzke@yale.edu, fyan.hepth@gmail.com

Abstract: We consider the *q-nonabelianization* map, which maps links L in a 3-manifold M to combinations of links $\widetilde{L}$ in a branched N-fold cover $\widetilde{M}$. In quantum field theory terms, q-nonabelianization is the UV-IR map relating two different sorts of defect: in the UV we have the six-dimensional $(2,0)$ superconformal field theory of type $\mathfrak{gl}(N)$ on $M \times \mathbb{R}^{2,1}$, and we consider surface defects placed on $L \times \{x^4 = x^5 = 0\}$; in the IR we have the $(2,0)$ theory of type $\mathfrak{gl}(1)$ on $\widetilde{M} \times \mathbb{R}^{2,1}$, and put the defects on $\widetilde{L} \times \{x^4 = x^5 = 0\}$. In the case $M = \mathbb{R}^3$, q-nonabelianization computes the Jones polynomial of a link, or its analogue associated to the group $\mathrm{U}(N)$. In the case $M = C \times \mathbb{R}$, when the projection of L to C is a simple non-contractible loop, q-nonabelianization computes the protected spin character for framed BPS states in 4d $\mathcal{N} = 2$ theories of class S. In the case $N = 2$ and $M = C \times \mathbb{R}$, we give a concrete construction of the q-nonabelianization map. The construction uses the data of the WKB foliations associated to a holomorphic covering $\widetilde{C} \to C$.

Keywords: Chern-Simons Theories, Quantum Groups, Supersymmetric Gauge Theory, Wilson, 't Hooft and Polyakov loops

ArXiv ePrint: 2002.08382

https://doi.org/10.1007/JHEP09(2020)153

Contents

JHEP09(2020)153

1 Introduction

This paper concerns a geometric construction which we call *q-nonabelianization*. In short, q-nonabelianization is an operation which maps links on a 3-manifold M to links on a branched N-fold cover $\widetilde{M}$. A bit more precisely, q-nonabelianization is a map of linear combinations of links modulo certain skein relations, encoded in *skein modules* associated to M and $\widetilde{M}$.

In this introduction we formulate the notion of q-nonabelianization rather generally: in particular, we discuss arbitrary N, and a general 3-manifold M. In the body of the paper, we describe a concrete way to construct q-nonabelianization in some detail, but only when $N = 2$ and $M = C \times \mathbb{R}$, with C a surface (which could be noncompact, e.g. $C = \mathbb{R}^2$). The extensions to higher N and general 3-manifolds M involve similar ideas but various new difficulties, and will appear in upcoming work.

The q-nonabelianization map we describe is related to many previous constructions in the literature, as we discuss in the rest of this introduction, and particularly close to the works [1–3] which provided important inspirations for our approach; indeed this paper was motivated by the problem of understanding their constructions in a more covariant and local way. Our description of q-nonabelianization can also be viewed as an extension of an

JHEP09(2020)153

approach to the Jones polynomial described in [4], particularly section 6.7 of that paper; from that point of view, what we are doing in this paper is explaining a way to replace $\mathbb{R}^3$ by $C \times \mathbb{R}$.

1.1 Physical setup

Our starting point is the six-dimensional $(2,0)$ superconformal field theory of type $\mathfrak{gl}(N)$, which we call $\mathfrak{X}[\mathfrak{gl}(N)]$. We will consider the theory $\mathfrak{X}[\mathfrak{gl}(N)]$ in six-dimensional spacetimes of the form

$$M \times \mathbb{R}^{2,1} \tag{1.1}$$

where M is a Riemannian manifold. We adopt coordinates as follows: M is coordinatized by $x^{1,2,3}$, $\mathbb{R}^{2,1}$ by $x^{4,5,0}$.

The theory $\mathfrak{X}[\mathfrak{gl}(N)]$ admits supersymmetric surface defects labeled by representations of $\mathfrak{gl}(N)$; in this paper we only consider the defect labeled by the fundamental representation. Given a 1-manifold (link) $L \subset M$, we insert this surface defect on a locus

$$L \times \{x^4 = x^5 = 0\} \subset M \times \mathbb{R}^{2,1}, \tag{1.2}$$

and call the resulting insertion $\mathbb{S}[L]$.

This kind of setup has been discussed frequently in the physics literature. As a tool for studying link invariants, it appears explicitly in [5], and its various dimensional reductions or M/string theory realizations have appeared in many other places, such as [6–8]. The case of $M = C \times \mathbb{R}$ with L at a fixed x^3-coordinate has also been studied in the context of line defects in class S theories, e.g. [9–12], while for more general M and L see e.g. [13].

1.2 The UV-IR map

Our approach to studying this setup is to pass to the "Coulomb branch" of the theory. The quickest way to understand what this means is to use the M-theory construction of the theory $\mathfrak{X}[\mathfrak{gl}(N)]$ on M. This construction involves N fivebranes wrapped on the zero section $M \subset T^*M$. To go to the Coulomb branch we consider instead one fivebrane wrapped on an N-fold cover $\widetilde{M} \subset T^*M$ (possibly branched). This construction has been used frequently in the study of class S and class R theories, e.g. [4, 12, 14–16].

Away from its branch locus the covering $\widetilde{M}$ is represented by N 1-forms λ_i on M. In order to preserve supersymmetry, the λ_i should be harmonic. In this paper, we will only consider two kinds of example:

1. $M = \mathbb{R}^3$, and the 1-forms λ_i are constants,

2. $M = C \times \mathbb{R}$ for a Riemann surface C, and the 1-forms λ_i are the real parts of meromorphic 1-forms on C.

(Case 1 is actually a special case of case 2 where we take $C = \mathbb{C}$, but it is interesting enough to merit mention on its own.)

JHEP09(2020)153

Now we ask the question: *what does* $\mathbb{S}[L]$ *look like in the IR?* In this limit the bulk theory is well approximated by the theory $\mathfrak{X}[\mathfrak{gl}(1)]$ on $\widetilde{M} \times \mathbb{R}^{2,1}$ [16]. In that theory we could consider surface defects $\widetilde{\mathbb{S}}[\widetilde{L}]$ on the loci

$$\widetilde{L} \times \{x^4 = x^5 = 0\} \subset \widetilde{M} \times \mathbb{R}^{2,1}, \tag{1.3}$$

for links $\widetilde{L} \subset \widetilde{M}$. The picture we propose, similar to e.g. [11, 17], is that $\mathbb{S}[L]$ *decomposes into a sum of defects* $\widetilde{\mathbb{S}}[\widetilde{L}]$, in the form

$$\mathbb{S}[L] \rightsquigarrow \sum_{\widetilde{L}} a(\widetilde{L}) \widetilde{\mathbb{S}}[\widetilde{L}]. \tag{1.4}$$

The meaning of the "coefficients" $a(\widetilde{L})$ is a bit subtle since we are not talking about local operators but rather extended ones. Nevertheless, we want to compute something concrete, and we proceed as follows. Eq. (1.4) implies a decomposition of the Hilbert space in the presence of the defect $\mathbb{S}[L]$ as a direct sum over Hilbert spaces associated to the IR defects, of the form

$$\mathcal{H}_L = \bigoplus_{\widetilde{L}} V_{a(\widetilde{L})} \otimes \mathcal{H}_{\widetilde{L}}. \tag{1.5}$$

What we will really compute is the Laurent polynomials $\alpha(\widetilde{L}) = \mathrm{Tr}_{V_{a(\widetilde{L})}}(-q)^{2J_3} q^{2I_3} \in \mathbb{Z}[q, q^{-1}]$ (see below).

1.3 Computing the UV-IR map

The construction of the UV-IR map (1.4) which we propose goes as follows. The links $\widetilde{L} \subset \widetilde{M}$ are built out of two sorts of local pieces:

- Lifts of segments of L to one of the sheets i of the covering $\widetilde{M} \to M$.

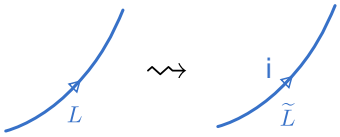

- Lifts to $\widetilde{M}$ of webs of strings, labeled by pairs ij of sheets of the covering $\widetilde{M} \to M$, ending on branch points of the covering or on the link L.

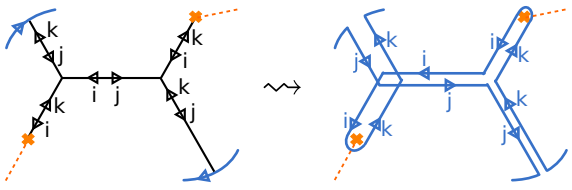

To each link $\widetilde{L}$ built from these pieces we assign a corresponding weight $\alpha(\widetilde{L}) \in \mathbb{Z}[q^{\pm 1}]$, built as a product of elementary local factors. Most of the difficulty in constructing the UV-IR map is to get these factors correct.

JHEP09(2020)153

In this paper we develop this scheme in detail only for $N = 2$. In the $N = 2$ case there are no trivalent string junctions, which enormously simplifies the situation: the only kinds of webs we have to deal with are the two shown below.

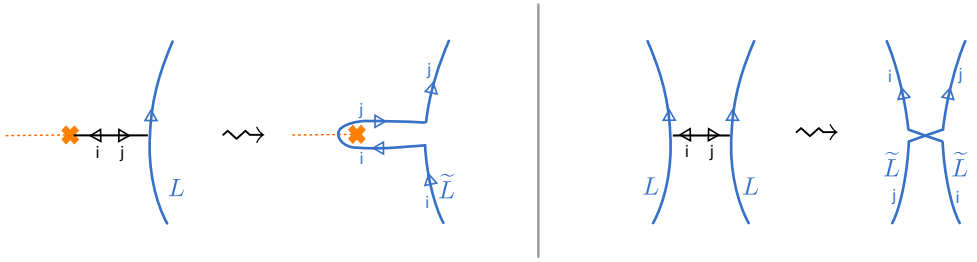

On the left is a string connecting the link L to a branch point of the covering $\widetilde{M} \to M$; the lift $\widetilde{L}$ takes a *detour* from the lift of L to the branch point along sheet i and back again along sheet j. On the right is a string connecting two different strands of L; we call this an *exchange*, because the two strands of the lift $\widetilde{L}$ exchange sheets along the lifted string.

There is an important difference between the detours and the exchanges. As we discuss in section 4, each exchange comes with a factor of $(q - q^{-1})$, so the contribution from exchanges vanishes at $q = 1$. (More generally, for $N > 2$, a web with k ends on L will come with a factor of $(q - q^{-1})^{k-1}$.) When we set $q = 1$, therefore, the only web contributions which survive are those from webs with exactly one end on L. Then our description of the UV-IR map reduces to a construction which already appeared in [12], for line defects in class S theories. In that context the webs attach to L only at places where L crosses the WKB spectral network. In contrast, when we allow $q \neq 1$, the webs can attach anywhere on L.

In [3] a version of the UV-IR map is described, in the language of spectral networks, which uses the detours but not the exchanges: in lieu of the exchanges one isotopes L to a specific profile relative to the spectral network, and then inserts by hand additional R-matrix factors. In our approach we do not make such an isotopy and we do not insert these R-matrix factors. The relation between the two approaches is roughly that, if we apply our approach to an L in this specific profile, then exchanges appear and produce automatically the off-diagonal parts of the R-matrix.

1.4 Skein relations

BPS quantities in the theory with surface defects $\mathbb{S}[L]$ inserted, such as supersymmetric indices, obey some relations. First, they depend only on the isotopy class of the link L, because deforming by an isotopy is a Q-exact deformation. Second, and more interestingly, there are also some Q-exact deformations which relate $\mathbb{S}[L]$ for non-isotopic links L.

We do not have a first-principles derivation of what these additional relations are, but to get a hint, we can use a picture from [5]: Euclideanize and compactify the x^0 direction, replace the x^4-x^5 directions by a cigar and compactify on its circular direction. The resulting effective theory is $\mathcal{N} = 4$ super Yang-Mills on $M \times \mathbb{R}_+$, with a boundary condition at the finite end. The operators $\mathbb{S}[L]$ reduce to supersymmetric Wilson lines in the boundary M.

From this point of view one should expect $\mathbb{S}[L]$ to obey the skein relations of analytically continued Chern-Simons theory. We formulate this as the conjecture that up to Q-exact

JHEP09(2020)153

deformations, $\mathbb{S}[L]$ is determined by the class of L in the *skein module* $\mathrm{Sk}(M, \mathfrak{gl}(N))$, described explicitly in section 3.1 below. This sort of skein relation in supersymmetric field theory has been discussed in many different contexts, e.g. [3, 10, 11, 17–19]. Similarly we propose that the IR defect $\widetilde{\mathbb{S}}[\widetilde{L}]$ depends only on the class of $\widetilde{L}$ in another skein module $\mathrm{Sk}(\widetilde{M}, \mathfrak{gl}(1))$, described in section 3.2.

The UV-IR decomposition takes Q-exact deformations in the UV to Q-exact deformations in the IR. It follows that it should descend to a map of skein modules,

$$F : \mathrm{Sk}(M, \mathfrak{gl}(N)) \to \mathrm{Sk}(\widetilde{M}, \mathfrak{gl}(1)). \tag{1.6}$$

This is a strong constraint, which in particular is strong enough to determine all the weight factors $\alpha(\widetilde{L})$. In section 7 we verify that our rules indeed satisfy this constraint in the $N = 2$ case. In case $M = C \times \mathbb{R}$, the skein modules are actually algebras, because of the operation of "stacking" links in the $\mathbb{R}$ direction (see section 3.3); this algebra structure gets related to the OPEs of the operators $\mathbb{S}[L]$ or $\mathbb{S}[\widetilde{L}]$, and F is then a homomorphism of algebras.

We should mention one subtlety we have been ignoring: the skein modules we consider involve *framed* links. The need to frame links, though familiar for Wilson lines in Chern-Simons theory, is not immediately obvious from the point of view of the theory $\mathfrak{X}[\mathfrak{gl}(N)]$. Nevertheless, it seems that they do need framing, and that shifting the framing in the $\mathfrak{gl}(N)$ theory by 1 unit is equivalent to changing the angular momentum of the defect in the x^4-x^5 direction by N units. It would be desirable to understand this in a more fundamental way.

1.5 Framed BPS state counting

In this subsection we discuss one application of the UV-IR map: it can be used to compute the spectrum of ground states of the bulk-defect system. This point of view unifies the computation of link polynomials and that of framed BPS states in 4d class S theories. When we say "framed BPS state" we also include states associated to a slightly unfamiliar sort of line defect which breaks rotation invariance; we call these "fat line defects" and discuss them in section 1.5.3 below.

1.5.1 Links in $\mathbb{R}^3$

The simplest case arises when we take

$$M = \mathbb{R}^3, \tag{1.7}$$

i.e. we consider $\mathfrak{X}[\mathfrak{gl}(N)]$ in the spacetime $\mathbb{R}^{5,1}$. This theory has 16 supercharges. For generic L, the defect $\mathbb{S}[L]$ preserves 2 of these supercharges [20]. The setup also preserves a rotational $\mathrm{U}(1)_P$ in the x^4-x^5 plane and a $\mathrm{U}(1)_R$ symmetry.

Now we make a "Coulomb branch" perturbation $\widetilde{M}$ as mentioned above. The ground states of the system form a vector space depending on the link L and the perturbation $\widetilde{M}$, which we call $\mathcal{H}_L(\widetilde{M})$. $\mathcal{H}_L(\widetilde{M})$ is a representation of $\mathrm{U}(1)_P \times \mathrm{U}(1)_R$.

It was proposed in [4, 5] following [7] that $\mathcal{H}_L(\widetilde{M})$ is a homological invariant of the link L, likely closely related to the *Khovanov-Rozansky homology*. The action of $\mathrm{U}(1)_P \times \mathrm{U}(1)_R$ is responsible for the bigrading of the link homology. In particular, suppose we let J_3

JHEP09(2020)153

denote the generator of $\mathrm{U}(1)_P$, and I_3 the generator of $\mathrm{U}(1)_R$. Then the proposal of [4, 5] implies that the generating function

$$\overline{\Omega}(L,\widetilde{M}) := \mathrm{Tr}_{\mathcal{H}_L(\widetilde{M})}(-q)^{2J_3}q^{2I_3} \in \mathbb{Z}[q,q^{-1}], \tag{1.8}$$

is related to the (un-normalized) HOMFLY polynomial $P_{\mathrm{HOMFLY}}(L)$. In our conventions the precise relation is

$$\overline{\Omega}(L,\widetilde{M}) = q^{Nw(L)}P_{\mathrm{HOMFLY}}(L, a=q^N, z=q-q^{-1}) \tag{1.9}$$

where $w(L)$ is the self-linking number of L. (In particular, this generating function is actually independent of the chosen perturbation $\widetilde{M}$, although *a priori* it might have depended on it.)

The generating function $\overline{\Omega}(L,\widetilde{M})$ can also be computed using the IR description of the theory. Indeed the IR skein module $\mathrm{Sk}(\widetilde{M},\mathfrak{gl}(1))$ is easy to understand: every $\widetilde{L}$ is equivalent to the class of some multiple of the empty link $[\cdot]$. It is not completely obvious what the contribution from the empty link to $\overline{\Omega}(L,\widetilde{M})$ should be (this amounts to counting the ground states of the system without a defect), but we propose that this contribution is just 1, and thus that

$$F([L]) = \overline{\Omega}(L,\widetilde{M})[\cdot]. \tag{1.10}$$

Thus, in this particular case, the UV-IR map described in section 1.2 must reduce to a method of computing the knot polynomial (1.9). We discuss this more in section 2 below.

1.5.2 Flat links in $C \times \mathbb{R}$

Now we consider the case

$$M = C \times \mathbb{R} \tag{1.11}$$

where C is a Riemann surface (perhaps with marked points.) In this case we take a twisted version of $\mathfrak{X}[\mathfrak{gl}(N)]$ in the spacetime $C \times \mathbb{R}^{3,1}$. This kind of twist was used in [14, 21]; it preserves 8 supercharges. If C is compact, then on flowing to the IR one arrives at an $\mathcal{N}=2$ theory of class S in $\mathbb{R}^{3,1}$; we denote this theory $\mathfrak{X}[C,\mathfrak{gl}(N)]$.

We are going to consider a link $L \subset M$ and a surface defect $\mathbb{S}[L]$. We fix a branched holomorphic N-fold covering $\widetilde{C} \to C$, where $\widetilde{C} \subset T^*C$. (Such a covering $\widetilde{C}$ is also a Seiberg-Witten curve, associated to a point of the Coulomb branch of the theory $\mathfrak{X}[C,\mathfrak{gl}(N)]$, as described in [14].) Then we define

$$\widetilde{M} = \widetilde{C} \times \mathbb{R}. \tag{1.12}$$

The symmetries preserved by the defect $\mathbb{S}[L]$ depend on how L is placed. In this section we consider the following: pick a simple closed curve $\wp \subset C$ and then take

$$L = \wp \times \{x^3 = 0\}. \tag{1.13}$$

We call such an L "flat" since it explores only 2 of the 3 dimensions of M. The remaining x^3-direction combines with the x^4-x^5 plane to give an $\mathbb{R}^3$, in which $\mathbb{S}[L]$ sits at the origin; thus in this setup we have 3-dimensional rotation invariance $\mathrm{SU}(2)_P$, and it turns out to also preserve R-symmetry $\mathrm{SU}(2)_R$, and 4 supercharges.

JHEP09(2020)153

For C compact and L flat, from the point of view of the reduced theory $\mathfrak{X}[C, \mathfrak{gl}(N)]$, $\mathbb{S}[L]$ is a $\frac{1}{2}$-BPS line defect. These line defects have been studied extensively, beginning with [9–11].[1] In particular, the vector space $\mathcal{H}_L(\widetilde{M})$ of ground states has been studied, e.g. in [2, 3, 11, 12]; it is called the space of *framed BPS states* of the line defect.[2]

$\mathcal{H}_L(\widetilde{M})$ admits a grading:

$$\mathcal{H}_L(\widetilde{M}) = \bigoplus_{\gamma \in \Gamma(\widetilde{M})} \mathcal{H}_{L,\gamma}(\widetilde{M}) \tag{1.14}$$

where $\Gamma(\widetilde{M}) = H_1(\widetilde{M}, \mathbb{Z})$ is the IR charge lattice of the four-dimensional theory $\mathfrak{X}[C, \mathfrak{gl}(N)]$, in the vacuum labeled by the covering $\widetilde{M}$. The grading by $\Gamma(\widetilde{M})$ keeps track of electromagnetic and flavor charges of the framed BPS states. Each $\mathcal{H}_{L,\gamma}(\widetilde{M})$ is a representation of $\mathrm{SU}(2)_P \times \mathrm{SU}(2)_R$.

Now fix Cartan generators J_3, I_3 of $\mathrm{SU}(2)_P$ and $\mathrm{SU}(2)_R$ respectively. Then we can consider the *protected spin character*[3]

$$\overline{\Omega}(L, \widetilde{M}, \gamma) := \mathrm{Tr}_{\mathcal{H}_{L,\gamma}(\widetilde{M})}(-q)^{2J_3} q^{2I_3} \in \mathbb{Z}[q, q^{-1}]. \tag{1.15}$$

Unlike the case of $M = \mathbb{R}^3$, here $\mathcal{H}_L(\widetilde{M})$ does depend strongly on $\widetilde{M}$; as we vary $\widetilde{M}$ (moving in the Coulomb branch) the invariants $\overline{\Omega}(L, \widetilde{M}, \gamma)$ can change. This is the phenomenon of *framed wall-crossing*. (We discuss this phenomenon in more detail in section 8, where we show that our map F obeys the expected framed wall-crossing formulas associated to BPS hypermultiplets and vector multiplets.)

Once again, we can compute the invariants $\overline{\Omega}(L, \widetilde{M}, \gamma)$ using the IR description of the theory on its Coulomb branch. In this case the IR skein module $\mathrm{Sk}(\widetilde{M}, \mathfrak{gl}(1))$ is more interesting: it has one generator X_γ for each class $\gamma \in H_1(\widetilde{C}, \mathbb{Z})$. Roughly speaking X_γ is just represented by a loop on $\widetilde{C}$ in class γ; see section 3.5 for the precise statement. A link in class X_γ gives an IR line defect carrying charge γ, which contributes one state to $\mathcal{H}_{L,\gamma}(\widetilde{M})$. This leads to the proposal

$$F([L]) = \sum_{\gamma \in H_1(\widetilde{C}, \mathbb{Z})} \overline{\Omega}(L, \widetilde{M}, \gamma) X_\gamma, \tag{1.16}$$

i.e., q-nonabelianization gives the generating function of the protected spin characters.

1.5.3 Non-flat links in $C \times \mathbb{R}$

Continuing with the case $M = C \times \mathbb{R}$, now we consider a more general link $L \subset M$. In this case we only have 2-dimensional rotation invariance $\mathrm{U}(1)_P$ (in the x^4-x^5 plane), and $\mathrm{U}(1)_R$, and 2 supercharges. From the point of view of symmetries, this is the same as the case of general links in $M = \mathbb{R}^3$ which we considered in section 1.5.1.

[1] More exactly, those works considered the case where the simple closed curve $\wp$ is not contractible. The case of contractible $\wp$ turns out to be a bit special, as we will see below.

[2] The "framed" in "framed BPS states" is not directly related to the framing of links; we will discuss the role of framing of links below.

[3] In comparing to [11] we have $q_{\text{here}} = -y_{\text{there}}$.

JHEP09(2020)153

What does the defect $\mathbb{S}[L]$ look like from the point of view of the reduced theory $\mathfrak{X}[C, \mathfrak{gl}(N)]$? In the IR, the position variations of the defect in the x^3 direction are suppressed, so the effective support of the defect in the spatial $\mathbb{R}^3$ is a point. Thus we obtain a $\frac{1}{4}$-BPS line defect in the theory $\mathfrak{X}[C, \mathfrak{gl}(N)]$.

If L is isotopic to a flat link, then we expect that this defect is actually $\frac{1}{2}$-BPS in the IR, and all the IR physics should be the same as in section 1.5.2. If L is not isotopic to a flat link, though, then the line defect we get is really only $\frac{1}{4}$-BPS. Moreover, in the UV the $\frac{1}{4}$-BPS defect breaks the rotational symmetry $\mathrm{SU}(2)_P$ to the $\mathrm{U}(1)_P$ rotation in the x^4-x^5 plane, and the full $\mathrm{SU}(2)_P$ need not be restored in the IR. Thus we expect that a general link $L \subset C \times \mathbb{R}$ corresponds to an unconventional sort of line defect in theory $\mathfrak{X}[C, \mathfrak{gl}(N)]$, which partially breaks rotation invariance in the spatial $\mathbb{R}^3$. We call these *fat line defects*.

As for a $\frac{1}{2}$-BPS line defect, we can consider a protected spin character $\underline{\Omega}(L, \widetilde{M}, \gamma) \in \mathbb{Z}[q, q^{-1}]$ for a fat line defect; it is defined by exactly the same equation (1.15) which we used before, with J_3 and I_3 the generators of $\mathrm{U}(1)_P$ and $\mathrm{U}(1)_R$. We propose that this protected spin character is also computed by q-nonabelianization, just as in (1.16) above.

1.5.4 Positivity

It was conjectured in [11] that, when L is flat and not contractible, the action of $\mathrm{SU}(2)_R$ on $\mathcal{H}_L$ is trivial; this is the "framed no-exotics" conjecture.[4] If the framed no-exotics conjecture is true, then when L is flat, (1.15) reduces to the simpler

$$\underline{\Omega}(L, \widetilde{M}, \gamma) := \mathrm{Tr}_{\mathcal{H}_{L,\gamma}(\widetilde{M})}(-q)^{2J_3}. \tag{1.17}$$

This would imply that the coefficients in the $(-q)$-expansion of $\underline{\Omega}(L, \widetilde{M}, \gamma)$ are all positive, and moreover they have symmetry and monotonicity properties following from the fact that they give a character of the full $\mathrm{SU}(2)_P$, not only of $\mathrm{U}(1)_P$.

For $N = 2$ the expected positivity has been established in [23, 24], for the version of F given in [1]. The expected monotonicity property has not been proven as far as we know.[5] We will see in various examples below that the coefficients in $\underline{\Omega}(L, \widetilde{M}, \gamma)$ computed from our F do have the expected properties; it would be very interesting to give a proof directly from our construction of F.

In contrast, for non-flat links L there is no reason to expect any kind of positivity property (and indeed, for a link contained in a ball in M we get the polynomial (1.9), which is in general not sign-definite.) Likewise when L is contractible we do not necessarily expect positivity, and indeed for a small unknot in M (even a flat one) we will get $F(L) = q + q^{-1}$, which does not have a positive expansion in $-q$.

1.6 Connections and future problems

1. In the language of theory $\mathfrak{X}[\mathfrak{gl}(N)]$, our UV-IR map can be interpreted roughly as follows. The direct lifts of L to $\widetilde{M}$ come from the usual symmetry-breaking phe-

[4] There is an analogous no-exotics conjecture for bulk BPS states. Important progress towards fully proving the no-exotics conjectures via physical arguments has been made by Clay Córdova and Thomas Dumitrescu [22].

[5] We thank Dylan Allegretti for several useful explanations about this.

JHEP09(2020)153

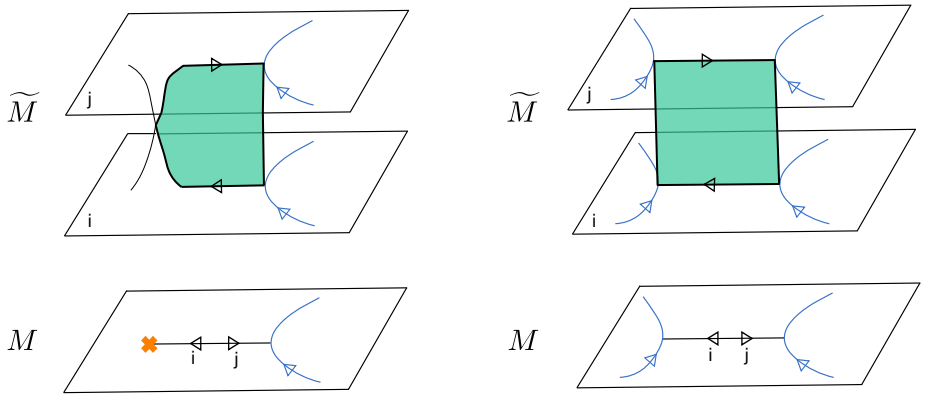

Figure 1. The interpretation of detour (left) and exchange (right) as M2-branes in T^*M bounded by $\widetilde{M}$ and the conormal to L.

nomenon: moving to the Coulomb branch breaks the symmetry locally from $\mathfrak{gl}(N)$ to its Cartan subalgebra of diagonal matrices, and correspondingly decomposes the fundamental representation of $\mathfrak{gl}(N)$ into N one-dimensional weight spaces. The terms involving webs are contributions from massive BPS strings of theory $\mathfrak{X}[\mathfrak{gl}(N)]$ on its Coulomb branch. In particular, a physical interpretation of the exchange factor for $N = 2$ has been given in [4]. Moreover its categorification in terms of knot homology was studied in [25]. We hope that similar interpretations also exist for generic web factors.

2. In the language of the M-theory construction of $\mathfrak{X}[\mathfrak{gl}(N)]$, compactifying the time direction to S^1 to compute the BPS indices could optimistically be understood as computing a partition function in Type IIA string theory on T^*M, with N D6-branes inserted on the zero section $M \subset T^*M$, and D4-branes placed on the conormal bundle to L in T^*M. Adding the parameter q would be implemented by making a rotation in the x^4-x^5 plane as we go around the S^1; from the Type IIA point of view this corresponds to activating a graviphoton background. Such a partition function is computed by the A model topological string on T^*M, with Lagrangian boundary conditions at the D-brane insertions, with string coupling g_s where $q = \mathrm{e}^{-g_s}$ [6].

   In this language the webs are interpreted as M2-branes in T^*M whose boundary lies partly on $\widetilde{M}$ and partly on the conormal to L. For $N = 2$ this is indicated in figure 1.

3. In the topological string approach to link invariants pioneered in [6], one takes the above setup with $M = S^3$, but then passes through the conifold transition. After the conifold transition we do not have the N D6-branes anymore, but we do have a compact holomorphic 2-cycle with volume Ng_s. In consequence, this sort of computation involves the variable N only through the combination $a = \mathrm{e}^{-Ng_s} = q^N$; so for example one gets the HOMFLY polynomial directly as a function of a, rather than its specialization (1.9) to a particular N. Recently this open topological string computation has been interpreted in the language of skein modules [26]. We want to emphasize that our computation is on the other side, "before" the conifold transition.

JHEP09(2020)153

4. We discuss in this paper mainly the cases $M = \mathbb{R}^3$ and $M = C \times \mathbb{R}$. Having come this far, it is natural to consider the case of a general 3-manifold M. There is a twist of $\mathfrak{X}[\mathfrak{gl}(N)]$ on $M \times \mathbb{R}^{2,1}$ which preserves 4 supercharges. If M is compact, then on flowing to the IR one arrives at a theory $\mathfrak{X}[M, \mathfrak{gl}(N)]$ in $\mathbb{R}^{2,1}$; examples of these theories have been studied e.g. in [13, 15, 27]. The surface defect $\mathbb{S}[L]$ gives in the IR a $\frac{1}{2}$-BPS line defect in theory $\mathfrak{X}[M, \mathfrak{gl}(N)]$.

   As before we could imagine perturbing the theory to reach a "Coulomb branch" using an N-fold covering $\widetilde{M} \to M$. Unlike the cases we have discussed up to now, though, here we do not have a good understanding of the IR physics. In particular, it is not clear to us that we can define a meaningful ground state Hilbert space $\mathcal{H}_L(\widetilde{M})$ in this case. Nevertheless, we could still think about the IR decomposition of line defects, and the corresponding map of skein modules. We believe that the same rules we use in this paper (in their covariant incarnation, section 6) will work for more general M, but there is a subtlety in formulating the skein module $\mathrm{Sk}(\widetilde{M}, \mathfrak{gl}(1))$ in this case: one needs to include corrections from boundaries of holomorphic discs in $T^*\widetilde{M}$. The $q = 1$ version of this problem will be treated in [28]; the case of general q is ongoing work.

5. One way of thinking of the skein modules is that they describe relations obeyed by Wilson lines in Chern-Simons theory. With that in mind, our q-nonabelianization map could be interpreted as part of a general relation between $\mathrm{GL}(N)$ Chern-Simons theory on M and $\mathrm{GL}(1)$ Chern-Simons theory on $\widetilde{M}$, with the latter corrected by holomorphic discs — or more succinctly, as a relation between the A model topological string on T^*M with N D-branes on M and the A model topological string on T^*M with 1 D-brane on $\widetilde{M}$. The possibility of such a relation was proposed in [2, 16]. Its avatar in classical Chern-Simons theory will appear in [28]. The existence of a relation between local systems on M and A branes in T^*M is also known in the mathematics literature, e.g. [29–31].

6. Quantization of character varieties, skein modules and skein algebras have recently been very fruitfully investigated from the point of view of topological field theory [32–35]. Roughly speaking, the underlying idea is that an appropriate version of the $\mathfrak{gl}(N)$ skein module of M can be identified with the space of states of a topologically twisted version of $\mathcal{N} = 4$ super Yang-Mills theory on $M \times \mathbb{R}$ with gauge group $\mathrm{U}(N)$. It seems natural to ask whether q-nonabelianization can be understood profitably in this language.[6]

7. As we have mentioned, the map F of skein modules which we construct for $N = 2$ in this paper closely resembles the "quantum trace" map constructed first in [1] and revisited in [3]. Our map cannot be precisely the same as the map considered there, if only because the relevant skein modules are different: ultimately this is related to the fact that we consider the $\mathfrak{gl}(2)$ theory while those references consider $\mathfrak{sl}(2)$.

[6] This perspective was emphasized to us by Davide Gaiotto and David Jordan.

JHEP09(2020)153

We believe that after appropriately decoupling the central $\mathfrak{gl}(1)$ factor, the maps are likely the same; we discuss this point a bit more in section 9.

Our map is also closely related to the computation of framed BPS states for certain interfaces between surface defects given in [2]; in particular, the writhe used in [2] is essentially the same as the power of q which appears in relating a class $[\widetilde{L}] \in \mathrm{Sk}(\widetilde{M}, \mathfrak{gl}(1))$ to a quantum torus generator X_γ, as described in section 3.5.

Nevertheless, our way of producing F looks quite different from the constructions in [1–3], and has some advantages: it is more local, it can be covariantly formulated on a general M, it does not require us to make a large isotopy of the link L to put it in some special position, and it makes the connections to the strings of the theory $\mathfrak{X}[\mathfrak{gl}(N)]$ or to holomorphic discs more manifest. We expect that these advantages will be useful for further developments. (In particular, for $N > 2$ our approach here is well suited for dealing with the case of theories $\mathfrak{X}[C, \mathfrak{gl}(N)]$ at general points of their Coulomb branch, involving more general spectral networks than the "Fock-Goncharov" type considered in [3].)

8. In this paper we compute indexed dimensions of spaces $\mathcal{H}_L(\widetilde{M})$ of framed BPS states. It would be very interesting to try to promote our construction to get the actual vector spaces $\mathcal{H}_L(\widetilde{M})$, with their bigrading by $\mathrm{U}(1)_P \times \mathrm{U}(1)_R$. When $M = \mathbb{R}^3$ this is expected to give some relative of the Khovanov-Rozansky homology as discussed e.g. in [4, 5, 7, 25, 36].

9. At least for flat links in $C \times \mathbb{R}$, there is also an algebraic approach to studying the framed BPS states. In [37–39] it was proposed that for theories of *quiver type* as studied in [40–46], framed BPS spectra of line defects could be computed by methods of quiver quantum mechanics. More recently this idea has been further developed in [47–50]. It would be nice to understand better the connection between this algebraic method and our geometric approach. One possibility might be to compare the method of *BPS graphs* as in [19, 51, 52] to the framed BPS quivers.

10. As we have mentioned, when $M = C \times \mathbb{R}$ our q-nonabelianization map is closely connected to the quantum trace of [1]. For other aspects of the quantum trace see e.g. [23, 24, 53–56]. It is also closely related to the quantum cluster structure on moduli spaces of flat connections, discussed in [57–59]; for some choices of the covering $\widetilde{C} \to C$, we expect that the formula (1.16) gives the expansion of a distinguished element $F([L])$ of the quantum cluster algebra, relative to the variables X_γ of a particular cluster determined by $\widetilde{C}$.

2 The state sum model revisited

We begin with the simplest case of our story. As we have discussed above, when $M = \mathbb{R}^3$, q-nonabelianization should boil down to a way of computing the specialization (1.9) of the HOMFLY polynomial.

JHEP09(2020)153

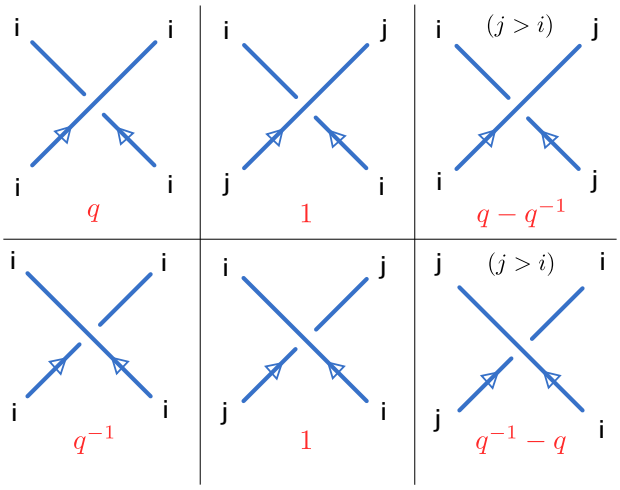

Figure 2. Multiplicative weights in the state sum model, associated to labeled crossings in a knot diagram.

The precise way in which this works depends on the shape of the covering $\widetilde{M} \to M$. If $\widetilde{M}$ is given by N constant 1-forms λ_i which are all nearly parallel, then q-nonabelianization is essentially equivalent to a known method of computing (1.9), known as the *state sum model*. In this section we first review the state sum model and then describe the ways in which q-nonabelianization generalizes it.

2.1 The state sum model

Choose a distinguished axis in $\mathbb{R}^3$, say the x^3-axis. This induces a projection $\mathbb{R}^3 \to \mathbb{R}^2$. We assume that L is in general position relative to this projection; if not, make a small isotopy so that it is. Then the projection induces an oriented knot diagram in $\mathbb{R}^2$.

A *labeling* ℓ of the knot diagram consists of an assignment of a label $i \in \{1, \dots, N\}$ to each arc. The state sum is a sum over all labelings. Each labeling ℓ is assigned a weight $\alpha(\ell) \in \mathbb{Z}[q, q^{-1}]$ according to the following rules:

- Each crossing gives a factor depending on the labels of the four involved arcs, as indicated in figure 2. If the labels at any crossing are not of one of the types shown in the figure, then the factor for that crossing is 0 (and thus $\alpha(\ell) = 0$).
- If the diagram includes crossings where the labels change, we "resolve" the crossings as shown in figure 3. After so doing, the diagram consists of loops, each carrying a fixed label i. We assign each such loop a factor $q^{w(N+1-2i)}$, where w is the winding number of the projection of the loop to $\mathbb{R}^2$ (so e.g. for a small counterclockwise loop the winding number is $+1$).[7]

[7] Our description of this factor is a bit different from what usually appears in the literature. One could equivalently define this factor by first making the stipulation that whenever there is a crossing, the orientations of both arcs in the crossing should have the same sign for their y-component (both up or both down), and then assigning factors $q^{\pm\frac{1}{2}(N-1-2i)}$ to local maxima and minima of y along arcs; these locations are sometimes called "cups" and "caps" in the knot diagram.

JHEP09(2020)153

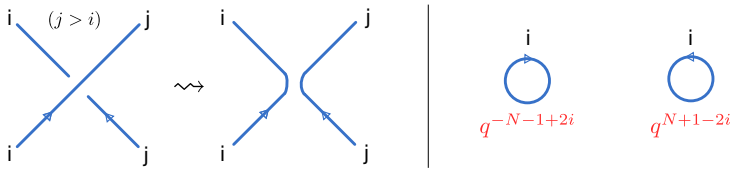

Figure 3. Left: resolving a labeled knot diagram. Right: multiplicative weights associated to winding of loops.

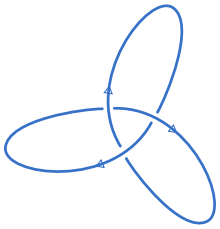

Figure 4. A diagram for the left-handed trefoil.

Then, the state sum formula is

$$\sum_{\ell} \alpha(\ell) = q^{Nw(L)} P_{\text{HOMFLY}}(L, a = q^N, z = q - q^{-1}), \tag{2.1}$$

where $w(L)$ is the writhe of the knot diagram (ie the number of overcrossings minus the number of undercrossings.)

Let us illustrate (2.1) with a few examples:

- The most trivial example is the unknot, placed in $\mathbb{R}^3$ so that its projection to $\mathbb{R}^2$ is a circle. The HOMFLY polynomial for this knot is

  $$P_{\text{HOMFLY}}(L, a, z) = z^{-1}(a - a^{-1}). \tag{2.2}$$

  Since the diagram has only one arc, the state sum model just sums over the N possible labels for that arc. Since there are no crossings, the weight $\alpha(\ell)$ reduces to the winding factor, giving

  $$\sum_{\ell} \alpha(\ell) = \sum_{i=1}^{N} q^{N+1-2i} = \frac{q^N - q^{-N}}{q - q^{-1}} = P_{\text{HOMFLY}}(L, a = q^N, z = q - q^{-1}) \tag{2.3}$$

  as desired.

- As a more interesting example, suppose we take L to be the left-handed trefoil, placed in $\mathbb{R}^3$ so that its projection to $\mathbb{R}^2$ is the diagram in figure 4.

  The HOMFLY polynomial for this knot is

  $$P_{\text{HOMFLY}}(L, a, z) = z^{-1}(a - a^{-1})(-a^4 + a^2 z^2 + 2a^2). \tag{2.4}$$

  Let us see how the state sum model reproduces this formula. The knot diagram in figure 4 has 6 arcs; thus the state sum model involves a sum over N^6 different arc label assignments ℓ. The ℓ for which $\alpha(\ell) \neq 0$ fall into five classes, as shown below:

JHEP09(2020)153

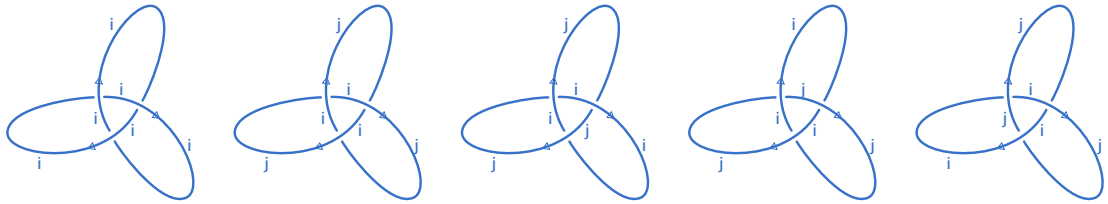

Figure 5. Arc labelings ℓ for which $\alpha(\ell) \neq 0$. The labels $i, j \in \{1, \dots, N\}$ and $j > i$.

Applying the state sum model rules, we obtain

$$\begin{aligned}\sum_{\ell} \alpha(\ell) &= q^{-3} \sum_{i=1}^{N} q^{-2N-2+4i} + \Big((q^{-1}-q)^3 + 3(q^{-1}-q)\Big) \sum_{1\le i<j\le N} q^{-2N-2+2i+2j} \\ &= q^{-3N} \frac{q^N - q^{-N}}{q-q^{-1}} \Big(-q^{4N} + q^{-2+2N} + q^{2+2N} \Big) \\ &= q^{-3N} P_{\text{HOMFLY}}(L, a = q^N, z = q - q^{-1})\end{aligned}$$

This matches (2.1) as desired, since the writhe of the diagram in figure 4 is $w = -3$.

2.2 Reinterpreting the state sum model

With an eye toward generalization, we now slightly reinterpret the state sum rules.

We think of the index i as labeling the i-th sheet of a trivial N-fold covering

$$\widetilde{M} \to M, \qquad M = \mathbb{R}^3, \qquad \widetilde{M} = \sqcup_{i=1}^{N} \mathbb{R}^3. \tag{2.5}$$

Each arc labeling ℓ with $\alpha(\ell) \neq 0$ gets interpreted as representing some link $\widetilde{L}$ in $\widetilde{M}$. If an arc in L is labeled i, it means $\widetilde{L}$ contains the lift of that arc to the i-th sheet in $\widetilde{M}$.

The simplest situation arises when all arcs in L carry the same label i: then $\widetilde{L}$ is just the lift of L to the i-th sheet. More generally, if the labels of the arcs change at the crossings, simply taking the lift of each arc would not give a closed link on $\widetilde{M}$. At such a crossing involving labels i and j, we insert two segments, traveling along the z-direction on sheets i and j in opposite directions, to close up the link, as shown in figure 3. We call this pair of segments an *exchange*. The resulting $\widetilde{L}$ is a disjoint union of closed links on various sheets of $\widetilde{M}$.

Now we reinterpret the weight factor $\alpha(\ell)$ in terms of the link $\widetilde{L}$:

- The weights $q^{\pm 1}$ assigned to crossings where all arc labels are the same give altogether $q^{\sum_{i=1}^{N} n_i}$, where n_i is the self-linking number of the part of $\widetilde{L}$ on sheet i. This factor can be understood as using the relations in $\mathrm{Sk}(\widetilde{M}, \mathfrak{gl}(1))$ to express $\widetilde{L}$ as a multiple of the empty link: $[\widetilde{L}] = q^{\sum_{i=1}^{N} n_i} [\cdot]$.

- The weights $\pm(q - q^{-1})$ assigned to crossings where the arc labels change are interpreted as universal factors associated to exchanges in $\widetilde{L}$.

- The winding factors $q^{w(N+1-2i)}$ can be interpreted as follows: for a loop of $\widetilde{L}$ on sheet i, we include a factor q^w for each $j > i$, and a factor q^{-w} for each $j < i$.

JHEP09(2020)153

2.3 q-nonabelianization as a generalization

The q-nonabelianization map can be thought of as a generalization of the state sum model. Some of the key elements are:

- The trivial covering of $\mathbb{R}^3$ given in (2.5) above is replaced by the (in general nontrivial) branched covering $\widetilde{M} \to M$, with $\widetilde{M} \subset T^*M$. The labels $i = 1, \dots, N$ which we used above are replaced by local choices of a sheet of this covering over a patch of M.

- The single projection $\mathbb{R}^3 \to \mathbb{R}^2$ along the z-axis is replaced by many different projections, along the leaves of $\binom{N}{2}$ different locally defined foliations of M, labeled by pairs of sheets ij. The directions of the different projections are determined by the 1-forms $\lambda_i - \lambda_j$. To define the winding factor for an arc on sheet i, we sum the winding of $N-1$ different projections of the arc to the leaf spaces of the $N-1$ ij-foliations. (In the case of the state sum model all of the foliations coincide, and so all of the projections also coincide, but the leaf space $\mathbb{R}^2$ gets a different orientation depending on whether $i > j$ or $i < j$; this recovers the recipe above.)

- Instead of simple exchanges built from segments traveling along the z-axis, we have to consider more general webs built out of segments of leaves of the $\binom{N}{2}$ foliations. Each end of each segment lies either on the link L, on the branch locus of $\widetilde{M} \to M$, or at a trivalent junction between three segments. Each such web comes with a weight factor generalizing the $\pm(q - q^{-1})$ we had above.

Even when $M = \mathbb{R}^3$, we can take $\widetilde{M}$ to be a general branched cover, and then q-nonabelianization looks quite different from the state sum model, involving sums over various sorts of webs; nevertheless it still computes (1.9) in the end. We will show how this works in a few examples in section 4.3 and section 5.1 below.

3 Skein modules

3.1 The $\mathfrak{gl}(N)$ skein module

Fix an oriented 3-manifold M. The $\mathfrak{gl}(N)$ skein module $\mathrm{Sk}(M, \mathfrak{gl}(N))$,[8] is the free $\mathbb{Z}[q^{\pm 1}]$-module generated by ambient isotopy classes of framed oriented links in M, modulo the submodule generated by the skein relations shown in figure 6.

In each skein relation, all the terms represent links which are the same outside a ball in M, and are as pictured inside that ball, with blackboard framing. Relation (II) can be thought of as a "change of framing" relation: the two links are isotopic as unframed links, but as framed links with blackboard framing, they differ by one unit of framing.

3.2 The $\mathfrak{gl}(1)$ skein module with branch locus

Now consider an oriented 3-manifold $\widetilde{M}$ decorated by a codimension-2 locus $\mathcal{F}$. (We sometimes call $\mathcal{F}$ the *branch locus* since in our application below, $\widetilde{M}$ will be a covering

[8] The literature contains a number of variants of this skein module; the one we consider here was also considered in [26] where it is called the "U(N) HOMFLYPT skein," except that $q_{\text{here}} = q_{\text{there}}^{\frac{1}{2}}$.

JHEP09(2020)153

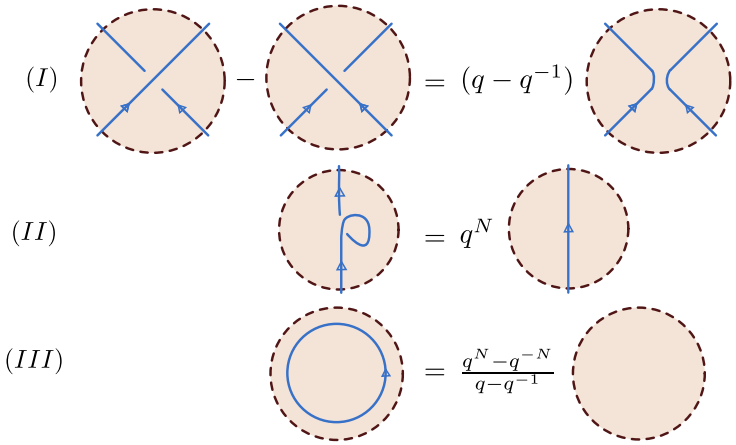

Figure 6. The skein relations defining $\mathrm{Sk}(M, \mathfrak{gl}(N))$.

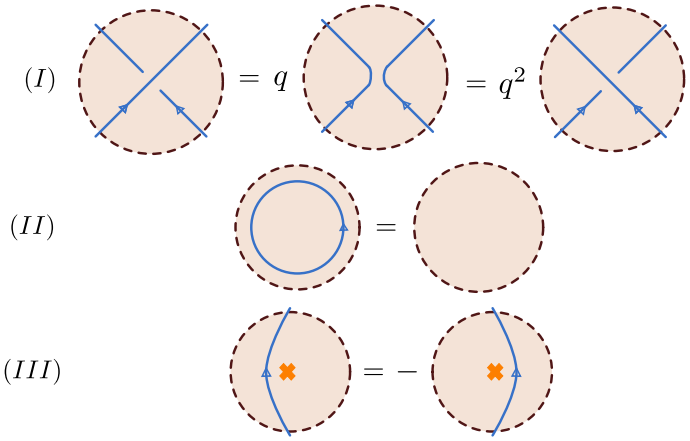

Figure 7. The skein relations defining $\mathrm{Sk}(\widetilde{M}, \mathfrak{gl}(1))$.

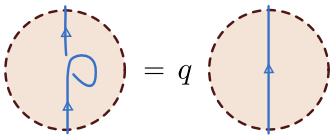

Figure 8. The change-of-framing relation in $\mathrm{Sk}(\widetilde{M}, \mathfrak{gl}(1))$.

of M, branched along $\mathcal{F}$.) The $\mathfrak{gl}(1)$ skein module with branch locus, $\mathrm{Sk}(\widetilde{M}, \mathfrak{gl}(1))$, is the free $\mathbb{Z}[q^{\pm 1}]$-module generated by ambient isotopy classes of framed oriented links in $\widetilde{M} \setminus \mathcal{F}$, modulo the submodule generated by the skein relations shown in figure 7.

In the skein relation (III) the orange cross represents the codimension-2 locus $\mathcal{F} \subset \widetilde{M}$. This skein relation says that we can isotope a link segment across $\mathcal{F}$ at the cost of a factor -1.

We remark that relations (I) and (II) imply a simple relation between links whose framings differ by one unit, parallel to what we had for $\mathfrak{gl}(N)$ above, as illustrated in figure 8.

JHEP09(2020)153

3.3 Skein algebras and their twists

Now we take $M = C \times \mathbb{R}$ and $\widetilde{M} = \widetilde{C} \times \mathbb{R}$,[9] where C and $\widetilde{C}$ are oriented surfaces. We take the orientation of M (resp. $\widetilde{M}$) to be the one induced from the orientation of C (resp. $\widetilde{C}$) and the standard orientation of $\mathbb{R}$.

In this case $\mathrm{Sk}(M, \mathfrak{gl}(N))$ and $\mathrm{Sk}(\widetilde{M}, \mathfrak{gl}(1))$ are algebras over $\mathbb{Z}[q^{\pm 1}]$, where the multiplication is given by "stacking" links along the $\mathbb{R}$ direction: $[L][L'] = [LL']$, where LL' is the link defined by superposing L' with the translation L^t of L in the positive x^3-direction, so that all points of L^t have larger $\mathbb{R}$ coordinate than all points of L'. We emphasize that this algebra structure comes from the $\mathbb{R}$ factor: for a general 3-manifold M, there is no algebra structure on $\mathrm{Sk}(M, \mathfrak{gl}(N))$.

We have to mention a little subtlety: the product structure that is most convenient for our purposes below is a *twisted* version of the usual one. Given two links L, L' in $C \times \mathbb{R}$, let $\epsilon(L, L') = \pm 1$ be the mod 2 intersection number of their projections to C. Then we define the twisted product in $\mathrm{Sk}(M, \mathfrak{gl}(N))$ by the rule

$$[L][L'] = \epsilon(L, L')[LL'] \tag{3.1}$$

and in $\mathrm{Sk}(\widetilde{M}, \mathfrak{gl}(1))$ by

$$[\widetilde{L}][\widetilde{L}'] = \epsilon(\pi(\widetilde{L}), \pi(\widetilde{L}'))[\widetilde{L}\widetilde{L}']. \tag{3.2}$$

In what follows we will only use the twisted products, not the untwisted ones. (The twisted and untwisted versions of the skein algebra are actually isomorphic, but not canonically so; to get an isomorphism between them one needs to choose a spin structure on C. For our purposes it will be more convenient not to make this choice.)

3.4 Standard framing

Another extra convenience in the case $M = C \times \mathbb{R}$ is that we have a distinguished framing available: as long as the projection of a link $L \subset M$ (resp. $\widetilde{L} \subset \widetilde{M}$) to C (resp. $\widetilde{C}$) is an immersion, we can equip the link with a framing vector pointing along the positive x^3-direction. We call this *standard framing* and will use it frequently.

3.5 The $\mathfrak{gl}(1)$ skein algebra is a quantum torus

When $\widetilde{M} = \widetilde{C} \times \mathbb{R}$ we can describe the skein algebra $\mathrm{Sk}(\widetilde{M}, \mathfrak{gl}(1))$ explicitly as follows. (Descriptions of the $\mathfrak{gl}(1)$ skein algebra similar to what follows have been used before in connection with $\mathfrak{gl}(1)$ Chern-Simons theory and BPS state counting, e.g. [2, 43, 60].)

Given any lattice Γ with a skew bilinear pairing $\langle \cdot, \cdot \rangle$, the *quantum torus* Q_Γ is a $\mathbb{Z}[q, q^{-1}]$-algebra with basis $\{X_\gamma\}_{\gamma \in \Gamma}$ and the product law

$$X_{\gamma_1} X_{\gamma_2} = (-q)^{\langle \gamma_1, \gamma_2 \rangle} X_{\gamma_1 + \gamma_2}. \tag{3.3}$$

Now let Γ be $H_1(\widetilde{C}, \mathbb{Z})$, with $\langle \cdot, \cdot \rangle$ the intersection pairing. Then, there is a canonical isomorphism

$$\iota : \mathrm{Sk}(\widetilde{M}, \mathfrak{gl}(1)) \quad \simeq \quad Q_\Gamma. \tag{3.4}$$

[9] For later convenience we sometimes call the $\mathbb{R}$-direction the "height" direction.

JHEP09(2020)153

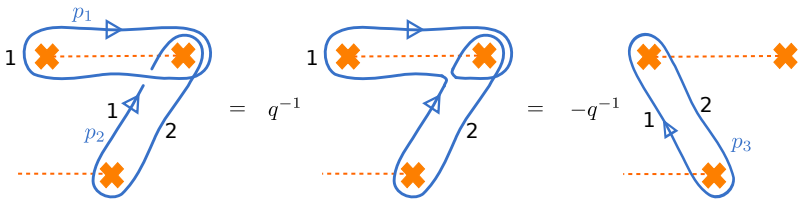

Figure 9. A sample quantum torus relation. We show a patch of $\widetilde{C}$, presented as a branched double cover of a patch of C. The covering is branched at the orange crosses, and branch cuts are shown as dashed orange segments. Labels 1 and 2 next to loop segments indicate which sheet of $\widetilde{C}$ they lie on. At a crossing between segments on the same sheet, the x^3-direction is represented as the "height" (loops which are closer to the eye are ones with a larger x^3 coordinate.) At a "non-local crossing" where two segments on different sheets of $\widetilde{C} \to C$ cross, we do not indicate the relative height.

The construction of ι is as follows. Suppose given a link $\widetilde{L}$ on $\widetilde{M}$ with standard framing. Let $n(\widetilde{L})$ be the writhe (number of overcrossings minus undercrossings) in the projection of $\widetilde{L}$ to $\widetilde{C}$, and let $n'(\widetilde{L})$ be the number of "non-local crossings" in the projection of $\widetilde{L}$ to $\widetilde{C}$: these are places which are not crossings on $\widetilde{C}$, but become crossings after further projecting from $\widetilde{C}$ to C. Then, we let

$$\iota([\widetilde{L}]) \;=\; (-1)^{n'(\widetilde{L})} q^{n(\widetilde{L})} X_{\gamma(\widetilde{L})} \tag{3.5}$$

where $\gamma(\widetilde{L}) \in H_1(\widetilde{M}, \mathbb{Z})$ is the homology class of $\widetilde{L}$.

To see that ι is really well defined, we must check that it respects the $\mathfrak{gl}(1)$ skein relations. For this the key point is that when we perturb the link $\widetilde{L}$ across a branch point we shift $n'(\widetilde{L})$ by 1, compatibly with relation (III) in figure 7.

We also need to check that ι respects the algebra structures. For this consider two loops $\widetilde{L}, \widetilde{L}'$. Let $k(\widetilde{L}, \widetilde{L}')$ be the signed number of crossings between $\widetilde{L}$ and $\widetilde{L}'$, and $k'(\widetilde{L}, \widetilde{L}')$ the number of non-local crossings. Then using the definition of ι we get directly

$$\begin{aligned}
\iota([\widetilde{L}\widetilde{L}']) &= (-1)^{n'(\widetilde{L})} q^{n(\widetilde{L})} (-1)^{n'(\widetilde{L}')} q^{n(\widetilde{L}')} (-1)^{k'(\widetilde{L},\widetilde{L}')} q^{k(\widetilde{L},\widetilde{L}')} X_{\gamma(\widetilde{L})+\gamma(\widetilde{L}')} && (3.6)\\
&= (-1)^{n'(\widetilde{L})} q^{n(\widetilde{L})} (-1)^{n'(\widetilde{L}')} q^{n(\widetilde{L}')} (-1)^{k'(\widetilde{L},\widetilde{L}')-k(\widetilde{L},\widetilde{L}')} X_{\gamma(\widetilde{L})} X_{\gamma(\widetilde{L}')} && (3.7)\\
&= (-1)^{k'(\widetilde{L},\widetilde{L}')-k(\widetilde{L},\widetilde{L}')} \iota([\widetilde{L}])\iota([\widetilde{L}']) && (3.8)\\
&= \epsilon(\pi(\widetilde{L}), \pi(\widetilde{L}'))\, \iota([\widetilde{L}])\iota([\widetilde{L}']), && (3.9)
\end{aligned}$$

so ι is indeed a homomorphism (recall the twisted algebra structure (3.2).)

For an example of a quantum torus relation see figure 9 below. The relation in $\mathrm{Sk}(\widetilde{M}, \mathfrak{gl}(1))$ shown there is

$$[p_1][p_2] = (-q^{-1})[p_3], \tag{3.10}$$

or equivalently

$$X_{\gamma_1} X_{\gamma_2} = (-q^{-1}) X_{\gamma_1+\gamma_2}, \tag{3.11}$$

matching (3.3).

JHEP09(2020)153

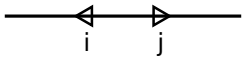

Figure 10. A leaf with its two orientations labeled.

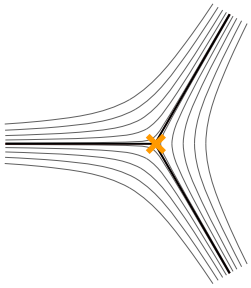

Figure 11. The local structure of the WKB foliation for $N = 2$ around a branch point. The branch point is represented by an orange cross. The dark lines represent critical leaves, while the lighter curves are generic leaves.

4 *q*-nonabelianization for $N = 2$

For the rest of this paper, we will focus on the case $N = 2$ and $M = C \times \mathbb{R}$. In this section we spell out the concrete q-nonabelianization map in this case.

4.1 WKB foliations

As we have discussed, we fix a complex structure on C and a holomorphic branched double cover $\widetilde{C} \to C$. Locally on C we then have 2 holomorphic 1-forms λ_i, corresponding to the two sheets of $\widetilde{C}$. We define a foliation of C using these one-forms: the leaves are the paths along which $\lambda_i - \lambda_j$ is real. The leaves are not naturally oriented, but if we choose one of the two sheets (say sheet i) then we get an orientation: the positive direction is the direction in which $\lambda_i - \lambda_j$ is negative; see figure 10. Thus the lift of a leaf to either sheet of $\widetilde{C}$ is naturally oriented.

At branch points of $\widetilde{C} \to C$ there is a three-pronged singularity as shown in figure 11.[10] The three leaves ending on each branch point are called *critical*.

Dividing C by the equivalence relation that identifies points lying on the same leaf, one obtains the *leaf space* of the foliation. This space is a trivalent tree, as indicated in figure 12. It will be convenient later to equip it (arbitrarily) with a Euclidean structure.

The WKB foliation of C also induces a foliation of $M = C \times \mathbb{R}$: the leaves on M are of the form $\ell \times \{x^3 = c\}$, where $\ell \subset C$ is a leaf, and c is any constant; we illustrate this in figure 13. Thus the leaf space of M is the product of a trivalent tree with $\mathbb{R}$, i.e. it is a collection of 2-dimensional "pages" glued together at 1-dimensional "binders." The leaf space inherits a natural Euclidean structure, so locally each page looks like a patch of $\mathbb{R}^2$. The pages do not carry canonical orientations, but locally choosing a sheet i induces an orientation. This induced orientation is determined by the orientation of leaves on sheet

[10] To understand this three-pronged structure note that around a branch point at $z = 0$ we have $\lambda^{(i)} - \lambda^{(j)} \sim cz^{\frac{1}{2}}\,\mathrm{d}z$, so $w^{(ij)} \sim cz^{\frac{3}{2}}$.

JHEP09(2020)153

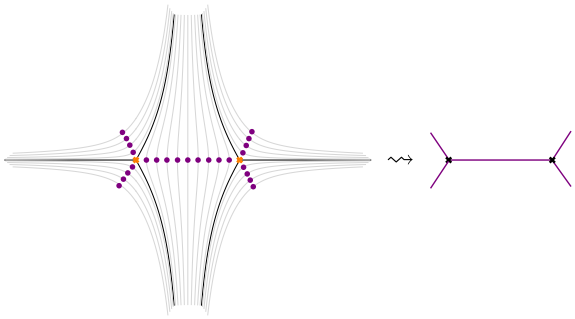

Figure 12. Left: a portion of the foliation on C. One point on each leaf is marked. Right: the corresponding portion of the leaf space, which is a trivalent tree.

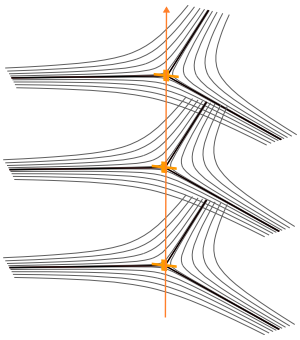

Figure 13. The local structure of the WKB foliation of $M = C \times \mathbb{R}$ for $N = 2$ around the branch locus. We explicitly show leaves at three discrete positions in the x^3-direction.

i and the ambient orientation of M: our convention is that the induced orientation is the *opposite* of the quotient orientation. Note that switching the choice of sheet reverses the leaf space orientation.

4.2 The q-nonabelianization map for $N = 2$

Now we are ready to define the q-nonabelianization map F.

Suppose given a framed oriented link L in $M = C \times \mathbb{R}$, with standard framing. Then $F([L])$ is given by

$$F([L]) = \sum_{\widetilde{L}} \alpha(\widetilde{L})[\widetilde{L}], \tag{4.1}$$

where $\widetilde{L}$ runs over all links in $\widetilde{M}$ built out of the following local constituents:

- *Direct lifts* of segments of L to $\widetilde{M}$: these are just the preimages of those strands under the covering map, as shown in figure 14.
- When a segment of L intersects a critical leaf, $\widetilde{L}$ may include a *detour* along the critical leaf, as shown in figure 15. Note that the orientation of the detour segments in $\widetilde{L}$ is constrained to match the orientations on the critical leaf; so e.g. in the situation of figure 15 we can have a detour from sheet i to sheet j, but not from sheet j to sheet i.

JHEP09(2020)153

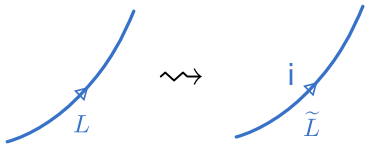

Figure 14. The direct lift of a segment of L to sheet i of the covering $\widetilde{M}$.

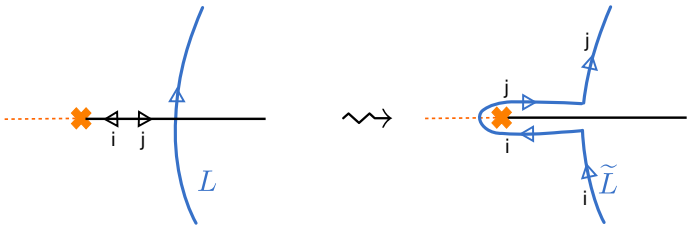

Figure 15. A detour lift of a segment of L which crosses a critical leaf.

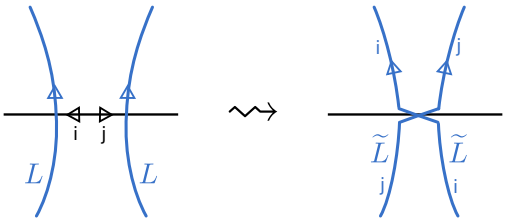

Figure 16. A lift including an exchange connecting two segments of L which cross the same ij-leaf.

- When two segments of L intersect a single ij-leaf in M, $\widetilde{L}$ can have an extra *lifted exchange* consisting of two new segments running along the lifts of the leaf to $\widetilde{M}$, as illustrated in figure 16.

  Again, the orientation of the lifted exchange in $\widetilde{L}$ is constrained to match the orientations on the ij-leaf.

We assume (by making a small perturbation if necessary) that L is sufficiently generic that detours and exchanges can only occur at finitely many places. (In particular, we always make a perturbation such that L is transverse to the "fixed height" slices $C \times \{x^3 = c\}$, since otherwise exchanges could occur in 1-parameter families instead of discretely.) Once this is done, the sum over $\widetilde{L}$ is a finite sum.

For each $\widetilde{L}$ the corresponding weight $\alpha(\widetilde{L}) \in \mathbb{Z}[q^{\pm 1}]$ is built as a product of elementary local factors, as follows:

- At every place where the projection of L onto C is tangent to a leaf, we get a contribution $q^{\pm\frac{1}{2}}$ to $\alpha(\widetilde{L})$, with the ign determined by the rules shown in figure 17. (Note that this is an overall factor, depending only on L, not on $\widetilde{L}$.)

- Each detour in $\widetilde{L}$ contributes a factor of $q^{\pm\frac{1}{2}}$ to $\alpha(\widetilde{L})$, with the sign determined by the tangent vector to L at the point where a strand of L meets the critical leaf. The factor is shown in figure 18 below.

JHEP09(2020)153

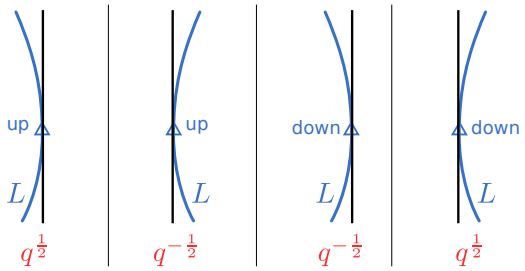

Figure 17. Framing factors contributing to the overall weight $\alpha(\widetilde{L})$. The black line denotes a leaf of the WKB foliation. Here the word "up" or "down" next to a segment of L indicates the behavior in the x^3-direction, which is not directly visible in the figure otherwise, since the figure shows the projection to C.

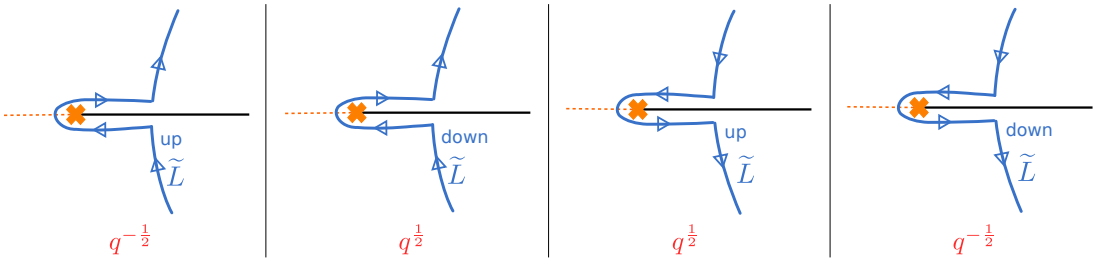

Figure 18. Detour factors contributing to the overall weight $\alpha(\widetilde{L})$. Notation is as in figure 17 above.

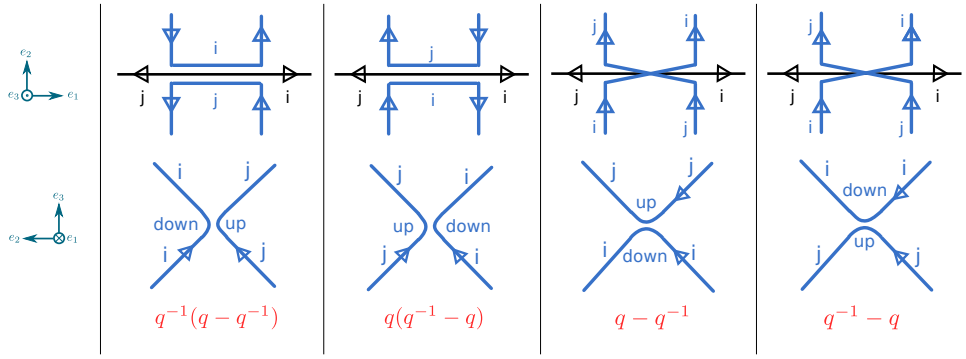

Figure 19. Exchange factors contributing to the overall weight $\alpha(\widetilde{L})$. The exchange factor depends on more data than we can represent in a single projection: we show the standard projection on top and the leaf space projection below. The picture represents $\widetilde{L}$ rather than L, so in the leaf space instead of a crossing we see its resolution. The words "up" and "down" here describe the behavior in the x^1-direction, since that is the direction not visible in the leaf space projection; hence "up" means pointing out of the paper and "down" means pointing into the paper.

- Each exchange in $\widetilde{L}$ contributes a factor to $\alpha(\widetilde{L})$. This factor depends on two things: first, it depends whether the two legs of L cross the exchange in the same direction or in opposite directions when viewed in the standard projection; second, it depends whether the crossing in the leaf space projection of L is an overcrossing or an undercrossing. See figure 19 for the factors in the four possible cases.

JHEP09(2020)153

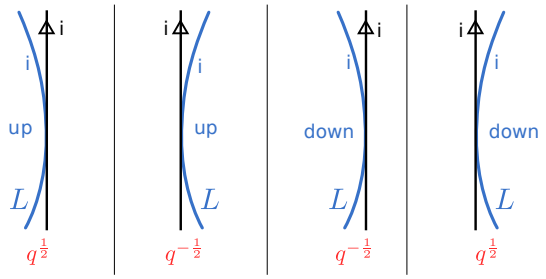

Figure 20. Factors contributing to the winding factor $q^{w(\widetilde{L})}$. The notation is as in figure 17, namely "up" and "down" refer to the tangency of L in the x^3-direction. The difference from figure 17 is that here we use the orientation of the ij-leaf and ignore that of the projection of L, while in figure 17 we used the orientation of the projection of L and ignored that of the ij-leaf.

- Finally there is a contribution from the "winding" of $\widetilde{L}$, or more precisely the winding of its projection to the leaf space of the foliation. This winding is defined as follows. Recall that the leaf space consists of "pages" each of which has a 2-dimensional Euclidean structure, glued together at 1-dimensional "binders." After perturbing $\widetilde{L}$ so that it meets each binder at a right angle, we can define a $\frac{1}{2}\mathbb{Z}$-valued winding number for the restriction of $\widetilde{L}$ to each page. (Recall that $\widetilde{L}$ is lifted to one of the two sheets of $\widetilde{M} \to M$, say sheet i, and this picks out the i-orientation on the leaf space; we use this orientation to define the winding number.) Summing up the winding of $\widetilde{L}$ on all of the pages, we get a $\mathbb{Z}$-valued total winding $w(\widetilde{L})$. We include a factor $q^{w(\widetilde{L})}$ in the weight $\alpha(\widetilde{L})$.

For practical computations, it is convenient to have a way of computing the winding factors $q^{w(\widetilde{L})}$ without explicitly drawing the leaf space projections. Here is one scheme that works. We consider all of the places where the projection of $\widetilde{L}$ to C is tangent to a leaf of the foliation.[11] For each such place we assign a factor $q^{\pm\frac{1}{2}}$ as indicated in figure 20.

Although the elementary local factors can involve half-integer powers of q, the total weight $\alpha(\widetilde{L})$ is valued in $\mathbb{Z}[q^{\pm 1}]$.

4.3 Simple unknot examples

In this section we illustrate concretely how q-nonabelianization works, in the simplest possible class of examples: we compute $F([K])$ where K is the unknot in standard framing. In this case we have $[K] = (q + q^{-1})[\cdot]$ in $\mathrm{Sk}(M, \mathfrak{gl}(2))$, and so since F factors through $\mathrm{Sk}(M, \mathfrak{gl}(2))$, the answer must be

$$F([K]) = q + q^{-1}. \tag{4.2}$$

The details of how this works out depend on what the WKB foliation of C looks like and how K is positioned relative to that foliation. In this section we describe how it works in some simple cases. We give more interesting unknot examples in section 5.1.1 below.

[11] We emphasize that we have to consider the full $\widetilde{L}$, not only the segments lifted directly from L; the winding does receive contributions from detours and exchanges.

JHEP09(2020)153

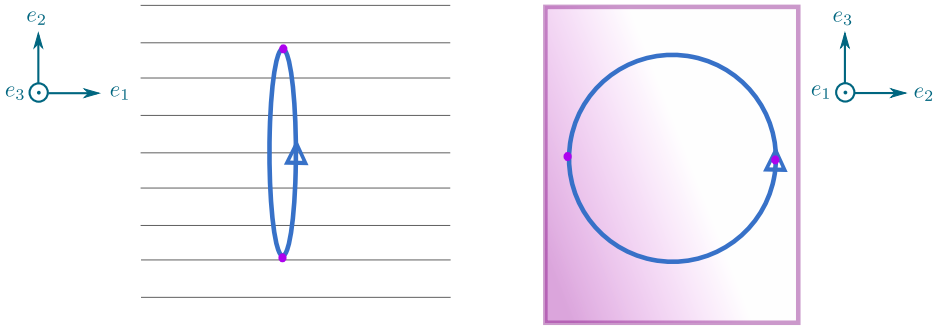

Figure 21. An unknot K. Left: the projection of K to C. The projections of leaves of the WKB foliation are shown in light gray. Right: the projection of K to the leaf space of the foliation. We use purple dots to mark the two points on K where the projection of K to C is tangent to a leaf. We will omit this information in the following figures.

lift	framing	exchange	detour	winding	[lift]	total
$\widetilde{K}_1$	1	1	1	q	1	q
$\widetilde{K}_2$	1	1	1	q^{-1}	1	q^{-1}

Table 1. Summary for the two lifts of the unknot K in figure 21.

First let us consider the case $C = \mathbb{C}$, with a trivial double covering $\widetilde{C} \to C$, for which the WKB foliation is just given by straight lines in the x^1-direction. We place the unknot K such that its projections to the x^1-x^2 plane and the x^2-x^3 plane are as shown in figure 21.

This is the simplest situation possible: there are no possible detours since the covering $\widetilde{M} \to M$ is unbranched, and there are no exchanges since each leaf meets K at most once. Thus the only contributions to $F([K])$ come from the direct lifts $\widetilde{K}_1$, $\widetilde{K}_2$ to the two sheets. Their weights are given simply by the winding factors, which are q and q^{-1} respectively, all other contributions being trivial. Finally, each lift $[\widetilde{K}_i]$ has self-linking number zero and thus is equivalent to the class $[\cdot]$ in $\mathrm{Sk}(\widetilde{M}, \mathfrak{gl}(1))$. We summarize the situation in table 1.

Thus we indeed get the expected answer (4.2). (In fact, the need to get this answer was our original motivation for including the winding factor in the q-nonabelianization map; see also [4] which includes a similar factor for a similar reason.)

Next we consider a slightly more interesting case: again we take $C = \mathbb{C}$ with a foliation by straight lines in the x^1-direction, but now take K as shown in figure 22.

In this case our path-lifting rules lead to three possible lifts:

- We could lift the whole link K to sheet 1 or sheet 2; this gives two lifts $\widetilde{K}_1$ and $\widetilde{K}_2$. Either of these lifts is contractible on $\widetilde{M}$ and has blackboard framing, so $[\widetilde{K}_1] = [\widetilde{K}_2] = [\cdot]$ in $\mathrm{Sk}(\widetilde{M}, \mathfrak{gl}(1))$. Each of these lifts has framing factor q, from the two places where the projection of K is tangent to the foliation of C. Each of these lifts has total winding zero, as we see from the leaf space projection on the right side of figure 22; thus the winding factor is trivial. (Another convenient way to count the winding is to use the rules of figure 20. The two tangencies contribute $q^{\frac{1}{2}}$ and $q^{-\frac{1}{2}}$ respectively,

JHEP09(2020)153

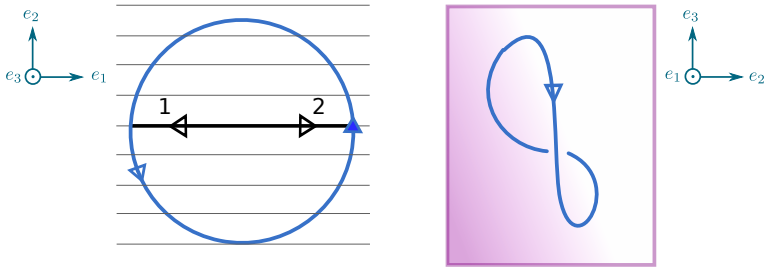

Figure 22. An unknot K. Left: the projection of K to C. The height (x^3) coordinate of K is taken as follows: as we travel counterclockwise around K the height monotonically increases, except for a small neighborhood of the filled arrow, where the height decreases. The projections of generic leaves of the WKB foliation are shown in light gray. The projection of the leaf segment along which an exchange may occur is shown in black. Right: the projection of K to the leaf space of the foliation. The position of the crossing in this projection corresponds to the location of the potential exchange.

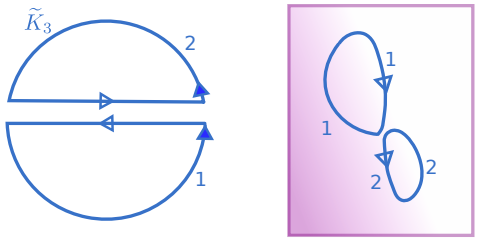

Figure 23. A lift $\widetilde{K}_3$ of K involving an exchange. Left: standard projection. Right: leaf space projection. Referring to the standard projection, the top half of K is lifted to sheet 2 of $\widetilde{M}$ while the bottom half is lifted to sheet 1. The 1-orientation of the leaf space is the standard orientation of the plane, while the 2-orientation is the opposite.

giving the total winding factor 1.) Thus these lifts have $\alpha(\widetilde{K}_1) = \alpha(\widetilde{K}_2) = q$, so they each contribute $q[\cdot]$ to $F([K])$.

- There is also a more interesting possibility shown in figure 23. Again $[\widetilde{K}_3] = [\cdot]$ in $\mathrm{Sk}(\widetilde{M}, \mathfrak{gl}(1))$ and the total framing factor is q. This time, however, the total winding is -2 instead of zero; this arises because $\widetilde{K}_3$ is divided into one loop on sheet 1 and one on sheet 2, and the 1-orientation and 2-orientation of the leaf space are opposite, so the windings from these two parts add instead of cancelling. Thus we get a winding factor q^{-2}. There is also an exchange factor of $q(q^{-1} - q)$, as we read off from figure 19; here we use the fact that the leaf space crossing is an undercrossing. Combining all these factors, this lift contributes $(q^{-1} - q)[\cdot]$ to $F([K])$. We summarize the situation in table 2.

Combining these three lifts we get

$$F([K]) = q + q + (q^{-1} - q) = q^{-1} + q \tag{4.3}$$

as expected.

JHEP09(2020)153

lift	framing	exchange	detour	winding	[lift]	total
$\widetilde{K}_1$	q	1	1	1	1	q
$\widetilde{K}_2$	q	1	1	1	1	q
$\widetilde{K}_3$	q	$q(q^{-1}-q)$	1	q^{-2}	1	$q^{-1}-q$

Table 2. Summary for the three lifts of the unknot K in figure 22.

As we remarked earlier, in this case our computation is similar to the state sum model reviewed in section 2, applied to the "figure-eight unknot" diagram we obtained by projecting to the leaf space (figure 22, right.) There is a slight difference: the state sum model computes with the blackboard framing in leaf space, which in this case differs by one unit from our standard framing. Thus the state sum model gives $q^{-2}(q^{-1}+q)$ instead of our result $q^{-1}+q$. Looking into the details of the computation one sees that the relative factor q^2 comes from two different places: our computation includes an extra q in the factors associated to the crossing, and also includes the framing factor q which has no direct analogue in the state sum model.

5 Examples

5.1 Knots in $\mathbb{R}^3$

In section 4.3 we have shown how our q-nonabelianization map F correctly produces the Jones polynomial for the simplest unknots in $\mathbb{R}^3$. In this section we show how it works in a few more intricate examples, with more interesting knots placed in more interesting positions relative to the WKB foliations. In all cases we have to get the Jones polynomial: this follows from the fact that F is a well defined map of skein modules, which we prove in section 7 below. Nevertheless it is interesting and reassuring to see how it works out explicitly in some concrete examples.

5.1.1 Unknots

We first look at an unknot K whose projection onto C is a small loop around a branch point of the covering $\widetilde{C} \to C$, as shown in figure 24. This case is more interesting since we will meet detours as well as exchanges.

In this case a direct lift of K is not allowed, since such a lift would not give a closed path on $\widetilde{M}$: we need to include an odd number of detours to get back to the initial sheet. Indeed, according to our rules there are five lifts $\widetilde{K}_n$ contributing to $F([K])$:

- There are three lifts which involve a single detour each, shown in figure 25. Each of these lifts is contractible in $\widetilde{M}$, and equipped with standard framing, so in $\mathrm{Sk}(\widetilde{M}, \mathfrak{gl}(1))$ we have
$$[\widetilde{K}_1] = [\widetilde{K}_2] = [\widetilde{K}_3] = [\cdot] = 1. \tag{5.1}$$
Moreover, each of these lifts has a total framing factor $q^{3/2}$ and detour factor $q^{-1/2}$. Finally, each of these lifts has total winding $w(\widetilde{K}_n) = 0$. Thus each of these lifts contributes q to $F([K])$.

JHEP09(2020)153

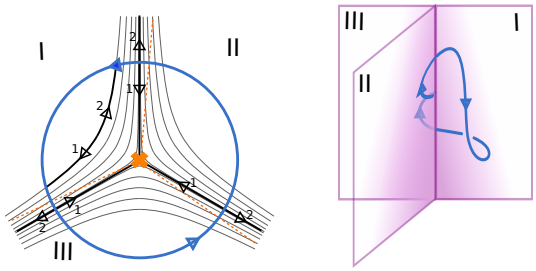

Figure 24. An unknot K encircling one strand of the branch locus of the covering $\widetilde{M} \to M$. Left: the projection of K to C. The height coordinate of K is taken as follows: as we travel counterclockwise around K the height monotonically increases, except for a small neighborhood of the filled arrow on K, where the height decreases. The projections of generic leaves of the WKB foliation are shown in light gray. The projections of special leaves, along which a detour or exchange may occur, are shown in black. Right: the projection of K to the leaf space of the foliation. The vertical direction in the leaf space corresponds to the height direction.

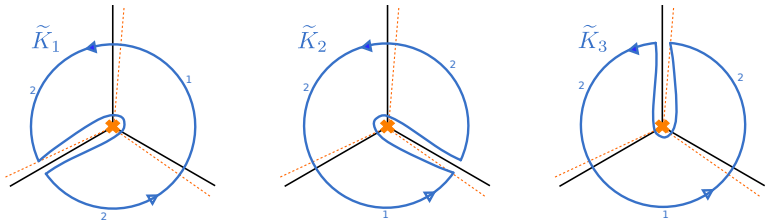

Figure 25. Three lifts $\widetilde{K}_n$ of K.

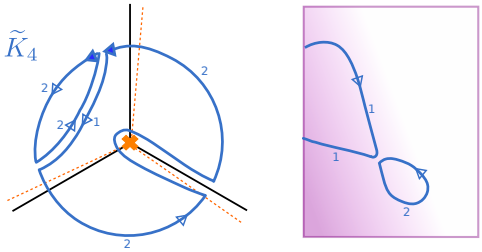

Figure 26. A lift $\widetilde{K}_4$ of K. Left: the standard projection. Right: the part of the leaf space projection involving the exchange.

- There is one lift $\widetilde{K}_4$ involving both a detour and an exchange, shown in figure 26:

  In $\mathrm{Sk}(\widetilde{M}, \mathfrak{gl}(1))$ again we have $[\widetilde{K}_4] = 1$. The framing factor, detour factor, and winding factor for this lift are $q^{3/2}$, $q^{-1/2}$, and q^{-2} respectively. The exchange carries a factor of $q(q^{-1} - q)$. Combining all these factors, altogether this lift contributes $q^{-1} - q$.

- Finally there is one lift $\widetilde{K}_5$ involving three detours, shown in figure 27.

  Resolving crossings using the $\mathfrak{gl}(1)$ skein relations, we find that $[\widetilde{K}_5]$ is q times the class of the link shown at the right of figure 27; in turn the class of that link is $-[\cdot]$ (the minus sign comes from deleting the loop in the middle, which winds once around

JHEP09(2020)153

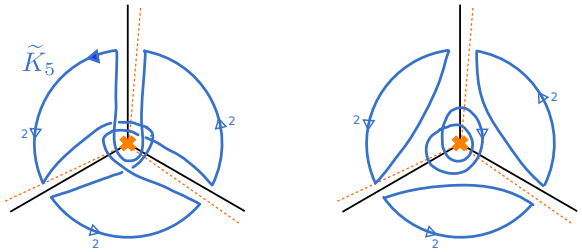

Figure 27. A lift $\widetilde{K}_5$ of K. Left: the standard projection. Right: a link obtained from $\widetilde{K}_5$ by applying $\mathfrak{gl}(1)$ skein relations.

lift	framing	exchange	detour	winding	[lift]	total
$\widetilde{K}_1$	$q^{3/2}$	1	$q^{-1/2}$	1	1	q
$\widetilde{K}_2$	$q^{3/2}$	1	$q^{-1/2}$	1	1	q
$\widetilde{K}_3$	$q^{3/2}$	1	$q^{-1/2}$	1	1	q
$\widetilde{K}_4$	$q^{3/2}$	$q(q^{-1}-q)$	$q^{-1/2}$	q^{-2}	1	$q^{-1}-q$
$\widetilde{K}_5$	$q^{3/2}$	1	$q^{-3/2}$	1	$-q$	$-q$

Table 3. Summary for the five lifts of the unknot K in figure 24.

the branch locus in $\widetilde{M}$); so altogether we get $[\widetilde{K}_5] = -q$. The framing factor is $q^{3/2}$, and the detour factor is $q^{-3/2}$. Finally, the total winding of $\widetilde{K}_5$ is zero, so there is no winding factor. Thus altogether this lift contributes $-q$. We summarize the situation in table 3.

Putting everything together, the image of $[K]$ under q-nonabelianization is

$$F([K]) = q + q + q + (q^{-1} - q) + (-q) = q + q^{-1}.$$

Again this matches the expected answer.

Next we look at an unknot K whose projection to C is a loop around two branch points of $\widetilde{C} \to C$, shown in figure 28.

This is the most detailed example which we will work out by hand. There are in total 17 lifts. Two of them, $\widetilde{K}_1$ and $\widetilde{K}_2$, are the direct lifts of K to the two sheets of $\widetilde{M}$. The next four lifts $\widetilde{K}_3$, $\widetilde{K}_4$, $\widetilde{K}_5$, $\widetilde{K}_6$ each involve two detours at the same branch point. They are shown in figure 29.

The next four lifts $\widetilde{K}_7$, $\widetilde{K}_8$, $\widetilde{K}_9$, $\widetilde{K}_{10}$ each involve two detours at two different branch points, as shown in figure 30.

The lifts $\widetilde{K}_{11}$ and $\widetilde{K}_{12}$ have three detours at one branch point and one detour at the other branch point, as illustrated in figure 31.

The next two lifts $\widetilde{K}_{13}$ and $\widetilde{K}_{14}$ have two detours at each branch point, as shown in figure 32.

Finally there are three lifts $\widetilde{K}_{15}$, $\widetilde{K}_{16}$ and $\widetilde{K}_{17}$ which have an exchange path as illustrated in figure 33.

This is our first example in which there is a nontrivial homology class on $\widetilde{C}$, and thus the contributions to $F([K])$ can be more interesting than just multiples of the unknot on

JHEP09(2020)153

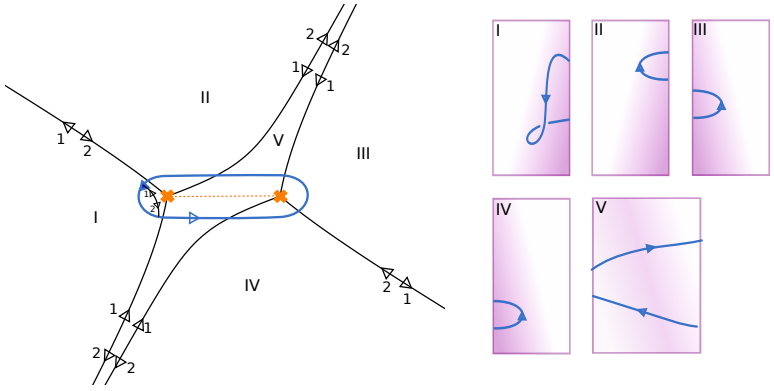

Figure 28. An unknot K encircling two strands of the branch locus of the covering $\widetilde{M} \to M$. Left: the projection of K to C. Right: the projections of K to five pieces of the leaf space. (For simplicity, we do not show the leaf spaces glued together.)

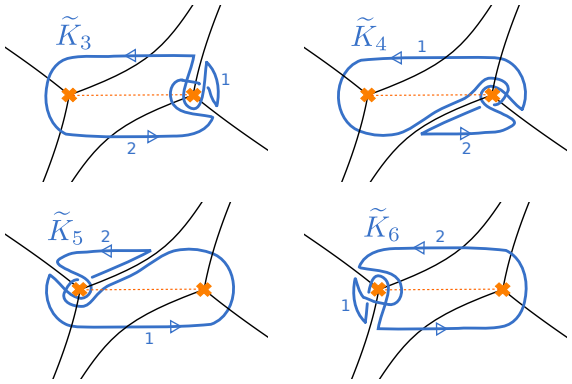

Figure 29. Four lifts of K to $\widetilde{C}$ which contribute to $F([K])$.

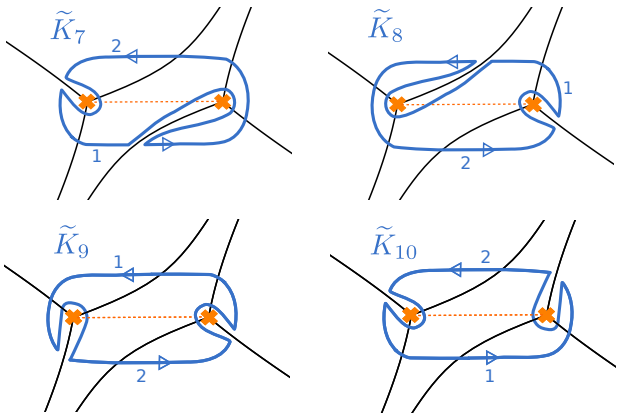

Figure 30. Four more lifts of K to $\widetilde{C}$ which contribute to $F([K])$.

$\widetilde{C}$: they can involve the other quantum torus generators. Explicitly, consider the oriented loop p in figure 34. According to the rules of section 3.5 we define the quantum torus generator $X_\gamma = [p] \in \mathrm{Sk}(\widetilde{M}, \mathfrak{gl}(1))$. The contributions from some of the lifts will involve

JHEP09(2020)153

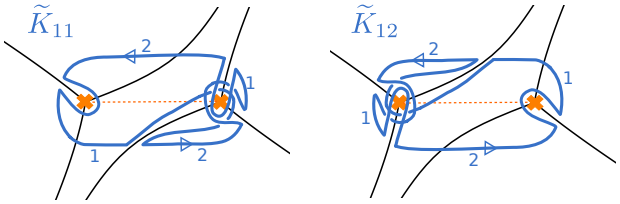

Figure 31. Two more lifts of K to $\widetilde{C}$ which contribute to $F([K])$.

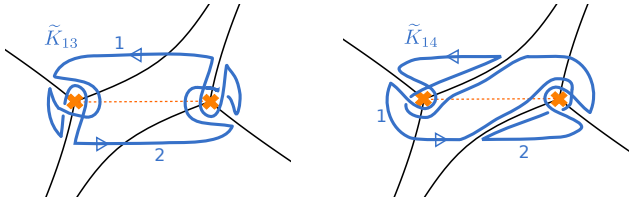

Figure 32. Two more lifts of K to $\widetilde{C}$ which contribute to $F([K])$.

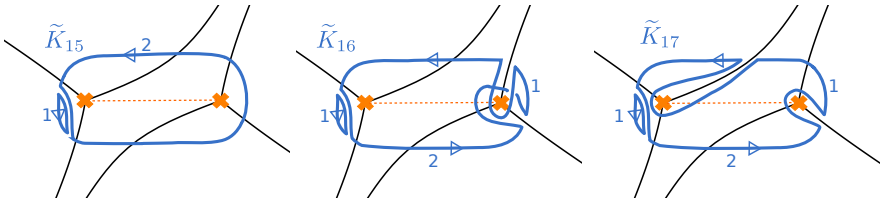

Figure 33. Three more lifts of K to $\widetilde{C}$ which contribute to $F([K])$.

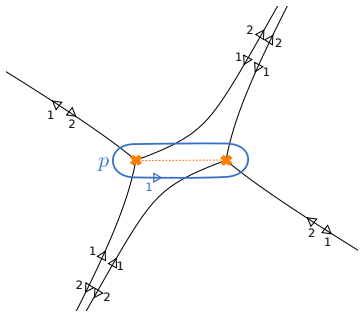

Figure 34. A cycle p on $\widetilde{C}$, with $[p] = X_\gamma$ in $\mathrm{Sk}(\widetilde{M}, \mathfrak{gl}(1))$.

the variable X_γ. We will not describe in detail the computations for all 17 lifts; see table 4 for a summary of the results.

Summing the 17 terms together gives once again the expected answer,

$$F([K]) = q + q^{-1}.$$

In particular, note that all the terms proportional to X_γ cancel among themselves, as do those proportional to $X_{-\gamma}$. This had to happen, since K is contained in a ball; in such cases we always just get the polynomial (1.9) for K, just as for $M = \mathbb{R}^3$. In more interesting examples where K represents a nontrivial class in $\pi_1(M)$, the X_γ will not cancel out.

JHEP09(2020)153

lift	framing	exchange	detour	winding	[lift]	total
$\widetilde{K}_1$	q^2	1	1	1	X_γ	q^2X_γ
$\widetilde{K}_2$	q^2	1	1	1	$X_{-\gamma}$	$q^2X_{-\gamma}$
$\widetilde{K}_3$	q^2	1	q^{-1}	1	$-qX_{-\gamma}$	$-q^2X_{-\gamma}$
$\widetilde{K}_4$	q^2	1	q^{-1}	1	$-qX_\gamma$	$-q^2X_\gamma$
$\widetilde{K}_5$	q^2	1	q^{-1}	1	$-qX_\gamma$	$-q^2X_\gamma$
$\widetilde{K}_6$	q^2	1	q^{-1}	1	$-q^{-1}X_{-\gamma}$	$-X_{-\gamma}$
$\widetilde{K}_7$	q^2	1	q^{-1}	1	1	q
$\widetilde{K}_8$	q^2	1	q^{-1}	1	1	q
$\widetilde{K}_9$	q^2	1	q^{-1}	1	1	q
$\widetilde{K}_{10}$	q^2	1	q^{-1}	1	1	q
$\widetilde{K}_{11}$	q^2	1	q^{-2}	1	$-q$	$-q$
$\widetilde{K}_{12}$	q^2	1	q^{-2}	1	$-q$	$-q$
$\widetilde{K}_{13}$	q^2	1	q^{-2}	1	$X_{-\gamma}$	$X_{-\gamma}$
$\widetilde{K}_{14}$	q^2	1	q^{-2}	1	q^2X_γ	q^2X_γ
$\widetilde{K}_{15}$	q^2	$q(q^{-1}-q)$	1	q^{-2}	$X_{-\gamma}$	$q(q^{-1}-q)X_{-\gamma}$
$\widetilde{K}_{16}$	q^2	$q(q^{-1}-q)$	q^{-1}	q^{-2}	$-qX_{-\gamma}$	$q(q-q^{-1})X_{-\gamma}$
$\widetilde{K}_{17}$	q^2	$q(q^{-1}-q)$	q^{-1}	q^{-2}	1	$q^{-1}-q$

Table 4. Summary for the seventeen lifts of the unknot K in figure 28.

5.1.2 Trefoils

In section 2 we obtained the Jones polynomial for a left-handed trefoil using the state-sum model. We could equally well apply our q-nonabelianization map to a left-handed trefoil K_{trefoil} in a single domain, equipped with standard framing. The calculation goes through in a similar fashion to the state-sum model. Explicitly, there are 6 lifts, whose contributions sum to

$$\begin{aligned} F([K_{\text{trefoil}}]) &= q^{-3}+q^{-3}+(q^{-1}-q)q^{-2}+(q^{-1}-q)q^{-2}+(q^{-1}-q)q^{2}+(q^{-1}-q)^3q^{-2} \\ &= q^{-5}+q^{-3}+q^{-1}-q^{3} \\ &= q^{-3\times 2}P_{\text{HOMFLY}}(K_{\text{trefoil}}, a=q^2, z=q-q^{-1}), \end{aligned}$$

which matches (2.1).

A more interesting example is a trefoil in the neighborhood of a branch point as shown in figure 35. There are in total 18 lifts, whose contributions sum up to give the expected answer,

$$\begin{aligned} F([K_{\text{trefoil}}]) = {} & (q^{-1}-q)-q(q^{-1}-q)^2+q^{-1}(q^{-1}-q)^2-q+q^{-1}+q^{-1}+q^{-5}+(q^{-1}-q) \\ & +q^{-2}(q^{-1}-q)-q^{-2}(q^{-1}-q)+q^{-1}(q^{-1}-q)^2+q^{-2}(q^{-1}-q)^3 \\ & -q^{-3}(q^{-1}-q)^2+q^{-1}+q^{-3}-q^{-3}+q^{-2}(q^{-1}-q)-q^{-3} \\ = {} & q^{-5}+q^{-3}+q^{-1}-q^{3}. \end{aligned}$$

JHEP09(2020)153

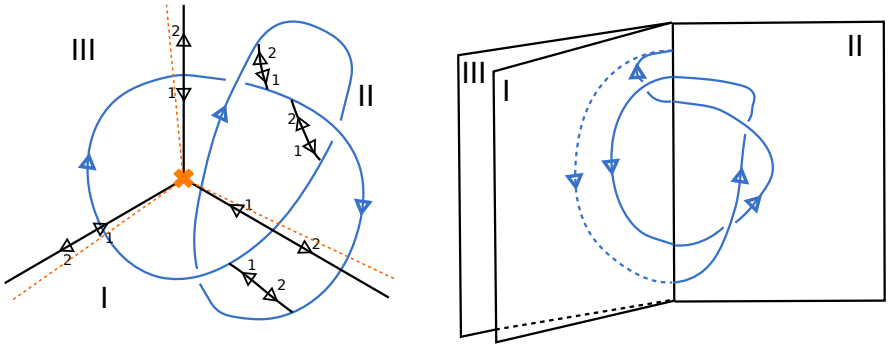

Figure 35. A left-handed trefoil in the neighborhood of a branch point in standard projection (left) and leaf space projection (right).

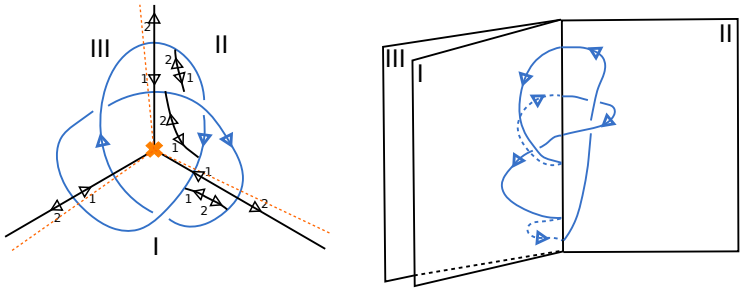

Figure 36. Another left-handed trefoil in the neighborhood of a branch point in standard projection (left) and leaf space projection (right).

Figure 36 shows another example of a left-handed trefoil knot in the neighborhood of a branch point. Here there are in total 30 lifts, whose contributions sum up to give once again the expected answer $q^{-5} + q^{-3} + q^{-1} - q^3$.

5.1.3 Figure-eight knot

In figure 37 we show a figure-eight knot $K_{\text{figure-8}}$ in standard projection and leaf space projection. There are in total 47 lifts, whose contributions sum up to

$$F([K_{\text{figure-8}}]) = q^5 + q^{-5}, \tag{5.2}$$

matching $P_{\text{HOMFLY}}(K_{\text{figure-8}}, a = q^2, z = q - q^{-1})$ as expected.[12]

5.2 A pure flavor line defect

Now we begin to consider examples of links which are homotopically nontrivial in M.

The simplest such example is a loop K whose standard projection encircles a puncture on C, as illustrated in figure 38.[13] K corresponds to a pure flavor line defect in a theory of class S.

[12] Although the standard projection of $K_{\text{figure-8}}$ has crossing number 4, its writhe is 0.

[13] The number of critical leaves going into the puncture depends on the example. However, that number is not important in this example, since there are no possible detours.

JHEP09(2020)153

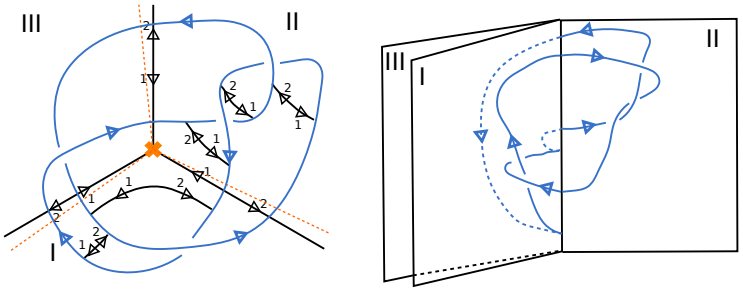

Figure 37. A figure-eight knot in the neighborhood of a branch point in standard projection (left) and leaf space projection (right).

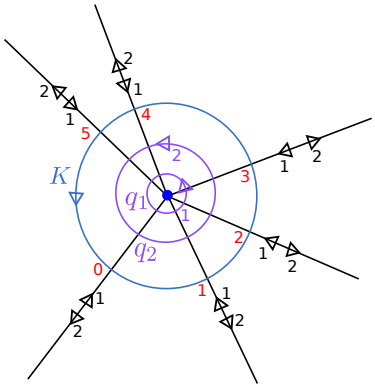

Figure 38. An unknot K whose standard projection is a small loop around a puncture (denoted as a blue dot) on C. For simplicity, in this and following examples, we do not draw the leaf space projection. Instead, we specify x^3-coordinates (in red) at points where the unknot meets a critical leaf. Between these points the x^3-coordinate varies as simply as possible: this means it varies monotonically, except for critical points which we place immediately before crossing a critical leaf. We also show cycles q_1, q_2 representing homology classes μ_1, μ_2 in $H_1(\widetilde{C}, \mathbb{Z})$ respectively.

In this case the only lifts of K allowed are the direct lifts $\widetilde{K}_1$ and $\widetilde{K}_2$ on sheet 1 and sheet 2 respectively. Moreover, the framing factor and winding factor for each of these are trivial, so we simply have $\alpha(\widetilde{K}_1) = \alpha(\widetilde{K}_2) = 1$ and thus

$$F([K]) = X_{\mu_1} + X_{\mu_2}. \tag{5.3}$$

So far we have been considering class S theories of type $\mathfrak{gl}(2)$, but in the following we will also discuss class S theories of type $\mathfrak{sl}(2)$, in order to be able to compare directly to previous results in the literature. The projection from $\mathfrak{gl}(2)$ to $\mathfrak{sl}(2)$ is discussed in section 9; roughly it amounts to replacing $X_\gamma \mapsto X_{\frac{1}{2}(\gamma - \sigma(\gamma))}$, where σ denotes the deck transformation exchanging the two sheets of $\widetilde{C} \to C$. In the following examples we first obtain the generating function $F([K])$ in a class S theory of type $\mathfrak{gl}(2)$, then apply this projection to get the result in the $\mathfrak{sl}(2)$ theory.

For a first example, we revisit the pure flavor line defect, now in a theory of class S of type $\mathfrak{sl}(2)$. The projection identifies $\mu_1 \sim -\mu_2 := \mu$, and the generating function is

$$F([K]) = X_\mu + X_{-\mu}. \tag{5.4}$$

JHEP09(2020)153

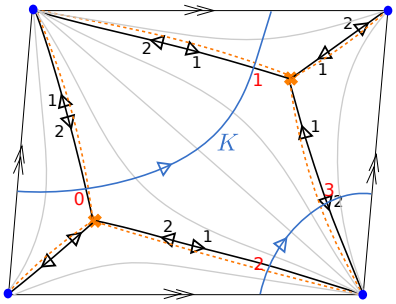

Figure 39. WKB foliation on a torus with one puncture (blue dot). We also show the standard projection of a loop K, whose x^3-profile is specified by the red numbers, following the convention we introduced in figure 38.

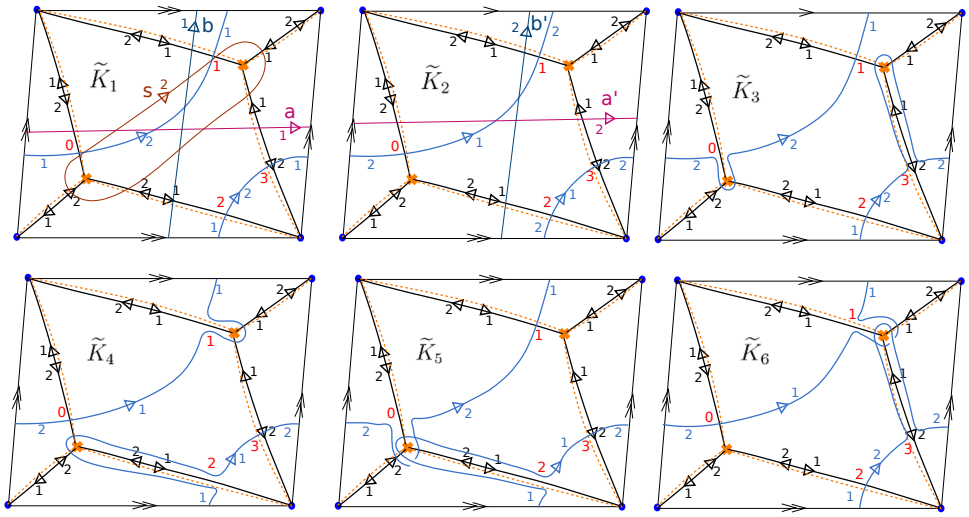

Figure 40. The six lifts $\widetilde{K}_i$ of K. We also show a basis $\{\gamma_1, \gamma_2, \gamma_3, \gamma_4, \gamma_5\}$ for $H_1(\widetilde{C}, \mathbb{Z})$ with representatives s, a, b, a', b' respectively.

5.3 SU(2) $\mathcal{N} = 2^*$ theory

Next we consider the SU(2) $\mathcal{N} = 2^*$ theory. This theory is obtained by giving a mass m to the adjoint hypermultiplet in the SU(2) $\mathcal{N} = 4$ theory. Its class S construction is given by compactifying the 6d (2,0) A_1 theory on a once-punctured torus C.

We choose m and the coupling τ such that the WKB foliation is as shown in figure 39. We consider a line defect corresponding to a loop K whose projection to C wraps both A-cycle and B-cycle once, as shown in figure 39.

We will first compute the generating function in the $\mathfrak{gl}(2)$ case. There are in total six lifts $\widetilde{K}_i$ as illustrated in figure 40. For each $\widetilde{K}_i$, the framing factor is trivial, while the winding factor and detour factors cancel out, so $\alpha(\widetilde{K}_i) = 1$. The question of finding $F([K])$ thus reduces to expressing $[\widetilde{K}_i]$ in terms of X_{γ_i}. Then according to the crossing-counting

JHEP09(2020)153

rules explained in section 3.5, we have

$$\begin{aligned}
[\widetilde{K}_1] &= X_{\gamma_2+\gamma_3}, & [\widetilde{K}_2] &= X_{\gamma_4+\gamma_5},\\
[\widetilde{K}_3] &= X_{\gamma_1+\gamma_3+\gamma_4}, & [\widetilde{K}_4] &= X_{-\gamma_1+\gamma_3+\gamma_4},\\
[\widetilde{K}_5] &= -q^{-1}X_{\gamma_3+\gamma_4}, & [\widetilde{K}_6] &= -qX_{\gamma_3+\gamma_4}
\end{aligned}$$

(recall that the factors of q come from the genuine crossings, and factors of -1 come from "non-local crossings.") Summing these up gives

$$F([K]) = X_{\gamma_2+\gamma_3} + X_{\gamma_4+\gamma_5} + X_{\gamma_1+\gamma_3+\gamma_4} + X_{-\gamma_1+\gamma_3+\gamma_4} - \left(q+q^{-1}\right)X_{\gamma_3+\gamma_4}.$$

This result obeys the expected positivity and monotonicity properties discussed in section 1.5.4.

To obtain the spectrum in the $\mathfrak{sl}(2)$ theory, we just perform the projection ρ, which has the effect of identifying $\gamma_4 \sim -\gamma_2$ and $\gamma_5 \sim -\gamma_3$. The resulting generating function is

$$F([K]) = X_{\gamma_2+\gamma_3} + X_{-\gamma_2-\gamma_3} + X_{\gamma_1-\gamma_2+\gamma_3} + X_{-\gamma_1-\gamma_2+\gamma_3} - (q+q^{-1})X_{-\gamma_2+\gamma_3}. \tag{5.5}$$

This agrees (modulo some shifts in conventions) with [3], where the same line defect was considered. We also remark that using the traffic rules of [11] one could compute the vacuum expectation value of this line defect, which agrees with the classical limit of our generating function (5.5).

5.4 SU(2) with $N_f = 4$ flavors

As our next example, we take C to be $\mathbb{CP}^1$ with four punctures, corresponding to $\mathcal{N} = 2$ SU(2) SYM with four fundamental hypermultiplets. Traditional $\frac{1}{2}$-BPS line defects in this theory have been systematically studied by many people, for example [9–11, 61]. Here we will consider both traditional and fat line defects.

Let z be a coordinate on $\mathbb{CP}^1$. We choose a complex structure such that the four punctures are located at $z = 1, \mathrm{i}, -1, -\mathrm{i}$ respectively. Moreover, we pick Coulomb branch and mass parameters such that the double cover $\widetilde{C}$ is

$$\widetilde{C} = \{\lambda : \lambda^2 + \phi_2 = 0\} \subset T^*C, \tag{5.6}$$

where

$$\phi_2 = -\frac{z^4+2z^2-1}{2(z^4-1)^2}\,\mathrm{d}z^2. \tag{5.7}$$

The WKB foliation structure on C is shown in figure 41.

As a warmup we consider a loop K_1 as shown on the left of figure 42. We choose a basis $\{\gamma_1, \gamma_2, \mu_1, \mu_2, \mu_3, \mu_4\}$ for $H_1^{\mathrm{odd}}(\widetilde{C}, \mathbb{Z})$, where $\langle\gamma_1, \gamma_2\rangle = -1$ and $\{\mu_i\}$ span the flavor charge lattice. Applying the rules from section 4 we obtain 11 lifts, whose total contribution is

$$\begin{aligned}
F([K_1]) = {} & X_{-\gamma_2-\mu_2+\mu_3} + X_{-\gamma_2-\mu_1-\mu_4} + X_{\gamma_1+\mu_1-\mu_4} + X_{-\gamma_1-\mu_1+\mu_4} + X_{\gamma_1-\gamma_2+\mu_1-\mu_4}\\
& + X_{\gamma_1-\gamma_2-\mu_2+\mu_3-2\mu_4} + X_{\gamma_1-2\gamma_2-\mu_2+\mu_3-2\mu_4},
\end{aligned}$$

This also agrees with the classical nonabelianization result in [11].

JHEP09(2020)153

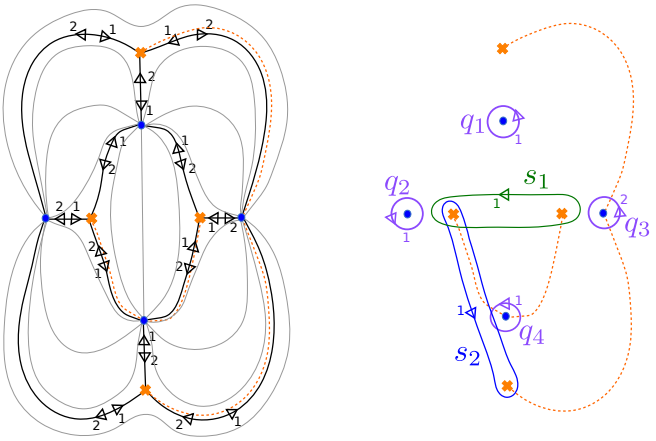

Figure 41. Left: WKB foliation structure on $\mathbb{CP}^1$ with four punctures (denoted as blue dots) with the parameters in (5.7). Right: a basis $\{\gamma_1, \gamma_2, \mu_1, \mu_2, \mu_3, \mu_4\}$ for $H_1^{\text{odd}}(\widetilde{C}, \mathbb{Z})$ with representative cycles $s_1, s_2, q_1, q_2, q_3, q_4$ respectively.

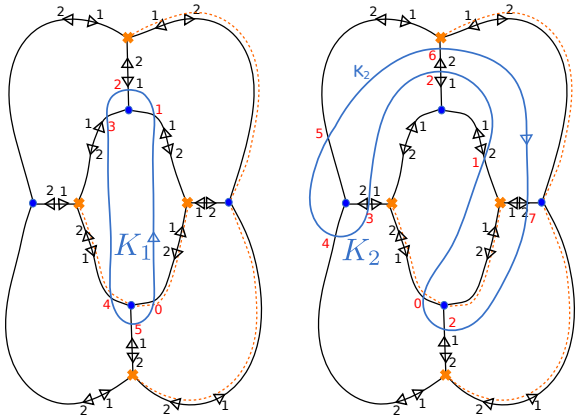

Figure 42. Standard projection of two loops K_1 and K_2 in $M = C \times \mathbb{R}$. Height profiles for these loops are specified in the same way as in figure 38.

As a more interesting example we consider the loop K_2 shown on the right of figure 42. K_2 has in total 48 lifts whose contributions sum up to

$$
\begin{aligned}
F([K_2]) = {} & X_{\gamma_1+\mu_1-\mu_3} + X_{\gamma_2+\mu_1-\mu_3} + X_{\gamma_1+\gamma_2+\mu_1-\mu_3} + X_{-\gamma_2-\mu_1+\mu_3} + X_{\gamma_1+\mu_1+\mu_3} \\
& + X_{\gamma_1-\gamma_2+\mu_1+\mu_3} + X_{2\gamma_1-3\gamma_2-\mu_2+2\mu_3-3\mu_4} - (q+q^{-1}) X_{2\gamma_1-2\gamma_2-\mu_2+2\mu_3-3\mu_4} \\
& + X_{2\gamma_1-\gamma_2-\mu_2+2\mu_3-3\mu_4} + X_{\gamma_1-2\gamma_2-\mu_1+\mu_3-2\mu_4} + X_{\gamma_1-\gamma_2-\mu_1+\mu_3-2\mu_4} \\
& + X_{\gamma_1+\mu_1+\mu_3-2\mu_4} - (q+q^{-1}) X_{2\gamma_1+\mu_1+\mu_3-2\mu_4} - (q+q^{-1}) X_{2\gamma_1-2\gamma_2+\mu_1+\mu_3-2\mu_4} \\
& + X_{\gamma_1-\gamma_2+\mu_1+\mu_3-2\mu_4} + (2+q^2+q^{-2}) X_{2\gamma_1-\gamma_2+\mu_1+\mu_3-2\mu_4} + X_{\gamma_1-\mu_2-\mu_4} \\
& + X_{\gamma_1-\gamma_2-\mu_2-\mu_4} + X_{\gamma_1+\mu_2-\mu_4} + X_{\gamma_1-\gamma_2+\mu_2-\mu_4} + X_{\gamma_1+2\mu_1+\mu_2-\mu_4} \\
& - (q+q^{-1}) X_{2\gamma_1+2\mu_1+\mu_2-\mu_4} + X_{2\gamma_1-\gamma_2+2\mu_1+\mu_2-\mu_4} + X_{\gamma_1+\gamma_2+2\mu_1+\mu_2-\mu_4} \\
& + X_{2\gamma_1+\gamma_2+2\mu_1+\mu_2-\mu_4} + X_{\gamma_1-2\gamma_2-\mu_2+2\mu_3-\mu_4} + X_{\gamma_1-\gamma_2-\mu_2+2\mu_3-\mu_4}.
\end{aligned}
$$

JHEP09(2020)153

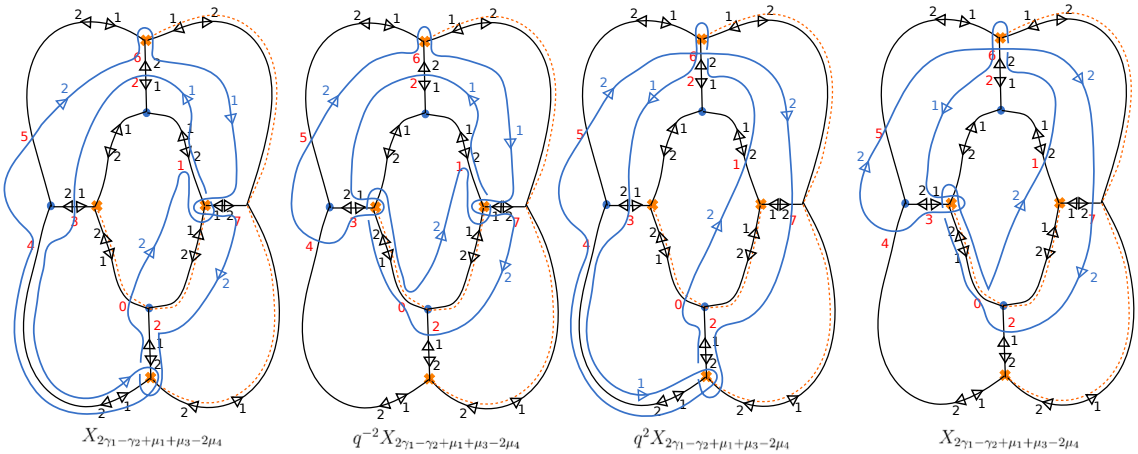

Figure 43. Lifts corresponding to framed BPS states in the charge sector $2\gamma_1 - \gamma_2 + \mu_1 + \mu_3 - 2\mu_4$ and their contributions to $F([K_2])$.

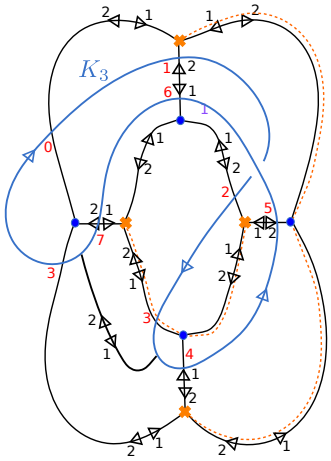

Figure 44. Standard projection of an unknot K_3 in $M = C \times \mathbb{R}$. Its height profile is specified in the same convention as in figure 38.

Once again the result has the expected properties: the coefficients of X_γ form characters of $\mathrm{SU}(2)_P$ representations, and framed BPS states that form even- (odd-) dimensional $\mathrm{SU}(2)_P$ representations contribute to the protected spin character with a minus (plus) sign.

The most interesting charge sector is the charge $2\gamma_1 - \gamma_2 + \mu_1 + \mu_3 - 2\mu_4$, where the framed BPS states form a direct sum of one-dimensional and three-dimensional $\mathrm{SU}(2)_P$ representations. We show the four lifts realizing these framed BPS states in figure 43.

As our final example, we consider the link K_3 shown in figure 44. K_3 has in total 52 lifts. Summing up their contributions, $F([K_3])$ is given by a long expression, which can be conveniently written in terms of $F([K_2])$ as follows:[14]

$$F([K_3]) = -F([K_2]) + q\big(X_{\mu_2} + X_{-\mu_2}\big)\big(X_{\mu_4} + X_{-\mu_4}\big). \tag{5.8}$$

[14]This relation could be obtained directly from the relations in the $\mathfrak{sl}(2)$ (Kauffman bracket) skein algebra.

JHEP09(2020)153

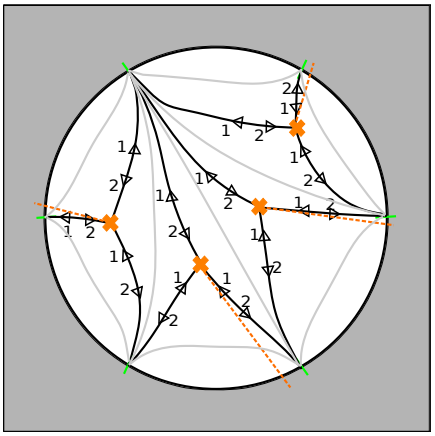

Figure 45. The WKB foliation at some point in the Coulomb branch of the (A_1, A_3) Argyres-Douglas theory. Here the irregular singularity is placed at $z = \infty$. The green markers on the boundary circle correspond to P_i, which are determined by the six rays going into the irregular singularity.

In particular, the positivity is violated, and even if we ignore this, the coefficients of X_γ in $F([K_3])$ do not in general form $\mathrm{SU}(2)_P$ characters (we have a q term but no corresponding $1/q$). This is as expected since K_3 corresponds to a fat line defect, as the standard projection of K_3 contains a crossing.

5.5 (A_1, A_N) Argyres-Douglas theories

In this section we briefly consider some theories whose class S construction involves irregular singularities: the (A_1, A_N) Argyres-Douglas theories [43]. These theories are obtained by taking $C = \mathbb{C}P^1$ with an irregular singularity at $z = \infty$, which prescribes that the coverings $\widetilde{C}$ that we consider have $\lambda \sim z^{\frac{N}{2}+1}\mathrm{d}z$ as $z \to \infty$.[15]

The local behavior of the WKB foliation in the neighborhood of an irregular singularity P is very different from that near a regular singularity. A generic leaf asymptotes tangentially to one of M,[16] rays near P. If we draw an infinitesimal circle S^1_P around P bounding an infinitesimal disk D_P, these M rays determine M marked points P_i on S^1_P, evenly distributed. In the examples that we will consider here $C = \mathbb{CP}^1 \setminus D_P$.

In the following we will use the (A_1, A_3) Argyres-Douglas theory as an example. We choose a point in the parameter space of this theory such that the covering $\widetilde{C}$ is given by

$$\widetilde{C} = \left\{ \lambda : \lambda^2 - \left(z^4 - \left(\frac{3}{2} + 2\mathrm{i} \right) z^2 + \left(1 - 2\mathrm{i} \right) z + \frac{3}{2}\mathrm{i} - \frac{3}{16} \right) \mathrm{d}z^2 = 0 \right\} \tag{5.9}$$

where z is a coordinate on C such that D_P is centered at $z = \infty$. Figure 45 shows the WKB foliation at this point in the moduli space.

[15] The rules we discuss in this section also apply to the (A_1, D_N) Argyres-Douglas theories, which have an irregular singularity at $z = \infty$ and also a regular singularity at $z = 0$. The spin content of framed BPS states for line defects in simple (A_1, D_N) theories has also been studied in [62].

[16] For (A_1, A_N) Argyres-Douglas theories, $M = N + 3$; for (A_1, D_N) Argyres-Douglas theories, $M = N$.

JHEP09(2020)153

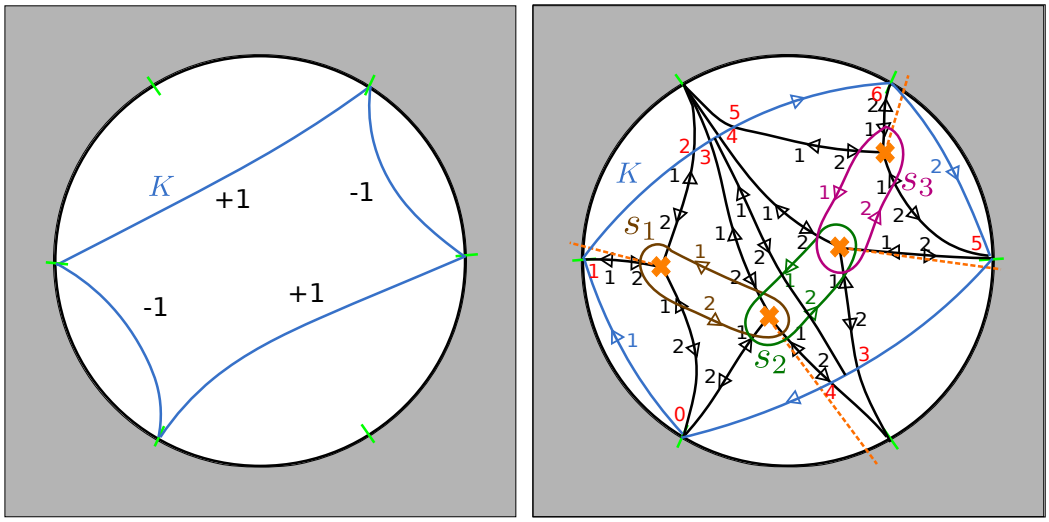

Figure 46. Left: a lamination which corresponds to a line defect in the (A_1, A_3) Argyres-Douglas theory. Here the irregular singularity is placed at infinity. The green markers represent the six marked points P_i. Right: standard projection of a collection K of arcs corresponding to the lamination. The height profile is specified in the same convention as figure 38. The open paths carrying -1 weight have a fixed lift, as indicated in blue. We also show a choice of basis $\{[\gamma_1], [\gamma_2], [\gamma_3]\}$ for $H_1(\widetilde{C}, \mathbb{Z})$ with representative cycles s_1 (brown), s_2 (green) and s_3 (purple).

In the presence of an irregular singularity, line defects do not correspond to ordinary links in $C \times \mathbb{R}$ anymore; we also need to include links which can have some endpoints on $S^1_P \times \mathbb{R}$. Here we focus on flat line defects, i.e. we only consider L' whose projection to C does not contain any crossings. The projection of such an L' to C is an oriented version of what was called a *lamination* in [11] following [57]. A lamination is a collection of paths on $C = \mathbb{CP}^1 \setminus D_P$, which can be either closed or open with ends on the marked points P_i. Each path carries an integer weight, subject to the constraint that paths that carry negative weights must be open and end at two adjacent marked points P_i, P_{i+1}, and the sum of the weights of paths ending at each P_i must be zero. For example, figure 46 illustrates a lamination corresponding to a line defect in the (A_1, A_3) Argyres-Douglas theory.

Now we state the extra ingredients in our q-nonabelianization rules to accommodate the presence of irregular singularities. For simplicity we just consider the case of laminations where all weights on paths are ± 1.

- Each open path carrying the weight -1 has to be lifted to a specific sheet of $\widetilde{M}$: its orientation has to match with the orientation of the leaves near the boundary circle. In figure 46 we show the lifts for the two open paths with -1 weight in that lamination.

- We enumerate all possible lifts $\widetilde{L}' \subset \widetilde{M}$ subject to these lifting constraints. Each $\widetilde{L}'$ is a link in $\widetilde{M}$, meeting $S^1_P \times \mathbb{R}$ at a finite number of points. We then apply our q-nonabelianization rules as usual, except that for computing $\alpha(\widetilde{L}')$, we do not include winding factors or framing weights for the lifts of paths carrying weight -1.

JHEP09(2020)153

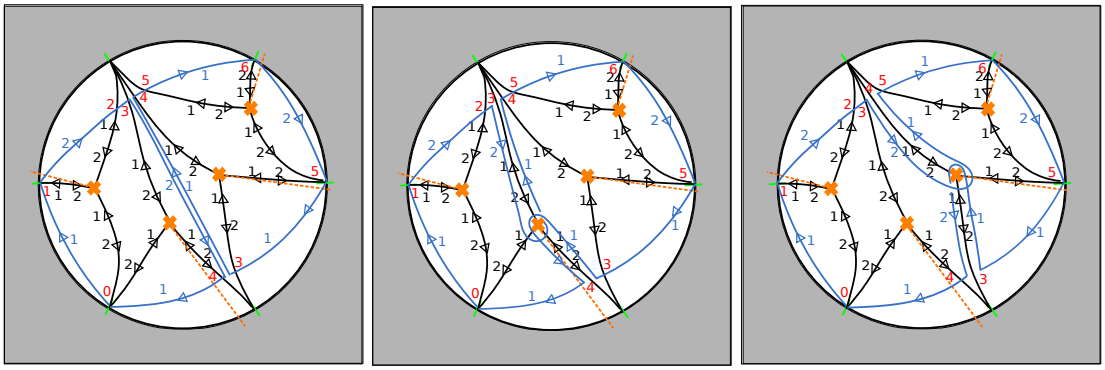

Figure 47. The standard projection of three lifts $\widetilde{K}_1$ (left), $\widetilde{K}_2$ (middle) and $\widetilde{K}_3$ (right) whose contributions sum up to $-(q+q^{-1})X_{\gamma_1-\gamma_3}$. Here we have denoted the sheet numbers of lifted strands in blue.

Applying these rules to the line defect in figure 46, we obtain the result:

$$F([K]) = X_{\gamma_1}+X_{\gamma_1+\gamma_2}+X_{-\gamma_3}-(q+q^{-1})X_{\gamma_1-\gamma_3}+X_{-\gamma_2-\gamma_3}+X_{\gamma_1-\gamma_2-\gamma_3}+X_{\gamma_1+\gamma_2-\gamma_3}. \quad (5.10)$$

This line defect was also studied in [11]; in particular the classical version of its generating function was given in (10.15) of that paper. Our q-nonabelianization computation refines the framed BPS state index from 2 to $-(q+q^{-1})$ in the charge sector $\gamma_1-\gamma_3$.

Let us take a closer look at the term $-(q+q^{-1})X_{\gamma_1-\gamma_3}$, which turns out to be the sum of contributions from three lifts $\widetilde{K}_1$, $\widetilde{K}_2$ and $\widetilde{K}_3$ shown in figure 47.

For all three lifts $\widetilde{K}_i$, there are four places where the standard projection of a strand with $+1$ weight is tangent to a WKB leaf. The associated local framing weight factors cancel out, so in the end each $\widetilde{K}_i$ has a trivial framing factor. The winding numbers of $\widetilde{K}_1$, $\widetilde{K}_2$ and $\widetilde{K}_3$ are -1, 0 and -1 respectively. Additionally $\widetilde{K}_1$ has an exchange factor of $q(q^{-1}-q)$, $\widetilde{K}_3$ has a detour factor of q, and $\widetilde{K}_2$ has trivial exchange and detour factors. In summary the total weights associated with the lifts are:

$$\alpha(\widetilde{K}_1) = q^{-1}-q, \quad \alpha(\widetilde{K}_2) = 1, \quad \alpha(\widetilde{K}_3) = 1. \quad (5.11)$$

Using the sign rules introduced in section 3.5, we get

$$[\widetilde{K}_1] = X_{\gamma_1-\gamma_3}, \quad [\widetilde{K}_2] = -q^{-1}X_{\gamma_1-\gamma_3}, \quad [\widetilde{K}_3] = -q^{-1}X_{\gamma_1-\gamma_3}. \quad (5.12)$$

Combining these gives

$$\sum_{i=1}^{3} \alpha(\widetilde{K}_i)[\widetilde{K}_i] = -(q+q^{-1})X_{\gamma_1-\gamma_3}. \quad (5.13)$$

6 A covariant version of q-nonabelianization

In section 4.2 above, we described the q-nonabelianization map F in a way that used the special structure $M = C \times \mathbb{R}$. For example, we always chose links with standard framing, and our explicit formulas for the weight factors $\alpha(\widetilde{L})$ involved the projection $M \to C$. In

JHEP09(2020)153

this section we reformulate F in a more covariant way. This reformulation will be useful for the future generalization to other 3-manifolds M. It will also prove to be convenient for the proof that F is a map of skein modules in section 7 below.

Given a framed link L in M, we again write

$$F([L]) = \sum_{\widetilde{L}} \alpha(\widetilde{L})[\widetilde{L}] \tag{6.1}$$

where $\widetilde{L}$ runs over links in $\widetilde{M}$ built from the same kinds of pieces as in section 4.2 as above. Now, however, we need to explain what framings we use.

- Direct lifts of portions of L to $\widetilde{M}$: these are equipped with a framing which just lifts the framing of L, using the projection to identify the tangent spaces to M and $\widetilde{M}$.

- Detours: each detour is equipped with a distinguished framing, as follows. Let p denote the point where the link L crosses the critical leaf. At p we have two distinguished tangent directions: the tangent t_w to the critical leaf (oriented toward the branch point) and the tangent t_L to L. Define $f_p := t_w \times t_L$. Without loss of generality, we may assume that the framing of L at p is given by f_p; then the framing of $\widetilde{L}$ as we approach p will also be given by f_p. (More generally if the framing of L is given by some $f \neq f_p$, we simply insert a rotation of the framing of $\widetilde{L}$ from along some arc a from f to f_p as we approach p along $\widetilde{L}$, and insert the opposite rotation from f_p back to f immediately after we leave p along $\widetilde{L}$. The homotopy class of the resulting framing of $\widetilde{L}$ is then independent of the choice of arc a, since a change of a cancels out.) Then, the framing of the lifted detour must start out from the framing f_p at the beginning of the lifted detour and end again at f_p at the end of the lifted detour. To get this interpolating framing we just choose any trivialization of TM in a neighborhood of the detour and then use that trivialization to extend f_p.

- Lifted exchanges: let p denote either of the two points where the exchange attaches to the link L. At p we have two distinguished tangent directions: the tangent t_e to the exchange (oriented away from p towards the exchange) and the tangent t_L to L. Define $f_p := t_e \times t_L$; without loss of generality, we may assume that the framing of L at p is given by f_p (if not we add interpolating arcs as above.) The framing of the exchange needs to interpolate between the two framings f_p at the two ends. Fortunately the normal bundle to the exchange has a canonical connection, coming from the fact that the exchange is a leaf of the foliation of M. We can use this connection to identify all the fibers with a single 2-dimensional vector space E. Then a framing of the exchange is a path in the circle $E/\mathbb{R}^+$, with its ends on the two points $[f_p]$. There are two distinguished such paths, one going the "short way" around the circle, the other going the "long way" around. We allow either of these framings; whichever one we choose, we use it on both sheets of the lift. (Thus when we consider a diagram involving n exchanges, the sum over $\widetilde{L}$ includes 2^n different terms associated to this diagram, differing only in their framing.)

JHEP09(2020)153

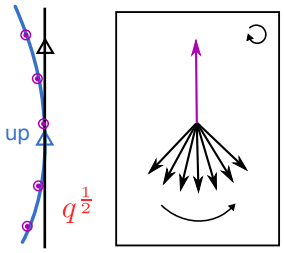

Figure 48. An example of the framing factor contribution to $\alpha(\widetilde{L})$ for $\widetilde{L}$ in standard framing. The framing vector is shown in purple while the foliation vector is shown in black.

The weight factor $\alpha(\widetilde{L})$ is given as follows:

- At every place where the framing of $\widetilde{L}$ is tangent to a leaf of the foliation of M, we include a contribution $q^{\pm\frac{1}{2}}$ to $\alpha(\widetilde{L})$, with the sign determined as follows. We consider the normal planes to $\widetilde{L}$ near the point where the tangency occurs. These planes are naturally oriented (since $\widetilde{L}$ and $\widetilde{M}$ are), and each contains two vectors, one given by the framing, the other by the foliation. At the point of tangency these two vectors coincide; as we move along $\widetilde{L}$ in the positive direction, the framing vector rotates across the foliation vector, either in the positive or negative direction. The factor is $q^{\frac{1}{2}}$ in the positive case, $q^{-\frac{1}{2}}$ in the negative case.

  To illustrate how this works, we revisit the first case in figure 17. In that case the link $\widetilde{L}$ was taken to carry standard framing. In figure 48 we show the framing vector and foliation vector in the normal plane to $\widetilde{L}$ near the tangency point. The framing vector rotates across the foliation vector in the positive direction, giving the framing factor $q^{\frac{1}{2}}$.

- For each lifted exchange, as we have explained, there are two possible framings: one going the "short way" and one going the "long way." When the framing goes the "long way" we include an extra factor -1 in $\alpha(\widetilde{L})$.

- Finally, the winding contribution $q^{w(\widetilde{L})}$ to $\alpha(\widetilde{L})$ is defined just as in section 4.2 (this definition was already covariant.)

This completes our description of the covariant rules. There are two special cases worth discussing:

- One can check directly that if we apply these covariant rules in the case where L has standard framing, we recover the rules of section 4.2 above. (When we frame a lifted exchange, since we apply the same framing to the lifts on both sheets, the terms using the "short way" and "long way" differ by a total of 2 units of framing. Thus altogether the two choices of framing give lifts differing by a factor $-q^2$. This is the origin of the exchange factors $\pm(q-q^{-1})$ in the rules of section 4.2.)

- Suppose $M=\mathbb{R}^3$ with the foliation in the x^3-direction. Then we can consider equipping L with "leaf space blackboard framing," i.e. choose the framing vector to point

JHEP09(2020)153

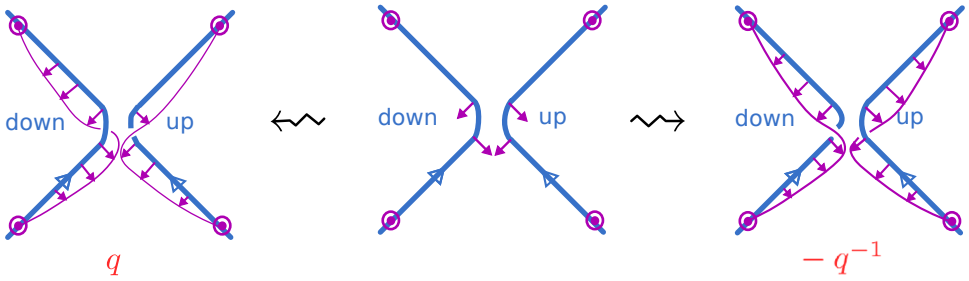

Figure 49. The sum over two framings for a lifted exchange, with the original link in blackboard framing. Middle: the blackboard framing far from the exchange, and the framings f_p near the exchange. Left: framing interpolated the "short way." This framing differs from the blackboard framing by a factor of q. Right: framing interpolated the "long way." This framing differs from the blackboard framing by a factor of q^{-1}. Summing over the two framings gives the factor $q - q^{-1}$.

in the x^3-direction. This framing is well defined provided that L is nowhere parallel to the x^3-direction. There is a slight technicality: our covariant rules cannot be applied directly because the framing is not generic enough. We perturb by rotating the framing everywhere very slightly in (say) the clockwise direction. After so doing, the covariant rules reduce exactly to the $N = 2$ state sum rules of section 2.1. In particular:

- The framing factor in the covariant rules is trivial (there are no points where the framing is tangent to the foliation.)
- The process of evaluating $[\widetilde{L}] \in \mathrm{Sk}(\widetilde{M}, \mathfrak{gl}(1))$ reduces to computing the self-linking number, which is given by a product over crossings, using the weights appearing in the first column of figure 2.
- The sum over framings for an exchange produces the $q - q^{-1}$ or $q^{-1} - q$ appearing in the last column of figure 2. For an example of how this works, see figure 49.
- The winding as defined in the covariant rules reduces to the winding of the link projection as used in the state sum rules.

7 Isotopy invariance and skein relations

In this section we give a sketch proof that F is well defined, i.e. that $F(L)$ really only depends on the class $[L] \in \mathrm{Sk}(M, \mathfrak{gl}(N))$.

The basic strategy is as follows. First we need to prove that $F(L)$ depends only on the framed isotopy class of L. For this purpose we use the covariant formulation of F, which we described in section 6. We check first that F is covariant under changes of framing. Next we turn to the question of isotopy. From the covariant rules it follows immediately that $F(L)$ is invariant under any isotopy which does not create or destroy exchanges and which leaves L untouched in some small neighborhood of the critical leaves. What remains is:

- To deal with processes in which exchanges are created or destroyed; since exchanges correspond to crossings in the leaf space projection, this boils down to checking

JHEP09(2020)153

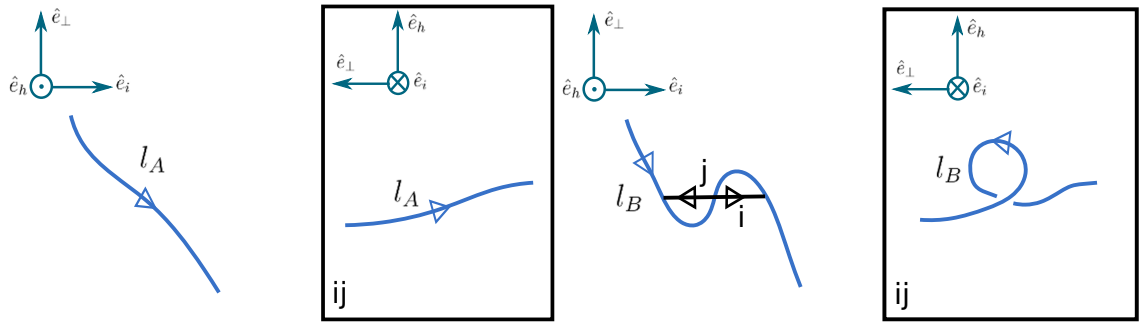

Figure 50. The first Reidemeister move. Here $\hat{e}_h$ is the unit vector along the height direction and $\hat{e}_i$ is the unit vector along the i-orientation of ij-leaves.

invariance under Reidemeister moves for that projection. We check this in section 7.2 below.

- To deal with processes which change L in a neighborhood of a critical leaf; here again a small isotopy does not change $F(L)$, but there are several Reidemeister-like moves which have to be considered, which create or destroy detours, or move detours across one another. We check invariance under these in section 7.3 below.

In each case we are free to choose any convenient framing; in practice the way we implement this is to choose a profile for the standard projection of L, and then use standard framing. Then for the actual computations we can use the concrete rules of section 4.2.

After this is done, we check that F preserves the skein relations. This check is simplified by the fact that we have already verified isotopy invariance, so we are free to put the link L in a simple position relative to the WKB foliation.

7.1 Changes of framing

Suppose L and L' are two links in M which differ only by a homotopy of the framing. Then we have $[L] = [L']$ in $\mathrm{Sk}(M, \mathfrak{gl}(2))$, and thus we must have $F(L) = F(L')$. This is relatively straightforward to check: as we vary the framing, the framing contributions $q^{\pm\frac{1}{2}}$ to $F(L)$ appear and disappear in cancelling pairs, while all other contributions vary continuously, so $F(L)$ is constant.

7.2 Isotopy invariance away from critical leaves

With an eye towards future generalization to $N > 2$, we use the notion of ij-leaf space; in the case of $N = 2$ we simply have $\{i, j\} = \{1, 2\}$.

In the following we denote the open strand configurations before and after each isotopy as l_A and l_B respectively. Correspondingly we denote its lifts before and after the isotopy as $\widetilde{l}_A^\kappa$ and $\widetilde{l}_B^\kappa$, where κ runs from 1 to the number of lifts.

7.2.1 The first Reidemeister move

In the following we consider the first Reidemeister move as shown in figure 50.

JHEP09(2020)153

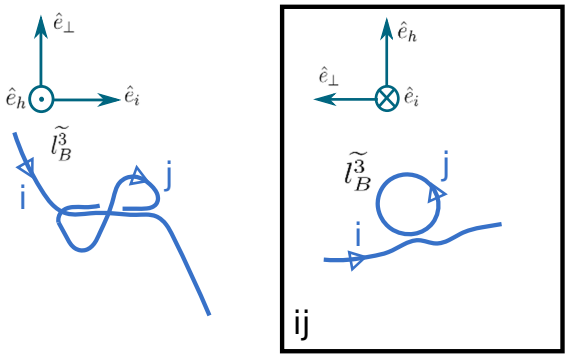

Figure 51. Lift of l_B that contains an exchange.

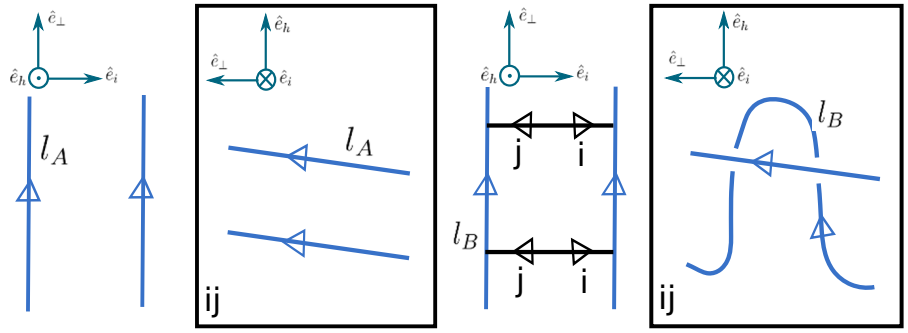

Figure 52. The second Reidemeister move.

l_A has two direct lifts to sheet i and sheet j, denoted as $\widetilde{l}_A^1$ and $\widetilde{l}_A^2$ respectively. l_B has two direct lifts $\widetilde{l}_B^1$ and $\widetilde{l}_B^2$, plus one lift $\widetilde{l}_B^3$ containing an exchange as shown in figure 51. Lifts of l_A carry no framing factor while lifts of l_B have a framing factor q. Denoting the winding of $\widetilde{l}_A^1$ as w, we have

$$\begin{aligned} F([l_B]) &= q^{(w+1)+1}[\widetilde{l}_A^1] + q^{-(w+1)+1}[\widetilde{l}_A^2] + (q^{-1}-q)q^{(w-1)+1}q[\widetilde{l}_A^1] \\ &= q^w[\widetilde{l}_A^1] + q^{-w}[\widetilde{l}_A^2] = F([l_A]). \end{aligned}$$

Here we have used $[\tilde{l}_B^1] = [\tilde{l}_A^1]$, $[\tilde{l}_B^2] = [\tilde{l}_A^2]$, $[\tilde{l}_B^3] = q[\tilde{l}_A^1]$ in $\mathrm{Sk}(\widetilde{M}, \mathfrak{gl}(1))$.

7.2.2 The second Reidemeister move

In figure 52 we illustrate the second Reidemeister move. Here both l_A and l_B have four direct lifts. It is easy to see that contributions from these direct lifts match with each other. l_B has two extra lifts $\widetilde{l}_B^5$ and $\widetilde{l}_B^6$ each containing an exchange, as shown in figure 53. So we only need to prove that the contributions from these two lifts cancel with each other. This works out simply because $[\tilde{l}_B^5] = [\tilde{l}_B^6]$ in $\mathrm{Sk}(\widetilde{M}, \mathfrak{gl}(1))$, and their weights differ by a minus sign due to the sign difference in exchange factors.

7.2.3 The third Reidemeister move

In this section we consider the third Reidemeister move as shown in figure 54.

JHEP09(2020)153

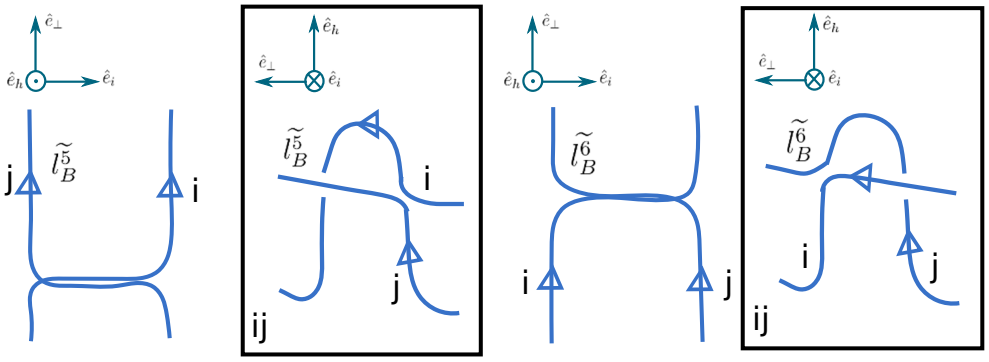

Figure 53. Two lifts of l_B whose contributions cancel each other.

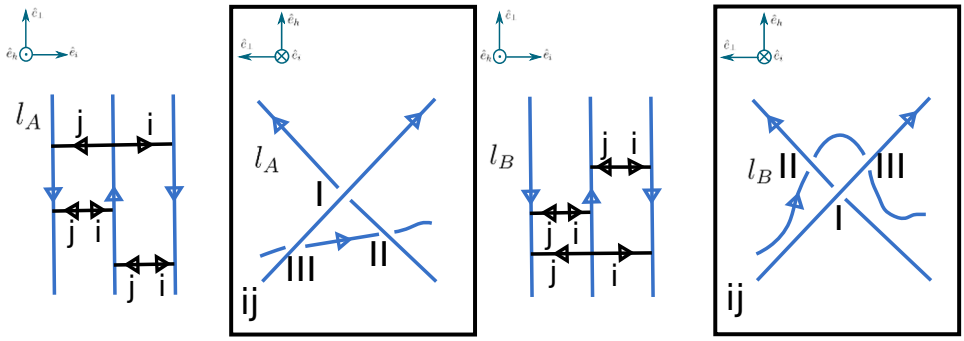

Figure 54. The third Reidemeister move.

Here l_A and l_B both have fifteen lifts, eight of which are direct lifts. It's easy to match contributions from twelve lifts of l_A and l_B on a term-by-term basis, so we only need to show contributions from the left-over three lifts match with each other. These three lifts are illustrated in figure 55, where $\widetilde{l^{1,2}_{A,B}}$ are lifts containing an exchange at leaf space crossing III and $\widetilde{l}^3_A, \widetilde{l}^3_B$ are lifts containing two exchanges at leaf space crossings I and II.

First, using the relations in $\mathrm{Sk}(\widetilde{M}, \mathfrak{gl}(1))$ we observe that

$$[\widetilde{l}^1_A] = q^{-1}[\widetilde{l}^3_A], \quad [\widetilde{l}^2_A] = q[\widetilde{l}^3_B], \quad [\widetilde{l}^1_B] = q[\widetilde{l}^3_A], \quad [\widetilde{l}^2_B] = q^{-1}[\widetilde{l}^3_B].$$

We denote the winding of $\widetilde{l}^3_A$ and $\widetilde{l}^3_B$ as w_1 and w_2. Then the weight factors associated to these six lifts are given as follows:

$$\begin{aligned}
&\alpha([\widetilde{l}^1_A]) = (q^{-1}-q)q^{w_1}, \quad \alpha([\widetilde{l}^2_A]) = (q^{-1}-q)q^{w_2}, \quad \alpha([\widetilde{l}^3_A]) = q(q^{-1}-q)q^{-1}(q-q^{-1})q^{w_1},\\
&\alpha([\widetilde{l}^1_B]) = (q^{-1}-q)q^{w_1}, \quad \alpha([\widetilde{l}^2_B]) = (q^{-1}-q)q^{w_2}, \quad \alpha([\widetilde{l}^3_B]) = q(q^{-1}-q)q^{-1}(q-q^{-1})q^{w_2}.
\end{aligned}$$

Therefore contributions from these three lifts do match with each other:

$$\sum_{i=1,2,3} \alpha([\widetilde{l}^i_A])[\widetilde{l}^i_A] = q(q^{-1}-q)q^{w_1}[\widetilde{l}^3_A] + q(q^{-1}-q)q^{w_2}[\widetilde{l}^3_B] = \sum_{i=1,2,3} \alpha([\widetilde{l}^i_B])[\widetilde{l}^i_B].$$

JHEP09(2020)153

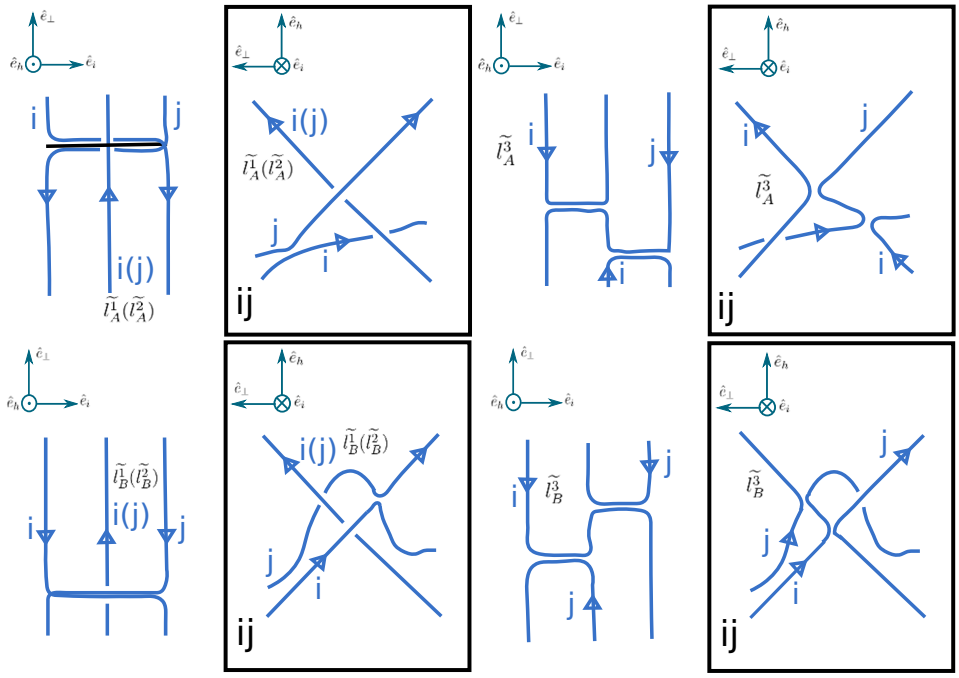

Figure 55. Three lifts of l_A and l_B.

7.3 Isotopy invariance near critical leaves

In this section we consider isotopies of open strands which involve critical leaves. All such isotopies can be perturbed into combinations of four basic moves, which are the analogues in this context of the Reidemeister moves.

Each basic move happens in a neighborhood of a branch point with three critical leaves emanating from it. In such a neighborhood, the leaf space of M topologically looks like three pages glued together at a "binder" corresponding to the branch locus. For convenience, we label these three pages as I, II, III, and illustrate the leaf space projection within each page.

7.3.1 Moving an exchange across a critical leaf

We first consider an isotopy which moves a leaf space crossing from one page to another, as shown in figure 56. There are in total eleven lifts on both sides. The comparison is reduced to matching contributions from the three lifts of l_A and l_B shown in figure 57.[17]

We denote the weights of $[\tilde{l}^1_A]$ and $[\tilde{l}^2_A]$ as α_1 and α_2. The weights of all the other lifts are then given by:

$$\alpha([\tilde{l}^1_B]) = \alpha_1, \quad \alpha([\tilde{l}^2_B]) = \alpha_2, \quad \alpha([\tilde{l}^3_A]) = (q-q^{-1})\alpha_2, \quad \alpha([\tilde{l}^3_B]) = (q-q^{-1})\alpha_1.$$

We also have the following relations in $\mathrm{Sk}(\widetilde{M}, \mathfrak{gl}(1))$:

$$[\tilde{l}^3_B] = q^{-1}[\tilde{l}^1_A] = q[\tilde{l}^1_B], \quad [\tilde{l}^3_A] = q[\tilde{l}^2_A] = q^{-1}[\tilde{l}^2_B].$$

Combining these we see that the contributions from these three lifts match on both sides.

[17] Here and below we omit the leaf space projection of the individual lifts.

JHEP09(2020)153

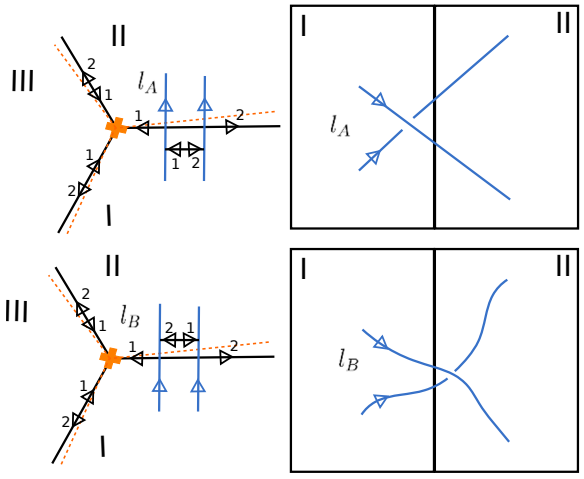

Figure 56. The first basic move in the neighborhood of a critical leaf.

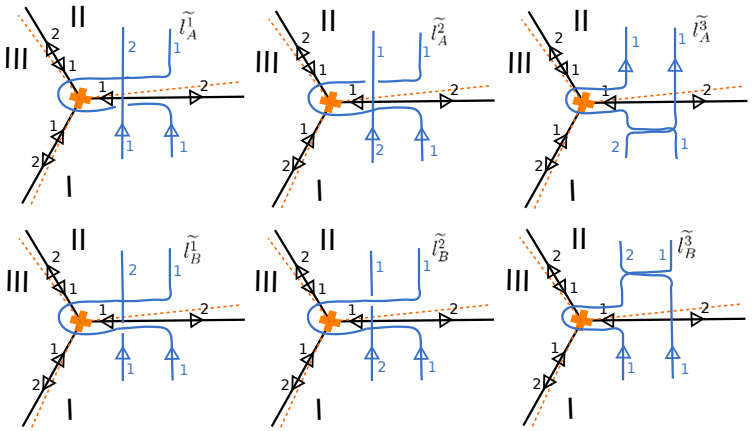

Figure 57. Three lifts of l_A and l_B making the same total contribution.

7.3.2 Height exchange for detours

In figure 58 we show another basic move in the neighborhood of a critical leaf. Here l_A has nine lifts while l_B has ten lifts in total. Eight lifts of l_A and eight lifts of l_B match on a term-by-term basis. The remaining two lifts of l_B make the same total contribution as the remaining lift of l_A. These terms are illustrated in figure 59.

Taking into account all the local factors, the weights associated to these lifts are related to each other as follows:

$$\alpha([\tilde{l}_B^2]) = (q - q^{-1})\alpha([\tilde{l}_A^1]) = (q - q^{-1})\alpha([\tilde{l}_B^1]).$$

We obtain the desired matching using the following relation in $\mathrm{Sk}(\widetilde{M}, \mathfrak{gl}(1))$:

$$[\tilde{l}_A^1] = q[\tilde{l}_B^2], \quad [\tilde{l}_B^1] = q^{-1}[\tilde{l}_B^2],$$

7.3.3 Moving a strand across a critical leaf

In this section we consider a basic isotopy where a strand is moved across a critical leaf. This is illustrated in figure 60. Here both l_A and l_B have two direct lifts with matching con-

JHEP09(2020)153

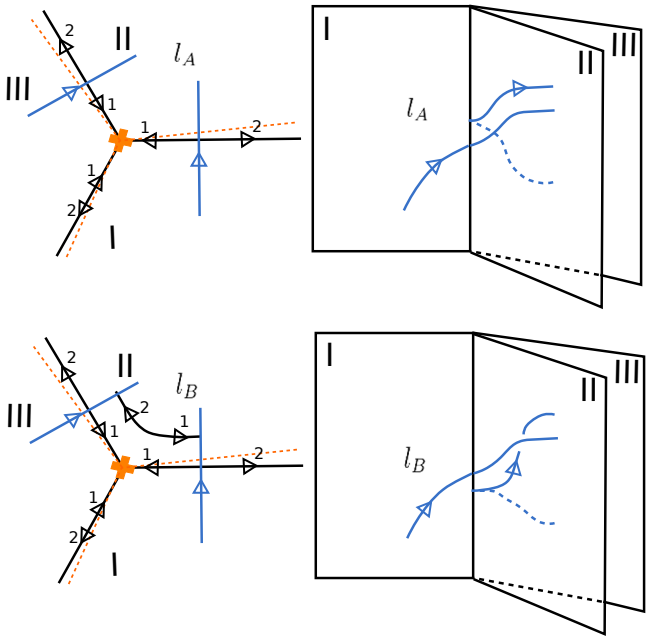

Figure 58. The height exchange for detours.

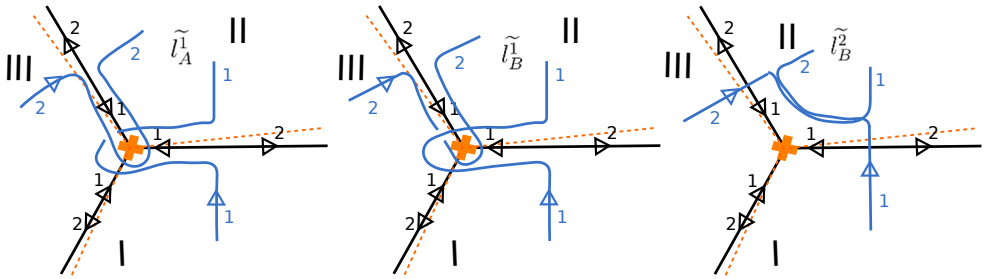

Figure 59. Two lifts of l_B which contribute the same as one lift of l_A.

tributions. l_B has two extra lifts involving detours, shown in figure 61, whose contributions cancel each other.

It is easy to see that $\widetilde{l}_B^1$ and $\widetilde{l}_B^2$ have the same winding and framing weight. However, their detour weights are inverse to each other, giving $\alpha([\widetilde{l}_B^1]) = q^{-1}\alpha([\widetilde{l}_B^2])$. Moreover, in $\mathrm{Sk}(\widetilde{M}, \mathfrak{gl}(1))$ we have $[\widetilde{l_B^1}] = -q[\widetilde{l_B^2}]$, as shown in figure 62. Combining these facts gives us the desired cancellation.

7.3.4 Moving a strand across a branch point

In this section we consider the basic isotopy where a strand is moved across a branch point. This is illustrated in figure 63.

l_A has three lifts which match three lifts of l_B on a term-by-term basis. These matching lifts are shown in figure 64. We take the pair $\widetilde{l}_A^1$ and $\widetilde{l}_B^1$ as an example. They clearly have the same winding. Moreover $\widetilde{l}_B^1$ has an extra framing factor $q^{-1/2}$ and an extra detour factor $q^{1/2}$. Therefore $\alpha([\widetilde{l}_A^1]) = \alpha([\widetilde{l}_B^1])$ and they make the same contribution to $F([l_{A,B}])$.

JHEP09(2020)153

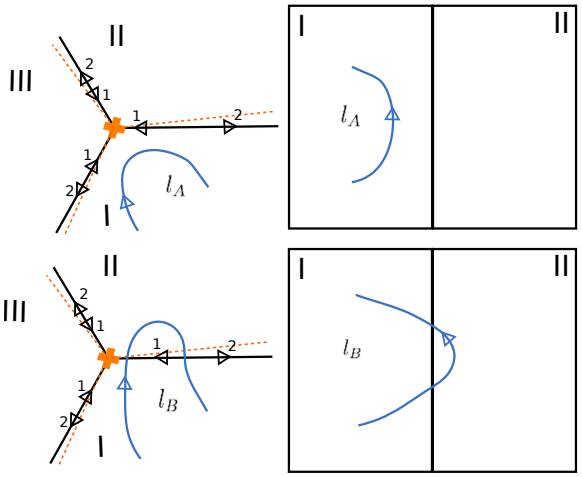

Figure 60. Moving a strand across a critical leaf.

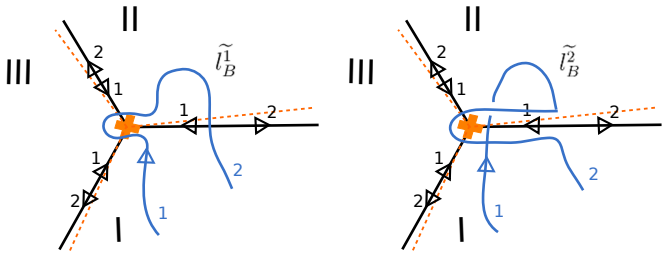

Figure 61. Two lifts of l_B whose contributions cancel each other.

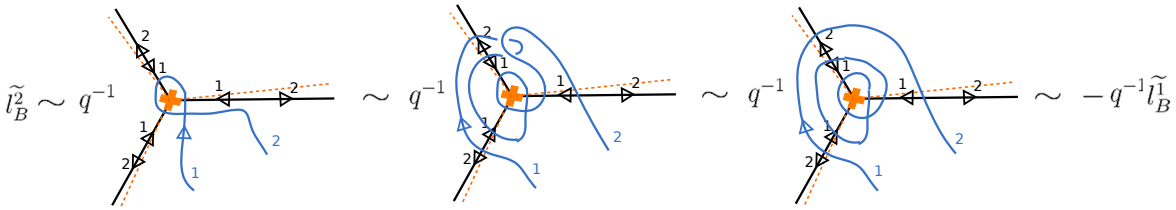

Figure 62. Moves illustrating the relation $[\widetilde{l}_B^2] = -q^{-1}[\widetilde{l}_B^1]$.

l_B also has two more lifts whose contributions are supposed to cancel with each other. These two lifts are illustrated in figure 65.

All local weights associated to $\widetilde{l}_B^4$ and $\widetilde{l}_B^5$ are the same except that $\widetilde{l}_B^5$ has an extra detour weight factor of q. Furthermore in $\mathrm{Sk}(\widetilde{M}, \mathfrak{gl}(1))$ we have $[\widetilde{l}_B^5] = -q^{-1}[\widetilde{l}_B^4]$, as shown in figure 66. Therefore the contributions from $\widetilde{l}_B^4$ and $\widetilde{l}_B^5$ cancel with each other.

7.4 The skein relations

In this section we prove that the skein relations are preserved by the q-nonabelianization map.

JHEP09(2020)153

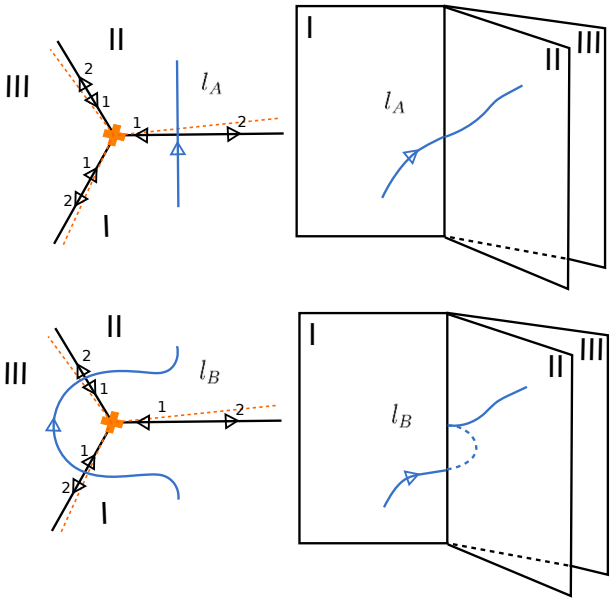

Figure 63. The fifth basic move in a neighborhood of a critical leaf. Here an open strand is moved across a branch point.

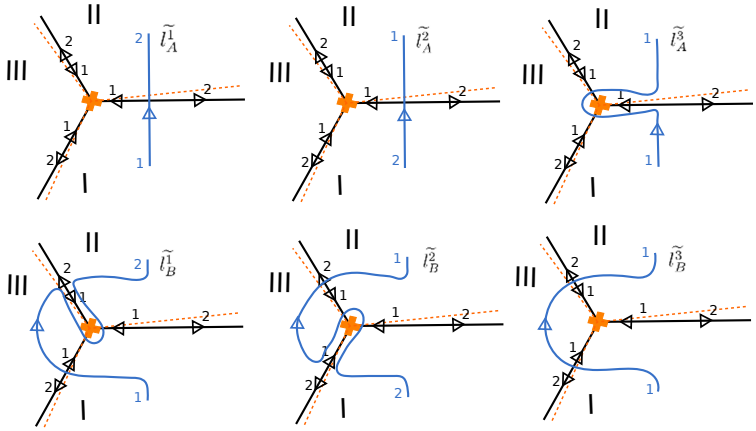

Figure 64. Three lifts of l_A and l_B with matching contributions.

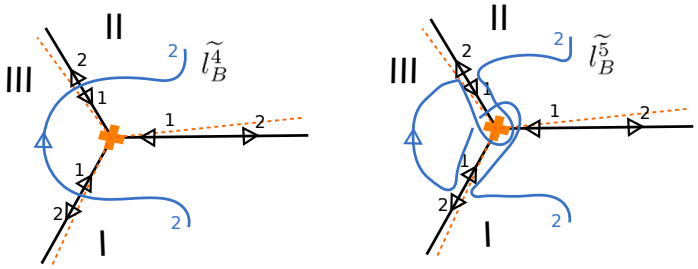

Figure 65. Two lifts of l_B whose contributions cancel with each other.

JHEP09(2020)153

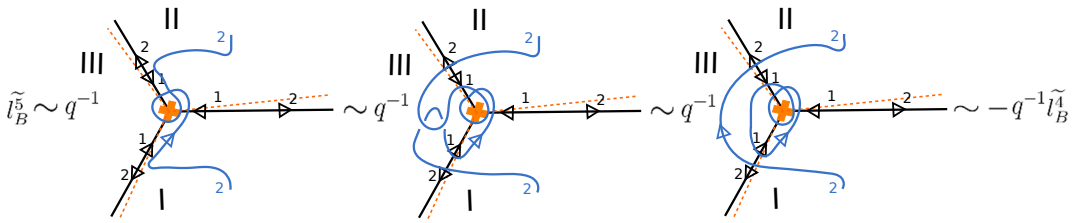

Figure 66. Moves illustrating the relation $[\widetilde{l}_B^5] = -q^{-1}[\widetilde{l}_B^4]$.

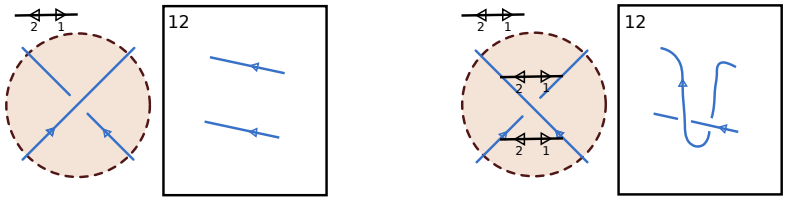

Figure 67. The two terms on the l.h.s. of skein relation (I) in $\mathrm{Sk}(M, \mathfrak{gl}(2))$. On the right, we show the loci where exchanges can occur.

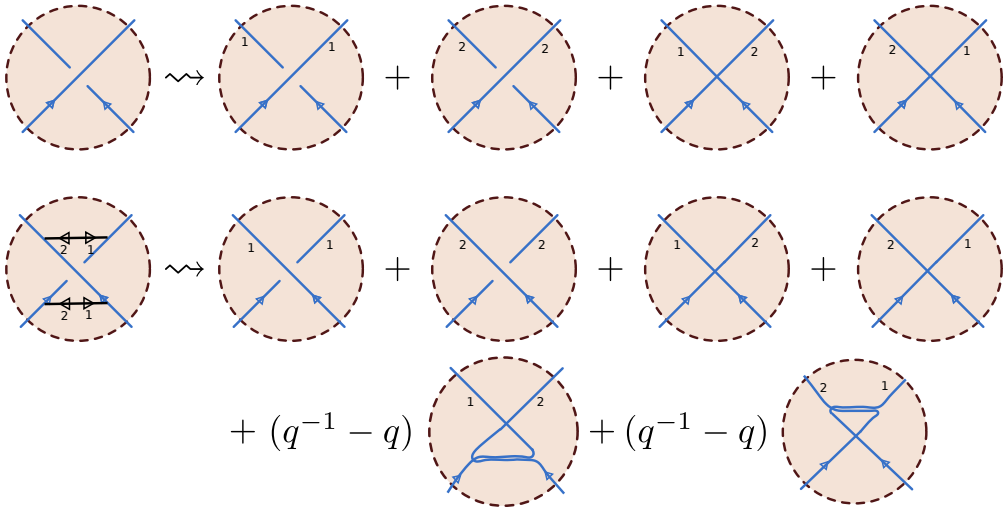

Figure 68. Applying F to the l.h.s. of skein relation (I) in $\mathrm{Sk}(M, \mathfrak{gl}(2))$.

We first look at the skein relation (I) in $\mathrm{Sk}(M, \mathfrak{gl}(2))$. Without loss of generality, we pick a specific direction for the leaves, and monotonic height profiles for the open strands,[18] as shown in figure 67.

We show lifts of these two terms in figure 68. In the second term, in addition to the direct lifts, there are two lifts involving exchanges. Now subtracting these two sets of lifts, and using the skein relations of $\mathrm{Sk}(\widetilde{M}, \mathfrak{gl}(1))$ on the r.h.s. , we get figure 69. The r.h.s. of that figure is indeed the lift of the right side of skein relation (I), as desired.

Next we consider skein relation (II) in $\mathrm{Sk}(M, \mathfrak{gl}(2))$ (the change-of-framing relation.) Again choose a generic direction for the foliation, and a simple monotonically decreasing

[18] We can safely do so as we have already proved the q-nonabelianization map is isotopy invariant.

JHEP09(2020)153

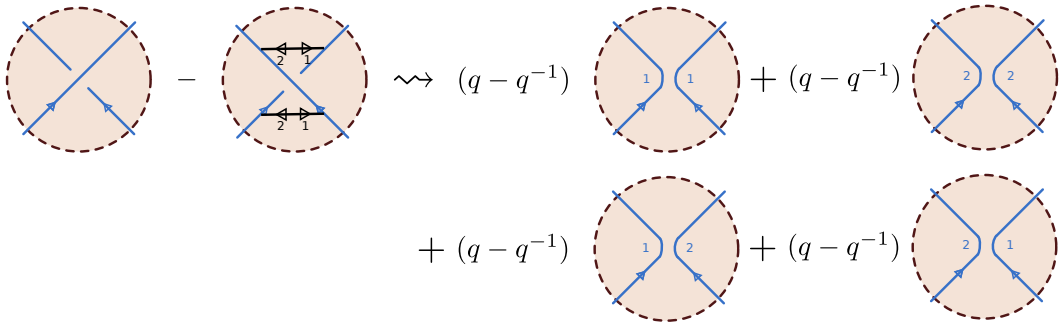

Figure 69. Applying F to the l.h.s. of skein relation (I) in $\mathrm{Sk}(M, \mathfrak{gl}(2))$.

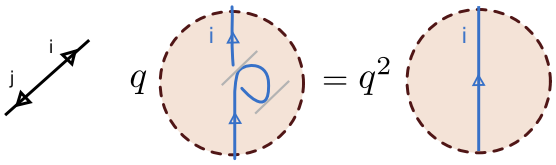

Figure 70. A direct lift of the open strand in skein relation (II), and its simplification in $\mathrm{Sk}(\widetilde{M}, \mathfrak{gl}(1))$.

height profile for the link strand. Due to the simple height profile the only lifts are direct lifts to sheet 1 and sheet 2. Each of these lifts comes with a framing fractor $q^{\frac{1}{2}} \times q^{\frac{1}{2}} = q$ from the two places where it is tangent to the foliation; combining this with the q from the skein relations in $\mathrm{Sk}(\widetilde{M}, \mathfrak{gl}(1))$ gives the desired factor q^2. This is shown in figure 70.

Finally, skein relation (III) in $\mathrm{Sk}(M, \mathfrak{gl}(2))$ follows from the fact that F assigns $q+q^{-1}$ to an unknot, which we have already checked in section 4.3 (and again in section 5.1.1.)

8 Framed wall-crossing

As we have discussed, the q-nonabelianization map for $M = C \times \mathbb{R}$ is defined using a WKB foliation associated to a covering $\widetilde{C} \to C$. As we vary the covering $\widetilde{C} \to C$ continuously, there are discrete moments at which the topology of the WKB foliation can jump. These jumps were called $\mathcal{K}$-walls in [12]. Following the topology change, the q-nonabelianization map is expected to jump according to the *framed wall-crossing* formula [11, 12, 14, 58, 63–65]. In this section we verify that this indeed happens.

8.1 The framed wall-crossing formula

Let us first quickly recall the framed wall-crossing formula.

From the point of view of the 4d $\mathcal{N} = 2$ theory $\mathfrak{X}[C, \mathfrak{g}]$, the framed wall-crossing behavior is determined by the bulk BPS spectrum. At any point in the Coulomb branch, the one-particle BPS Hilbert space is graded by the IR charge lattice Γ, $\mathcal{H} = \oplus_{\gamma \in \Gamma} \mathcal{H}_\gamma$. We factor out the center-of-mass degrees of freedom by writing

$$\mathcal{H}_\gamma = [(\mathbf{2}, \mathbf{1}) \oplus (\mathbf{1}, \mathbf{2})] \otimes h_\gamma, \tag{8.1}$$

JHEP09(2020)153

and consider the *protected spin character* [11]:

$$\Omega(\gamma, q) := \mathrm{Tr}_{h_\gamma}(-q)^{2J_3} q^{2I_3} = \sum_{n=1}^{\infty} \Omega_n(\gamma) q^n, \tag{8.2}$$

where J_3, I_3 are Cartan generators of $\mathrm{SU}(2)_P$ and $\mathrm{SU}(2)_R$ respectively. The integers $\Omega_n(\gamma)$ are conveniently packaged into the *Kontsevich-Soibelman factor*,

$$K(q; X_\gamma; \Omega_n(\gamma)) := \prod_{n=1}^{\infty} E_q\left(\sigma(\gamma)(-1)^n q^n X_\gamma\right)^{(-1)^n \Omega_n(\gamma)}, \tag{8.3}$$

where $E_q(z)$ is the quantum dilogarithm defined as

$$E_q(z) := \prod_{j=0}^{\infty} \left(1 + q^{2j+1} z\right)^{-1}, \tag{8.4}$$

and $\sigma(\gamma) = \pm 1$ is a certain quadratic refinement defined in [14]. The $\mathcal{K}$-walls are the (real codimension 1) loci in the Coulomb branch where, for some charge γ, the central charge $Z_\gamma \in \mathbb{R}_-$ and the Kontsevich-Soibelman factor $K(q; X_\gamma; \Omega_n(\gamma)) \neq 1$.

Fix a framed link L in M, and let $F_-([L])$ and $F_+([L])$ be the values of $F([L])$ before and after crossing a $\mathcal{K}$-wall in the *positive* direction, i.e. the direction in which Im Z_γ goes from negative to positive. The framed wall-crossing formula is [11, 64]:

$$F_+([L]) = K F_-([L]) K^{-1}, \qquad K := K(q; X_\gamma; \Omega_i(\gamma)). \tag{8.5}$$

In the following we will verify that our map F indeed satisfies (8.5), in the two simplest situations:

- A BPS hypermultiplet $\mathcal{K}$-wall: then $K = E_q(-X_\gamma)$ for some γ, which gives using (3.3)

$$K X_\mu K^{-1} = \begin{cases} X_\mu & \text{for } \langle \gamma, \mu \rangle = 0, \\ X_\mu \prod_{j=1}^{|\langle \gamma, \mu \rangle|} \left(1 - q^{\mathrm{sgn}(\langle \gamma, \mu \rangle)(2j-1)} X_\gamma\right)^{\mathrm{sgn}(\langle \gamma, \mu \rangle)} & \text{for } \langle \gamma, \mu \rangle \neq 0. \end{cases} \tag{8.6}$$

- A BPS vector multiplet $\mathcal{K}$-wall: then $K = E_q(-qX_\gamma) E_q(-q^{-1} X_\gamma)$ for some γ, which gives

$$K X_\mu K^{-1} = \begin{cases} X_\mu & \text{for } \langle \gamma, \mu \rangle = 0, \\ X_\mu \prod_{j=1}^{\langle \gamma, \mu \rangle} \left(1 - q^{2j} X_\gamma\right)\left(1 - q^{2j-2} X_\gamma\right) & \text{for } \langle \gamma, \mu \rangle > 0, \\ X_\mu \prod_{j=1}^{\langle \mu, \gamma \rangle} \left(1 - q^{-2j} X_\gamma\right)^{-1}\left(1 - q^{2-2j} X_\gamma\right)^{-1} & \text{for } \langle \gamma, \mu \rangle < 0. \end{cases} \tag{8.7}$$

JHEP09(2020)153

8.2 Relative skein modules

To compare F_+ to F_- it will be convenient to observe that the definition of F is local, in the following sense.

Let $M^\circ \subset M$ be a submanifold with boundary (and perhaps corners) such that no leaf meets ∂M transversely, i.e., the WKB foliation of M by 1-manifolds restricts to a foliation of ∂M by 1-manifolds. Also fix a 0-chain S in ∂M°, given by a finite subset of ∂M° with each point labeled by ± 1. Then we can define a relative skein module $\mathrm{Sk}(M^\circ, S, \mathfrak{gl}(2))$, by applying exactly the rules of section 3.1, except that instead of oriented links L, we use oriented tangles L, with boundary $\partial L = S$. Also let $\widetilde{M}^\circ \to M^\circ$ be the branched double cover of M° obtained by restricting $\widetilde{M} \to M$. Then we define a relative skein module $\mathrm{Sk}(M^\circ, S, \mathfrak{gl}(1))$ by applying again the rules of section 3.2 to oriented tangles $\widetilde{L}$, where we allow $\partial\widetilde{L}$ to be any 0-chain which projects to S. Our construction of F applies directly in this relative situation, to give a map

$$F : \mathrm{Sk}(M^\circ, S, \mathfrak{gl}(2)) \to \mathrm{Sk}(\widetilde{M}^\circ, S, \mathfrak{gl}(1)). \tag{8.8}$$

Now we can formulate the crucial locality property of F. Suppose M° is obtained by gluing M_1° and M_2° along part of their boundary, and $L \subset M^\circ$ is a link, divided into $L_1 = L \cap M_1^\circ$ and $L_2 = L \cap M_2^\circ$. Then we have

$$F_{M^\circ}(L) = F_{M_1^\circ}(L_1) \cdot F_{M_2^\circ}(L_2) \tag{8.9}$$

where the $\cdot$ on the right is defined by concatenation of tangles.

The relative skein module $\mathrm{Sk}(\widetilde{M}^\circ, S, \mathfrak{gl}(1))$ is a two-sided module over the (absolute) skein algebra $\mathrm{Sk}(\widetilde{M}^\circ, \mathfrak{gl}(1))$. For each relative homology class a we define an element $X_a \in \mathrm{Sk}(\widetilde{M}^\circ, S, \mathfrak{gl}(1))$, by the same rule we used to define X_γ for ordinary homology classes γ in section 3.5. Then we have the analog of (3.3),

$$X_\gamma X_a = (-q)^{\langle \gamma, a \rangle} X_{\gamma + a}. \tag{8.10}$$

8.3 The hypermultiplet $\mathcal{K}$-wall

We begin by considering a hypermultiplet $\mathcal{K}$-wall.

The transformation of the WKB foliation which occurs at such a $\mathcal{K}$-wall is described in [12]. The only nontrivial change occurs in the neighborhood of a saddle connection on C, as shown in figure 71.

Let C° denote the region shown in figure 71, and let $l_1, \ldots, l_m$ be the components of the intersection $L \cap (C^\circ \times \mathbb{R})$. By an isotopy of L, we may assume that each l_n crosses C° in one of the simple ways shown in figure 72.

Moreover, we may assume that each l_n has x^3-coordinate monotonically increasing from a_n to b_n, with $b_n < a_{n+1}$. Then we divide M into the disjoint regions $M_n^\circ = C^\circ \times [a_n, b_n]$ and the complementary region M_0°. We will prove that, in each region M_n°, we have

$$F_{M_n^\circ, +}(l_n) = K F_{M_n^\circ, -}(l_n) K^{-1}, \tag{8.11}$$

JHEP09(2020)153

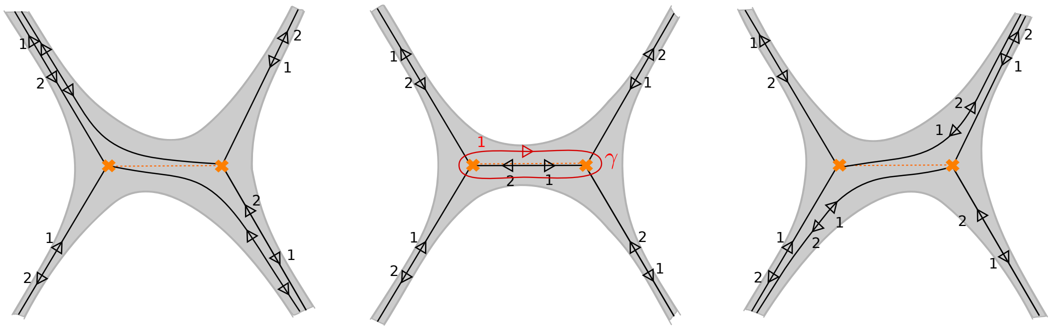

Figure 71. A region C° of C bounded by generic leaves of the WKB foliation, and the critical leaves contained therein, before (left) and after (right) crossing a hypermultiplet $\mathcal{K}$-wall. The charge γ of the hypermultiplet is also shown.

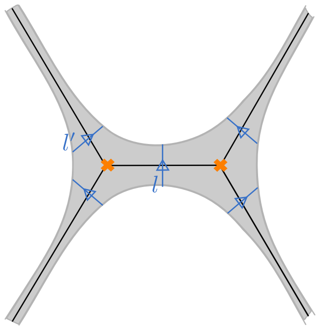

Figure 72. Five ways in which the projection of L could cross C°; by an isotopy of L we can arrange that all crossings are of one of these five types.

where the conjugation acts concretely by (8.6), and in M_0° we have

$$F_{M_0^\circ,+}(l_n) = F_{M_0^\circ,-}(l_n). \tag{8.12}$$

Using the locality of F this then implies the desired formula (8.5).

First we consider the region M_0°. In this region the topology of the WKB foliation does not change as we cross the $\mathcal{K}$-wall; (8.12) follows directly.

Next we consider a region M_n° containing an open strand l_n isotopic to the l in figure 72. l has five lifts $\tilde{l}^1, \ldots, \tilde{l}^5$ either before or after crossing the $\mathcal{K}$-wall, as shown in figure 73. Using p^i for the standard projection of $\tilde{l}^i$, $F_\pm([l])$ are:

$$F_-([l]) = \sum_{i=1}^{4} q^{w_i} X_{p^i} + q^{w_2} X_{p^2+\gamma} = q^{w_1} X_{p^1} + q^{w_2} X_{p^2}(1 - q^{-1} X_\gamma) + \sum_{i=3,4} q^{w_i} X_{p^i}, \tag{8.13}$$

$$F_+([l]) = \sum_{i=1}^{4} q^{w_i} X_{p^i} + q^{w_1} X_{p^1+\gamma} = q^{w_1} X_{p^1}(1 - q X_\gamma) + q^{w_2} X_{p^2} + \sum_{i=3,4} q^{w_i} X_{p^i}, \tag{8.14}$$

where w_i is the winding of p^i and we have used (8.10) to rewrite $F_\pm([l])$. Now (8.14) is obtained from (8.13) by the substitutions $X_{p^1} \to X_{p^1}(1 - qX_\gamma)$, $X_{p^2} \to X_{p^2}(1 - q^{-1}X_\gamma)^{-1}$, leaving all other X_a alone; this matches the expected (8.11).

JHEP09(2020)153

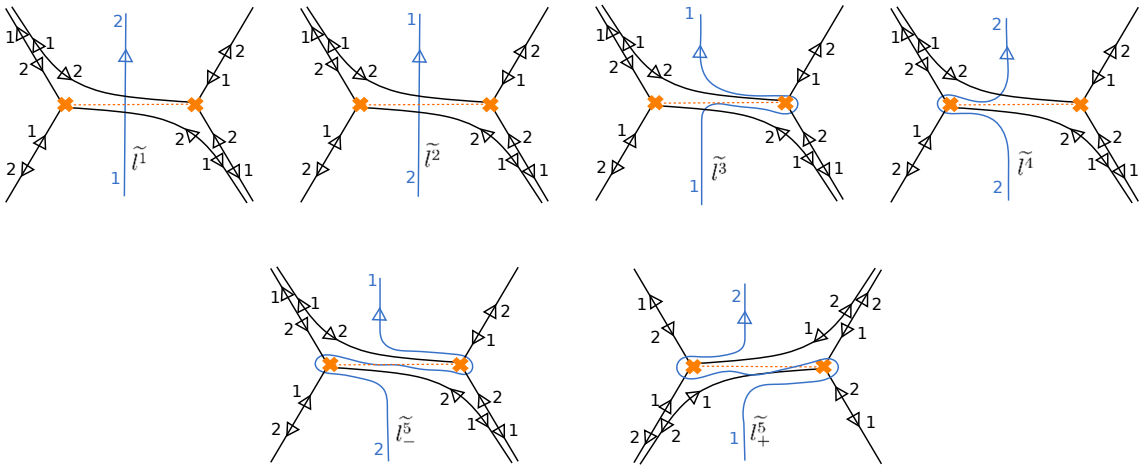

Figure 73. Top: four lifts $\tilde{l}^1, \ldots, \tilde{l}^4$ of the open strand l which are present both before and after the flip. Bottom left: a lift $\tilde{l}^5_-$ which is present only before the flip. Bottom right: a lift $\tilde{l}^5_+$ which is present only after the flip.

Finally we consider a region M_n° containing an open strand l_n isotopic to the l' in figure 72. There are two direct lifts of l', which are the same on both sides of the $\mathcal{K}$-wall; we denote their standard projections p^2, p^3. On the $+$ side of the wall there is one lift containing a detour, with standard projection p^1. On the $-$ side there are two lifts containing detours. Altogether we find:

$$F_+([l']) = q^{w_1} X_{p^1} + \sum_{i=2,3} q^{w_i} X_{p^i},$$
$$F_-([l']) = q^{w_1}(X_{p^1} + X_{p^1+\gamma}) + \sum_{i=2,3} q^{w_i} X_{p^i} = q^{w_1} X_{p^1}(1 - q^{-1} X_\gamma) + \sum_{i=2,3} q^{w_i} X_{p^i}.$$

This again agrees with the expected (8.11), using $\langle \gamma, p^1 \rangle = -1$, $\langle \gamma, p^2 \rangle = 0$, $\langle \gamma, p^3 \rangle = 0$.

8.4 The vector multiplet $\mathcal{K}$-wall

Now we turn to the vector multiplet $\mathcal{K}$-wall, where the WKB foliation develops an annulus of closed trajectories. Here the transformation of the WKB foliation which occurs at the wall is subtler to describe. As described in [12, 14], as we approach the $\mathcal{K}$-wall from either direction, the WKB foliation in the annulus undergoes an infinite sequence of flips, which accumulate at the $\mathcal{K}$-wall. The $F_\pm$ we are after in this case therefore have to be understood as the *limits* of F as we approach the $\mathcal{K}$-wall from the two sides. Moreover, the meaning of $F_\pm$ is a bit subtle: they involve infinite sums of terms, so they really lie in some completion of the skein module; we will optimistically gloss over this point here, so what we are really giving here is a proof sketch rather than a complete proof.

Similarly to the classical case discussed in [12], we can compute $F_\pm([l])$ by considering the limiting behavior of the critical leaves of the foliation as we approach the wall. A schematic picture of the limits is shown in figure 74 (see also [12, 14] for more such pictures). The degenerated critical leaves wind infinitely many times around the annulus. Concretely

JHEP09(2020)153

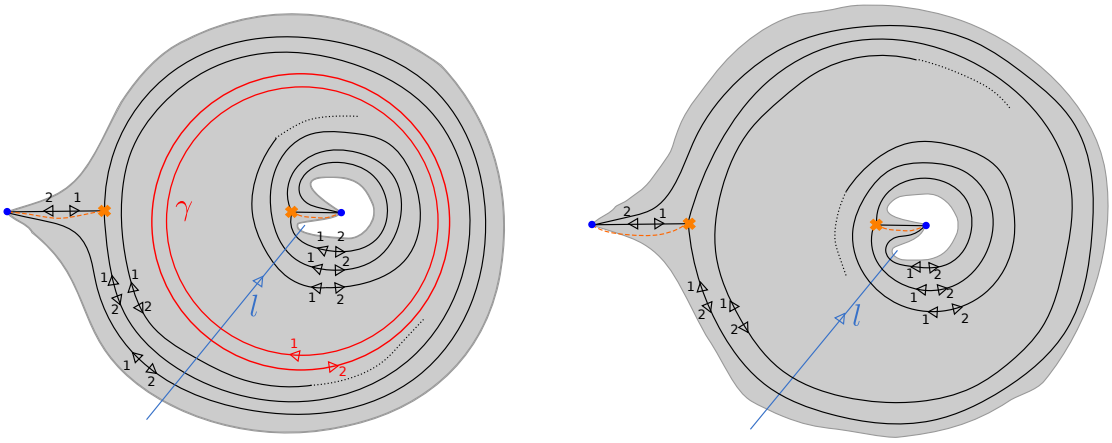

Figure 74. A region C° of C bounded by generic leaves of the WKB foliation, and degenerated versions of the WKB foliation contained therein, immediately before (left) and after (right) crossing a vector multiplet $\mathcal{K}$-wall. The picture is a bit schematic; the leaves which end in dotted lines should be understood as winding infinitely many times around the annulus, and l crosses each of these leaves infinitely many times. The charge γ of the vector multiplet is also shown on the left.

speaking, to compute $F_\pm([l])$, we sum over direct lifts and detours along critical leaves in the usual way; the only tricky point is that even for a compact l, $F_\pm([l])$ may involve an infinite sum over detours, since l may meet one of the degenerated critical leaves infinitely many times.

Now we follow the same strategy we used for the hypermultiplet. The key computation is to compare the two limits $F_\pm([l])$, where l is an open strand crossing C° as shown in figure 74, with its x^3-coordinate increasing monotonically.

We need some notation for various paths in C°. Let $a_{12}, a_{21}, b_{12}, b_{21}$ be the detour paths shown in figure 75. Let p^1, p^2 be the standard projection of the direct lifts of l to sheet 1, 2 respectively. Finally, divide each p^i into initial, middle and final segments p^i_-, p^i_0, p^i_+ respectively, in such a way that the following paths are connected:

$$
\begin{aligned}
p^{11} &:= p^1_- + a_{12} + p^2_0 + b_{21} + p^1_+, \quad p^{22} := p^2_- + a_{21} + p^1_0 + b_{12} + p^2_+, \\
p^{12} &:= p^1_- + a_{12} + p^2_0 + p^2_+, \quad p'^{12} := p^1_- + p^1_0 + b_{12} + p^2_+, \\
p^{21} &:= p^2_- + a_{21} + p^1_0 + p^1_+, \quad p'^{21} := p^2_- + p^2_0 + b_{21} + p^1_+.
\end{aligned}
$$

Let $F_\pm([l])^{(ij)}$ $(i, j \in \{1, 2\})$ be the contribution to $F_\pm([l])$ from lifts that start on sheet i and end on sheet j. For example, one lift of l that contributes to $F_-([l])^{(12)}$ is shown in figure 76. Let w^{ij} be the winding of the corresponding open strands in $\widetilde{C}$.[19] A direct

[19]Due to the monotonic height profile, the lift in the class $p + n\gamma$ has the same winding as the lift in the class p.

JHEP09(2020)153

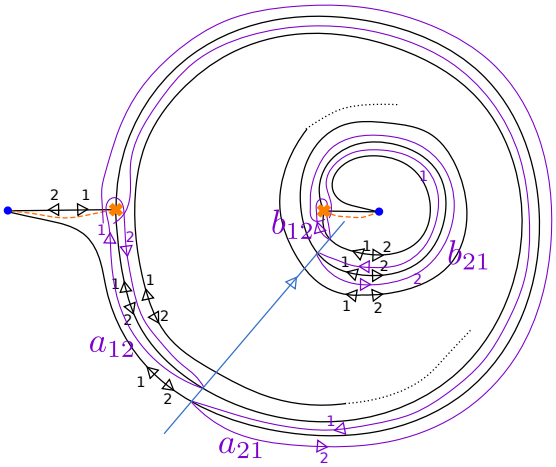

Figure 75. Basic constituents of open paths $\{p\}$ on $\widetilde{C}$. The (minimal) detours $a_{12}, a_{21}, b_{12}, b_{21}$ are shown in purple.

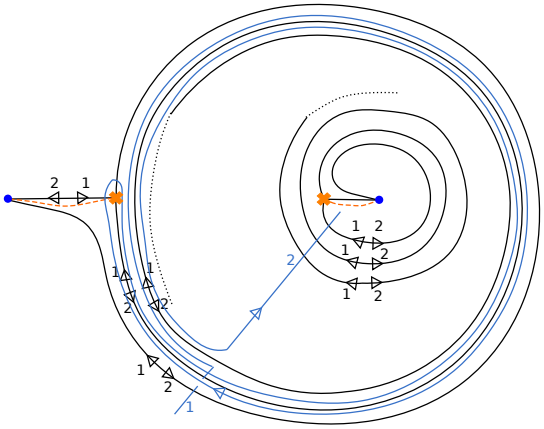

Figure 76. One of the lifts contributing to $F_-([l])^{(12)}$. This specific lift contributes $-q^{w^{12}-\frac{3}{2}}X_{p^{12}+\gamma}$.

enumeration of all the allowed lifts gives:

$$\begin{aligned} F_-([l])^{(11)} &= q^{w^{11}}\left(X_{p^1}+\sum_{n_1,n_2=0}^{\infty}(-q)^{-n_1+n_2}X_{p^{11}+(n_1+n_2)\gamma}\right) \\ &= q^{w^{11}}\left(X_{p^1}+X_{p^{11}}\frac{1}{1-X_\gamma}\frac{1}{1-q^2X_\gamma}\right), \\ F_+([l])^{(11)} &= q^{w^{11}}\left(\sum_{n_1,n_2=0}^{\infty}(-q)^{-n_1+n_2}X_{p^1+(n_1+n_2)\gamma}+X_{p^{11}}\right) \\ &= q^{w^{11}}\left(X_{p^1}\frac{1}{1-X_\gamma}\frac{1}{1-q^2X_\gamma}+X_{p^{11}}\right), \end{aligned}$$

JHEP09(2020)153

$$
\begin{aligned}
F_-([l])^{(22)} &= q^{w^{22}}\left(\sum_{n_1,n_2=0}^{\infty}(-q)^{-n_1+n_2}X_{p^2+(n_1+n_2)\gamma}+X_{p^{22}}\right)\\
&= q^{w^{22}}\left(X_{p^2}\frac{1}{1-X_\gamma}\frac{1}{1-q^2X_\gamma}+X_{p^{22}}\right),\\
F_+([l])^{(22)} &= q^{w^{22}}\left(X_{p^2}+\sum_{n_1,n_2=0}^{\infty}(-q)^{-n_1+n_2}X_{p^{22}+(n_1+n_2)\gamma}\right)\\
&= q^{w^{22}}\left(X_{p^2}+X_{p^{22}}\frac{1}{1-X_\gamma}\frac{1}{1-q^2X_\gamma}\right),\\
F_-([l])^{(12)} &= q^{w^{12}-\frac{1}{2}}\left(\sum_{n_1,n_2=0}^{\infty}(-q)^{-n_1+n_2}X_{p^{12}+(n_1+n_2)\gamma}+X_{p'^{12}}\right)\\
&= q^{w^{12}-\frac{1}{2}}\left(X_{p^{12}}\frac{1}{1-X_\gamma}\frac{1}{1-q^2X_\gamma}+X_{p'^{12}}\right),\\
F_+([l])^{(12)} &= q^{w^{12}-\frac{1}{2}}\left(X_{p^{12}}+\sum_{n_1,n_2=0}^{\infty}(-q)^{-n_1+n_2}X_{p'^{12}+(n_1+n_2)\gamma}\right)\\
&= q^{w^{12}-\frac{1}{2}}\left(X_{p^{12}}+X_{p'^{12}}\frac{1}{1-X_\gamma}\frac{1}{1-q^2X_\gamma}\right),\\
F_-([l])^{(21)} &= q^{w^{21}+\frac{1}{2}}\left(X_{p^{21}}+\sum_{n_1,n_2=0}^{\infty}(-q)^{-n_1+n_2}X_{p'^{21}+(n_1+n_2)\gamma}\right)\\
&= q^{w^{21}+\frac{1}{2}}\left(X_{p^{21}}+X_{p'^{21}}\frac{1}{1-X_\gamma}\frac{1}{1-q^2X_\gamma}\right),\\
F_+([l])^{(21)} &= q^{w^{21}+\frac{1}{2}}\left(\sum_{n_1,n_2=0}^{\infty}(-q)^{-n_1+n_2}X_{p^{21}+(n_1+n_2)\gamma}+X_{p'^{21}}\right)\\
&= q^{w^{21}+\frac{1}{2}}\left(X_{p^{21}}\frac{1}{1-X_\gamma}\frac{1}{1-q^2X_\gamma}+X_{p'^{21}}\right).
\end{aligned}
$$

From these expressions one sees directly that $F_+([l]) = KF_-([l])K^{-1}$, with K given by (8.7), as desired.

9 Reduction to $\mathfrak{sl}(2)$

9.1 The Kauffman bracket skein module

In this final section we briefly discuss the $\mathfrak{sl}(2)$ variant of the skein module, which we denote $\mathrm{Sk}(M,\mathfrak{sl}(2))$; it is also known as the Kauffman bracket skein module (see [66] for a review). In this version of the skein module we use unoriented links and $\mathbb{Z}[(-q)^{\frac{1}{2}},(-q)^{-\frac{1}{2}}]$ coefficients; the skein relations are shown in figure 77. Reflecting the relation $\mathfrak{gl}(2) = \mathfrak{sl}(2)\oplus\mathfrak{gl}(1)$ there is a map of skein modules

$$
\mathrm{Sk}(M,\mathfrak{gl}(2)) \;\to\; \mathrm{Sk}(M,\mathfrak{sl}(2))\otimes \mathrm{Sk}^{\frac{1}{2}}(M,\mathfrak{gl}(1)), \tag{9.1}
$$

JHEP09(2020)153

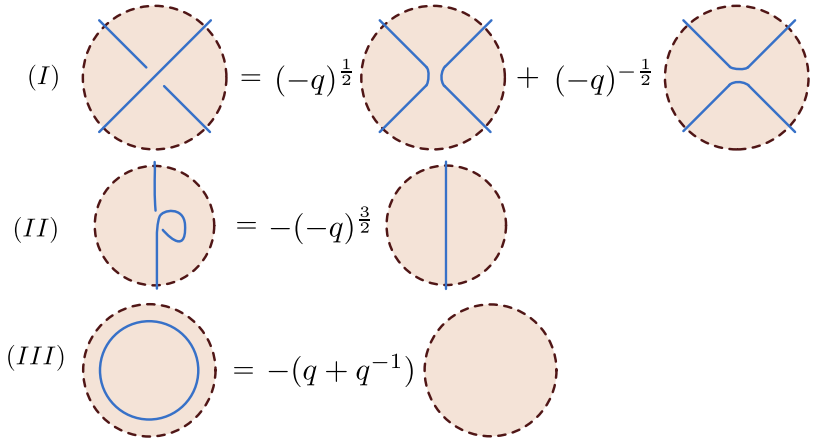

Figure 77. Skein relations defining $\mathrm{Sk}(M, \mathfrak{sl}(2))$.

where by $\mathrm{Sk}^{\frac{1}{2}}$ we mean the skein module with the replacement $q \mapsto -(-q)^{\frac{1}{2}}$. The map is given by the obvious operation, $[L] \mapsto [L] \otimes [L]$, which one can check directly respects the skein relations.

9.2 Factorization of q-nonabelianization, for $M = C \times \mathbb{R}$

Now suppose $M = C \times \mathbb{R}$. Let $\Gamma = H_1(\widetilde{C}, \mathbb{Z})$, and let σ be the involution on Γ induced by the deck transformation of $\widetilde{C}$. Then we have the map

$$\begin{aligned} \Gamma &\to \frac{1}{2}\Gamma^{\mathrm{odd}} \times \frac{1}{2}\Gamma^{\mathrm{even}} \\ \gamma &\mapsto \left(\frac{1}{2}(\gamma - \sigma(\gamma)), \frac{1}{2}(\gamma + \sigma(\gamma))\right), \end{aligned} \tag{9.2}$$

which preserves the pairings and thus induces a map

$$Q_\Gamma \to Q_{\frac{1}{2}\Gamma^{\mathrm{odd}}} \otimes Q_{\frac{1}{2}\Gamma^{\mathrm{even}}}, \tag{9.3}$$

where the quantum tori $Q_{\frac{1}{2}\Gamma^{\mathrm{odd}}}$, $Q_{\frac{1}{2}\Gamma^{\mathrm{even}}}$ are algebras over $\mathbb{Z}[(-q)^{\pm\frac{1}{4}}]$, because the intersection pairings on these lattices take values in $\frac{1}{4}\mathbb{Z}$.

We conjecture that the q-nonabelianization map F can be factorized into odd and even parts, or more precisely, that there is a commuting diagram

$$\begin{array}{ccc} \mathrm{Sk}(M, \mathfrak{gl}(2)) & \xrightarrow{\quad F \quad} & \mathrm{Sk}(\widetilde{M}, \mathfrak{gl}(1)) = Q_\Gamma \\ \downarrow & & \downarrow \\ \mathrm{Sk}(M, \mathfrak{sl}(2)) \otimes \mathrm{Sk}^{\frac{1}{2}}(M, \mathfrak{gl}(1)) & \xrightarrow{F^{\mathrm{odd}} \otimes F^{\mathrm{even}}} & Q_{\frac{1}{2}\Gamma^{\mathrm{odd}}} \otimes Q_{\frac{1}{2}\Gamma^{\mathrm{even}}}, \end{array} \tag{9.4}$$

where

$$F^{\mathrm{even}}([L]) = q^{\frac{1}{2}w(L)} X_{\frac{1}{2}\pi^{-1}(L)}, \tag{9.5}$$

$$F^{\mathrm{odd}}([L]) = q^{-\frac{1}{2}w(L)} \rho(F([L])), \qquad \rho(X_\gamma) = X_{\frac{1}{2}(\gamma - \sigma(\gamma))}, \tag{9.6}$$

JHEP09(2020)153

and the map F^{odd} coincides with the quantum trace map of [1]. One approach to verifying this factorization would be to interpret $Q_{\frac{1}{2}\Gamma^{\text{odd}}}$ directly as a variant of the skein module which includes factors associated to non-local crossings. We will not undertake this verification here, but remark that a similar comparison (between the approach of [3] to q-nonabelianization and the quantum trace of [1]) was carried out in [55].

Acknowledgments

We thank Dylan Allegretti, Jørgen Andersen, Sungbong Chun, Clay Córdova, Davide Gaiotto, Po-Shen Hsin, Saebyeok Jeong, David Jordan, Pietro Longhi, Rafe Mazzeo, Gregory Moore, Du Pei, Pavel Putrov, Shu-Heng Shao, and Masahito Yamazaki for extremely helpful discussions. We thank Dylan Allegretti, Pietro Longhi, Gregory Moore, and Du Pei for extremely helpful comments on a draft. AN is supported in part by NSF grant DMS-1711692. FY is supported by DOE grant DE-SC0010008. This work benefited from the 2019 Pollica summer workshop, which was supported in part by the Simons Collaboration on the Non-Perturbative Bootstrap and in part by the INFN.

References

[1] F. Bonahon and H. Wong, *Quantum traces for representations of surface groups in SL_2*, *Geom. Topol.* **15** (2011) 1569 [arXiv:1003.5250v4].

[2] D. Galakhov, P. Longhi and G.W. Moore, *Spectral Networks with Spin*, *Commun. Math. Phys.* **340** (2015) 171 [arXiv:1408.0207] [INSPIRE].

[3] M. Gabella, *Quantum Holonomies from Spectral Networks and Framed BPS States*, *Commun. Math. Phys.* **351** (2017) 563 [arXiv:1603.05258] [INSPIRE].

[4] D. Gaiotto and E. Witten, *Knot Invariants from Four-Dimensional Gauge Theory*, *Adv. Theor. Math. Phys.* **16** (2012) 935 [arXiv:1106.4789] [INSPIRE].

[5] E. Witten, *Fivebranes and Knots*, arXiv:1101.3216 [INSPIRE].

[6] H. Ooguri and C. Vafa, *Knot invariants and topological strings*, *Nucl. Phys. B* **577** (2000) 419 [hep-th/9912123] [INSPIRE].

[7] S. Gukov, A.S. Schwarz and C. Vafa, *Khovanov-Rozansky homology and topological strings*, *Lett. Math. Phys.* **74** (2005) 53 [hep-th/0412243] [INSPIRE].

[8] S. Chun, S. Gukov and D. Roggenkamp, *Junctions of surface operators and categorification of quantum groups*, arXiv:1507.06318 [INSPIRE].

[9] N. Drukker, D.R. Morrison and T. Okuda, *Loop operators and S-duality from curves on Riemann surfaces*, *JHEP* **09** (2009) 031 [arXiv:0907.2593] [INSPIRE].

[10] N. Drukker, J. Gomis, T. Okuda and J. Teschner, *Gauge Theory Loop Operators and Liouville Theory*, *JHEP* **02** (2010) 057 [arXiv:0909.1105] [INSPIRE].

JHEP09(2020)153

[11] D. Gaiotto, G.W. Moore and A. Neitzke, *Framed BPS States*, *Adv. Theor. Math. Phys.* **17** (2013) 241 [arXiv:1006.0146] [INSPIRE].

[12] D. Gaiotto, G.W. Moore and A. Neitzke, *Spectral networks*, *Annales Henri Poincaré* **14** (2013) 1643 [arXiv:1204.4824] [INSPIRE].

[13] T. Dimofte, D. Gaiotto and S. Gukov, *3-Manifolds and 3d Indices*, *Adv. Theor. Math. Phys.* **17** (2013) 975 [arXiv:1112.5179] [INSPIRE].

[14] D. Gaiotto, G.W. Moore and A. Neitzke, *Wall-crossing, Hitchin Systems, and the WKB Approximation*, arXiv:0907.3987 [INSPIRE].

[15] T. Dimofte, D. Gaiotto and S. Gukov, *Gauge Theories Labelled by Three-Manifolds*, *Commun. Math. Phys.* **325** (2014) 367 [arXiv:1108.4389] [INSPIRE].

[16] S. Cecotti, C. Cordova and C. Vafa, *Braids, Walls, and Mirrors*, arXiv:1110.2115 [INSPIRE].

[17] I. Coman, M. Gabella and J. Teschner, *Line operators in theories of class $\mathcal{S}$, quantized moduli space of flat connections, and Toda field theory*, *JHEP* **10** (2015) 143 [arXiv:1505.05898] [INSPIRE].

[18] Y. Tachikawa and N. Watanabe, *On skein relations in class S theories*, *JHEP* **06** (2015) 186 [arXiv:1504.00121] [INSPIRE].

[19] P. Longhi, *Wall-Crossing Invariants from Spectral Networks*, *Annales Henri Poincaré* **19** (2018) 775 [arXiv:1611.00150] [INSPIRE].

[20] K. Zarembo, *Supersymmetric Wilson loops*, *Nucl. Phys. B* **643** (2002) 157 [hep-th/0205160] [INSPIRE].

[21] D. Gaiotto, $N = 2$ *dualities*, *JHEP* **08** (2012) 034 [arXiv:0904.2715] [INSPIRE].

[22] C. Cordova and T. Dumitrescu, *Current algebra constraints on BPS particles*, to appear.

[23] D.G.L. Allegretti, *A duality map for the quantum symplectic double*, arXiv:1605.01599 [INSPIRE].

[24] S.Y. Cho, H. Kim, H.K. Kim and D. Oh, *Laurent Positivity of Quantized Canonical Bases for Quantum Cluster Varieties from Surfaces*, *Commun. Math. Phys.* **373** (2019) 655 [arXiv:1710.06217] [INSPIRE].

[25] D. Galakhov and G.W. Moore, *Comments On The Two-Dimensional Landau-Ginzburg Approach To Link Homology*, arXiv:1607.04222 [INSPIRE].

[26] T. Ekholm and V. Shende, *Skeins on Branes*, arXiv:1901.08027 [INSPIRE].

[27] T. Dimofte, M. Gabella and A.B. Goncharov, *K-Decompositions and 3d Gauge Theories*, *JHEP* **11** (2016) 151 [arXiv:1301.0192] [INSPIRE].

[28] D. Freed and A. Neitzke, *3d spectral networks*, to appear.

[29] D. Nadler and E. Zaslow, *Constructible sheaves and the Fukaya category*, math/0604379.

[30] D. Nadler, *Microlocal branes are constructible sheaves*, math/0612399.

[31] X. Jin, *Holomorphic lagrangian branes correspond to perverse sheaves*, *Geom. Topol.* **19** (2015) 1685 [arXiv:1311.3756].

[32] D. Ben-Zvi, A. Brochier and D. Jordan, *Integrating quantum groups over surfaces*, arXiv:1501.04652 [INSPIRE].

JHEP09(2020)153

[33] D. Ben-Zvi, A. Brochier and D. Jordan, *Quantum character varieties and braided module categories*, arXiv:1606.04769.

[34] I. Ganev, D. Jordan and P. Safronov, *The quantum frobenius for character varieties and multiplicative quiver varieties*, arXiv:1901.11450.

[35] S. Gunningham, D. Jordan and P. Safronov, *The finiteness conjecture for skein modules*, arXiv:1908.05233 [INSPIRE].

[36] D. Gaiotto, G.W. Moore and E. Witten, *Algebra of the Infrared: String Field Theoretic Structures in Massive $\mathcal{N} = (2,2)$ Field Theory In Two Dimensions*, arXiv:1506.04087 [INSPIRE].

[37] C. Córdova and A. Neitzke, *Line Defects, Tropicalization, and Multi-Centered Quiver Quantum Mechanics*, *JHEP* **09** (2014) 099 [arXiv:1308.6829] [INSPIRE].

[38] M. Cirafici, *Line defects and (framed) BPS quivers*, *JHEP* **11** (2013) 141 [arXiv:1307.7134] [INSPIRE].

[39] W.-y. Chuang, D.-E. Diaconescu, J. Manschot, G.W. Moore and Y. Soibelman, *Geometric engineering of (framed) BPS states*, *Adv. Theor. Math. Phys.* **18** (2014) 1063 [arXiv:1301.3065] [INSPIRE].

[40] M.R. Douglas and G.W. Moore, *D-branes, quivers, and ALE instantons*, hep-th/9603167 [INSPIRE].

[41] M.R. Douglas, B. Fiol and C. Romelsberger, *Stability and BPS branes*, *JHEP* **09** (2005) 006 [hep-th/0002037] [INSPIRE].

[42] M.R. Douglas, B. Fiol and C. Romelsberger, *The Spectrum of BPS branes on a noncompact Calabi-Yau*, *JHEP* **09** (2005) 057 [hep-th/0003263] [INSPIRE].

[43] S. Cecotti, A. Neitzke and C. Vafa, *R-Twisting and 4d/2d Correspondences*, arXiv:1006.3435 [INSPIRE].

[44] M. Alim, S. Cecotti, C. Cordova, S. Espahbodi, A. Rastogi and C. Vafa, *$\mathcal{N} = 2$ quantum field theories and their BPS quivers*, *Adv. Theor. Math. Phys.* **18** (2014) 27 [arXiv:1112.3984] [INSPIRE].

[45] S. Cecotti and M. Del Zotto, *On Arnold's 14 'exceptional' $N = 2$ superconformal gauge theories*, *JHEP* **10** (2011) 099 [arXiv:1107.5747] [INSPIRE].

[46] M. Del Zotto, *More Arnold's $N = 2$ superconformal gauge theories*, *JHEP* **11** (2011) 115 [arXiv:1110.3826] [INSPIRE].

[47] M. Cirafici and M. Del Zotto, *Discrete Integrable Systems, Supersymmetric Quantum Mechanics, and Framed BPS States — I*, arXiv:1703.04786 [INSPIRE].

[48] M. Cirafici, *Quivers, Line Defects and Framed BPS Invariants*, *Annales Henri Poincaré* **19** (2018) 1 [arXiv:1703.06449] [INSPIRE].

[49] M. Cirafici, *On Framed Quivers, BPS Invariants and Defects*, arXiv:1801.03778 [INSPIRE].

[50] M. Cirafici, *Quantum Line Defects and Refined BPS Spectra*, *Lett. Math. Phys.* **110** (2019) 501 [arXiv:1902.08586] [INSPIRE].

[51] M. Gabella, P. Longhi, C.Y. Park and M. Yamazaki, *BPS Graphs: From Spectral Networks to BPS Quivers*, *JHEP* **07** (2017) 032 [arXiv:1704.04204] [INSPIRE].

JHEP09(2020)153

[52] D. Gang, P. Longhi and M. Yamazaki, S *duality and framed BPS states via BPS graphs*, *Adv. Theor. Math. Phys.* **23** (2019) 1361 [arXiv:1711.04038] [INSPIRE].

[53] T.T.Q. Le, *Quantum Teichmüller spaces and quantum trace map*, arXiv:1511.06054 [INSPIRE].

[54] D.G.L. Allegretti and H.K. Kim, *A duality map for quantum cluster varieties from surfaces*, *Adv. Math.* **306** (2017) 1164 [arXiv:1509.01567] [INSPIRE].

[55] H.K. Kim and M. Son, SL_2 *quantum trace in quantum Teichmüller theory via writhe*, arXiv:1812.11628 [INSPIRE].

[56] J. Korinman and A. Quesney, *The quantum trace as a quantum non-abelianization map*, arXiv:1907.01177.

[57] V. Fock and A. Goncharov, *Moduli spaces of local systems and higher Teichmüller theory*, *Publ. Math. IHES* **103** (2006) 1 [math/0311149].

[58] V.V. Fock and A.B. Goncharov, *Cluster ensembles, quantization and the dilogarithm*, math/0311245 [INSPIRE].

[59] A. Goncharov and L. Shen, *Quantum geometry of moduli spaces of local systems and representation theory*, arXiv:1904.10491.

[60] T. Dimofte, *Perturbative and nonperturbative aspects of complex Chern–Simons theory*, *J. Phys. A* **50** (2017) 443009 [arXiv:1608.02961] [INSPIRE].

[61] L.F. Alday, D. Gaiotto, S. Gukov, Y. Tachikawa and H. Verlinde, *Loop and surface operators in $N = 2$ gauge theory and Liouville modular geometry*, *JHEP* **01** (2010) 113 [arXiv:0909.0945] [INSPIRE].

[62] A. Neitzke and F. Yan, *Line defect Schur indices, Verlinde algebras and* $U(1)_r$ *fixed points*, *JHEP* **11** (2017) 035 [arXiv:1708.05323] [INSPIRE].

[63] D. Gaiotto, G.W. Moore and A. Neitzke, *Four-dimensional wall-crossing via three-dimensional field theory*, *Commun. Math. Phys.* **299** (2010) 163 [arXiv:0807.4723] [INSPIRE].

[64] M. Kontsevich and Y. Soibelman, *Stability structures, motivic Donaldson-Thomas invariants and cluster transformations*, arXiv:0811.2435 [INSPIRE].

[65] T. Dimofte, S. Gukov and Y. Soibelman, *Quantum Wall Crossing in $N = 2$ Gauge Theories*, *Lett. Math. Phys.* **95** (2011) 1 [arXiv:0912.1346] [INSPIRE].

[66] J.H. Przytycki, *Fundamentals of Kauffman bracket skein modules*, *Kobe J. Math.* **16** (1999) 45.

JHEP09(2020)153